CANADIAN THESES ON MICROFICHE

THÈSES CANADIENNES SUR MICROFICHE

National Library of Canada
Collections Development Branch

Canadian Theses on
Microfiche Service

Ottawa, Canada
K1A 0N4

Bibliothèque nationale du Canada
Direction du développement des collections

Service des thèses canadiennes
sur microfiche

NOTICE

The quality of this microfiche is heavily dependent upon the quality of the original thesis submitted for microfilming. Every effort has been made to ensure the highest quality of reproduction possible.

If pages are missing, contact the university which granted the degree.

Some pages may have indistinct print especially if the original pages were typed with a poor typewriter ribbon or if the university sent us an inferior photocopy.

Previously copyrighted materials (journal articles, published tests, etc.) are not filmed.

Reproduction in full or in part of this film is governed by the Canadian Copyright Act, R.S.C. 1970, c. C-30. Please read the authorization forms which accompany this thesis.

AVIS

La qualité de cette microfiche dépend grandement de la qualité de la thèse soumise au microfilmage. Nous avons tout fait pour assurer une qualité supérieure de reproduction.

S'il manque des pages, veuillez communiquer avec l'université qui a conféré le grade.

La qualité d'impression de certaines pages peut laisser à désirer, surtout si les pages originales ont été dactylographiées à l'aide d'un ruban usé ou si l'université nous a fait parvenir une photocopie de qualité inférieure.

Les documents qui font déjà l'objet d'un droit d'auteur (articles de revue, examens publiés, etc.) ne sont pas microfilmés.

La reproduction, même partielle, de ce microfilm est soumise à la Loi canadienne sur le droit d'auteur, SRC 1970, c. C-30. Veuillez prendre connaissance des formules d'autorisation qui accompagnent cette thèse.

THIS DISSERTATION
HAS BEEN MICROFILMED
EXACTLY AS RECEIVED

LA THÈSE A ÉTÉ
MICROFILMÉE TELLE QUE
NOUS L'AVONS REÇUE

Canadä

NL 339 (r. 86/09)

(21)

0-315-21217-9

National Library
of Canada

Canadian Theses Division

Ottawa, Canada
K1A 0N4

Bibliothèque nationale
du Canada

Division des thèses canadiennes

PERMISSION TO MICROFILM — AUTORISATION DE MICROFILMER

- Please print or type — Écrire en lettres moulées ou dactylographier

Full Name of Author — Nom complet de l'auteur
JOHN DAVID WILSON

Date of Birth — Date de naissance
8 MAY 1957

Country of Birth — Lieu de naissance
TRINIDAD, W.I.

Permanent Address — Résidence fixe
[redacted]

21 DIANA DR. APT. 3
DOWNS VIEW ONT
M3M 2W2

Title of Thesis — Titre de la thèse
COLD STARTING OF A DIESEL ENGINE USING A TIMED SPARK DISCHARGE

University — Université
UNIVERSITY OF ALBERTA

Degree for which thesis was presented — Grade pour lequel cette thèse fut présentée
M.Sc. (MECHANICAL ENGINEERING)

Year this degree conferred — Année d'obtention de ce grade
SPRING 1985

Name of Supervisor — Nom du directeur de thèse
DR. J.D. DALE

Permission is hereby granted to the NATIONAL LIBRARY OF CANADA to microfilm this thesis and to lend or sell copies of the film.

The author reserves other publication rights, and neither the thesis nor extensive extracts from it may be printed or otherwise reproduced without the author's written permission.

L'autorisation est, par la présente, accordée à la BIBLIOTHÈQUE NATIONALE DU CANADA de microfilmer cette thèse et de prêter ou de vendre des exemplaires du film.

L'auteur se réserve les autres droits de publication; ni la thèse ni de longs extraits de celle-ci ne doivent être imprimés ou autrement reproduits sans l'autorisation écrite de l'auteur.

Date
14 DEC 84

Signature
J Wilson

NL-91 (4/77)

THE UNIVERSITY OF ALBERTA

COLD STARTING OF A DIESEL ENGINE USING A TIMED SPARK IGNITION

by

©

JOHN D. WILSON

A THESIS

SUBMITTED TO THE FACULTY OF GRADUATE STUDIES AND RESEARCH

IN PARTIAL FULFILMENT OF THE REQUIREMENTS FOR THE DEGREE

OF MASTER OF SCIENCE

DEPARTMENT OF MECHANICAL ENGINEERING

EDMONTON, ALBERTA

SPRING 1985

THE UNIVERSITY OF ALBERTA

RELEASE FORM

NAME OF AUTHOR JOHN D. WILSON

TITLE OF THESIS COLD STARTING OF A DIESEL ENGINE USING A TIMED SPARK IGNITION

DEGREE FOR WHICH THESIS WAS PRESENTED MASTER OF SCIENCE

YEAR THIS DEGREE GRANTED SPRING 1985

Permission is hereby granted to THE UNIVERSITY OF ALBERTA LIBRARY to reproduce single copies of this thesis and to lend or sell such copies for private, scholarly or scientific research purposes only.

The author reserves other publication rights, and neither the thesis nor extensive extracts from it may be printed or otherwise reproduced without the author's written permission.

(SIGNED) J Wilson

PERMANENT ADDRESS:
c/o VAL & CAROL
16208 87 AVE
EDM., ALTA. T5R 4G9.

DATED 26 JANUARY 1985

THE UNIVERSITY OF ALBERTA

FACULTY OF GRADUATE STUDIES AND RESEARCH

The undersigned certify that they have read, and recommend to the Faculty of Graduate Studies and Research, for acceptance, a thesis entitled COLD STARTING OF A DIESEL ENGINE USING A TIMED SPARK IGNITION submitted by JOHN D. WILSON in partial fulfilment of the requirements for the degree of MASTER OF SCIENCE.

J.D. Dale
Supervisor

Peter R. Smy

Date December 14, 1984

To my parents, Valentine and Carol Wilson

ABSTRACT

This study investigates the development and adaptation of a timed spark discharge system to aid a multi-cylinder automotive-type indirect injection (I.D.I.) Diesel engine, for low temperature starting. Its performance was compared with factory installed glow plugs which are commonly used on this type of engine.

Pressure and temperature measurements of the cylinder charge were taken during cranking with a high speed computer controlled data acquisition system. This was done to obtain measurements of cylinder gas density in ambient temperatures down to -33°C and to estimate heat transfer rates to the cylinder during cranking. The maximum cylinder gas density needed to be identified in order to develop an ignition system with high energy voltage capability to properly breakdown the spark gaps.

In order to perform breakdown voltage tests on spark plugs, a high pressure cell was designed and built. It was cylindrical in shape, 10 cm long and 8 cm in diameter, fitted with glass windows (2.44 cm thick) on each end. This cell was capable of withstanding sustained internal pressures of up to 2 MPa. The cell was also used in conjunction with a Schlieren system to show the effect of plug geometry on spark kernel mobility. Here an orificed plasma plug was used and photographs were taken to show the hot plasma plume generated within the plug cavity, as it travels across the cell. The system had sufficient

resolution to be able to clearly see the shock wave travelling away from the plug.

For this engine, access to the pre-chamber, where the spark plugs were to be installed, was so limited that special experimental small diameter surface gap plugs (Champion G508V) had to be installed in the engine.

The timed spark discharge system developed and adapted to the test engine produced starts in 30% to 40% of the cranking time required with the factory installed glow plug. Furthermore, only 50% of the total starting energy required with the glow plugs was used with the timed spark discharge system.

ACKNOWLEDGEMENTS

I would first of all like to express my appreciation to my supervisor, Dr. J.D. Dale, for his consistent advice, support (both financial and otherwise) and availability throughout this study.

The patience and optimism of Dr. J. Santiago exhibited throughout the experimentation was invaluable. Doug Way-Nee's technical help was also very much appreciated.

I am most grateful to Dr. D. Checkel for his help setting up the Data Acquisition System used in this study.

Thanks are also extended to the Department of Mechanical Engineering (University of Alberta) for the pleasure of studying in such a conducive environment, and for the assistance offered by the technicians and machinists, in particular, the very fine work of Albert Yuen throughout the project.

I am also grateful to the Natural Sciences and Engineering Research Council of Canada for supporting this work through grant G0290.

Special thanks go to two collegues, Dave MacKay and Björn Ystad for their friendship and counsel over the past two years.

I would especially like to thank my wife, Caroline, for her love and encouragement, and for her tireless effort textforming this thesis.

Table of Contents

Chapter Page

1. INTRODUCTION 1
    - 1.1 Historical Review of Engine Starting Aids 1
    - 1.2 Timed Spark Discharge as a Starting Aid 3
2. HEAT TRANSFER ANALYSIS 10
    - 2.1 Analytical Approaches to Heat Loss Problem 10
    - 2.2 Instrumentation 12
        - 2.2.1 Charge Temperature Measurements 13
        - 2.2.2 Pressure Measurement 15
        - 2.2.3 Data Acquisition 16
    - 2.3 Calculation of Charge Temperature using Two Thermocouples with Different Junction Sizes 22
    - 2.4 Cylinder Pressure Measurement 30
    - 2.5 Determination of Isentropic Charge Temperature .30
    - 2.6 Charge Density Determination 34
    - 2.7 Isentropic Work added to Charge 35
    - 2.8 Heat Lost from Charge 37
    - 2.9 Average Cylinder Heat Transfer Coefficient 41
    - 2.10 Cylinder Nusselt and Reynolds Numbers 43
3. HIGH PRESSURE CELL 56
    - 3.1 Cell Design 56
        - 3.1.1 Design Criteria 56
        - 3.1.2 Cell Performance 57
        - 3.1.3 Cell Features 57
        - 3.1.4 Pressure-Deflection Testing 60
    - 3.2 Cell - Schlieren System 63
        - 3.2.1 Schlieren Technique 63

3.2.2 Cell-Schlieren System Integration 65

3.2.3 Operation of the System 66

3.2.4 Photographic Results 67

4. SPARK PLUG SELECTION AND CIRCUIT DESIGN 71

4.1 Influence of Charge Density and Plug Geometry on Breakdown Voltage 71

4.2 Problems with Pre-Chamber Access - Special Designs 76

4.3 Ignition System 78

4.3.1 Introduction 78

4.3.2 Power Supplies 80

4.3.3 Trigger Circuits 80

4.3.4 SCR Switched Capacitor and Ignition Coil .80

4.3.5 Main Discharge Capacitor 82

5. STARTING EXPERIMENTS 84

5.1 Low Temperature Chamber 84

5.2 Engine Modifications 84

5.3 Power Supplies, Fuel and Lubrication 86

5.4 Starting Procedure 88

5.5 Results 89

5.6 Effects of Fuel Injection Timing on Ignition Delay 97

6. SUMMARY 104

REFERENCES 109

APPENDIX A: Internal energy of air and ratio of specific heats as a function of temperature 112

APPENDIX B: Correlation of Nu for Flow over a Single Sphere 118

APPENDIX C: Listing of Heat Transfer Analysis Program;CYANAL 119

APPENDIX D: Detailed Cell Design 135
APPENDIX E: Surface Gap Plugs Used in Study 152
APPENDIX F: Ignition System Parts List 155
APPENDIX G: Technical Data on Diesel Fuel 163

List of Tables

Table Page

2.1 Engine Specifications 13

2.2 Coefficients for Calculation of Heat Transfer on a Circular Cylinder with Air Flowing Normal to its Axis 27

A.1 Air Composition 113

B.1 Coefficients for Calculation of Heat Transfer on a Sphere with Air Flowing over it 118

G.1 Diesel Fuel Specifications 163

G.2 Diesel Fuel Distillations, Cloud Point and Pour Point Test Results 164

List of Figures

Figure Page

1.1 Block Diagram of Ignition Circuit 6

2.1 Cross-section of Engine Showing Location of Thermocouples and Pressure Transducer 14

2.2 Schematic of Engine - Data Acquisition Set-up for Heat Transfer 17

2.3 Flow Chart for D.E.C. LSI 11 Data Acquisition System Showing Software Use 21

2.4 Average Nusselt Number for Heating or Cooling of Air Flowing across a Single Cylinder (from McAdams [17]) 26

2.5 Measured Cylinder Pressure During Compression Stroke 31

2.6 Measured and Calculated Charge Temperatures during the Compression stroke 33

2.7 Charge Density during Compression 36

2.8 Incremental Isentropic Work Added to Charge and Incremental Heat Lost from Charge during each Interval throughout Compression Process 38

2.9 Cumulative Isentropic Work added to Charge and Cumulative Heat Lost from Charge during each Interval throughout Compression Process 39

2.10 Average Cylinder Heat-Transfer Coefficient at each Point in the Charge Compression 42

2.11 Charge Velocity Extracted from Flow Conditions over Thermocouple Junctions (assuming cylindrically shaped junctions) 47

2.12 Average Nuselt number for Heating or Cooling of Air Flowing across a Single Sphere (from McAdams [17]) 50

Figure Page

2.13 Average Cylinder Nusselt Number for Heating of Air (charge) during Compression Stroke @ T = -26.5°C (assuming t.c. junction is a cylinder) 51

2.14 Average Cylinder Nusselt Number for Heating of Air (charge) during Compression Stroke @ T = -26.5°C (assuming t.c. junction is a sphere) 52

2.15 Average Cylinder Nusselt Number for Heating of Air (charge) during Compression Stroke @ T = -33°C (assuming t.c. junction is a cylinder) 53

2.16 Average Cylinder Nusselt Number for Heating of Air (charge) during Compression Stroke @ T = +27°C (assuming t.c. junction is a cylinder) 54

3.1 High Pressure Cell 58

3.2 Load-Deflection Test of Glass Window 62

3.3 Cell-Schlieren System 64

3.4 Plume Penetration at Ambient Pressure after 115 µs 68

3.5 Plume Penetration at Ambient Pressure after 1065 µs 69

4.1 Charge Density during Compression Stroke @ -33°C 72

4.2 Cross-Sections of Spark Plug Types 73

4.3 Spark Plug Breakdown Voltage Dependence on Ambient Air Density 75

4.4 Schematic of the Four Cylinder Ignition System Driving External Gaps and Spark Plugs 79

4.5 Typical Ignition Circuit Input Signal 81

5.1 Schematic of High Energy Ignition Adapted to Engine in Cold Room 85

Figure Page

5.2 Cross Section of Engine Showing Fuel Injector and Starting Aid Location 87

5.3 Cranking Times for Engine with Starting Aids 91

5.4 Effect of Ambient Temperature on Spark Timing Window 92

5.5 Mercedes-Benz Starting - Running Characteristics with Factory Installed Glow Plug Aid 93

5.6 Effect of Ambient Temperature of Engine Cranking Speed 95

5.7 Mercedes-Benz Starting - Running Characteristics with Timed Spark Discharge Aid 96

5.8 Typical Pressure Buildup in Fuel Injector Line during Cranking for Cylinder #1, Temperature -34°C 98

5.9 Pressure - Time Diagram for Mechanical-Injection Engine Running at Full Load 100

5.10 Four Stages of Diesel Combustion (Mercedes-Benz Fuel Injection Period measured @ -34°C) 100

5.11 Schematic of Disintegration of a Fuel Jet 101

D.1 Variation of Radial and Tangential Stresses in a Thick Wall Cylinder 137

D.2 Schematic of Glass Window 140

D.3 Pressure-Time Trace used as the Starting Point in Glass Design 145

D.4 Recommended Working Pressure and Low Risk Loading Curve for Glass 148

E.1 Homebuilt Surface Gap Plug 153

E.2 Champion G508V Surface Gap Plug 154

Figure Page

F.1 Schematic of Ignition Circuit (a) DC-DC Converter, (b) Main Discharge Capacitor, (c) Ignition Coil (1 of 4), (d) SCR Switched Capacitor 156

F.2 Schematic of Trigger Circuit (1 of 4) (e) 159

F.3 Schematic of +5 v Regulated Power Supply to Trigger Circuit (f) 162

NOMENCLATURE

a_i - NBS Type T thermocouple polynomial coefficient

A - area (m^2)

°BTDC - degrees before top dead centre

C - specific heat of thermocouple junction

C_p - specific heat of ideal gas at constant pressure (kJ/kg-K)

C_v - specific heat of ideal gas at constant volume (kJ/kg-K)

d - inside diameter of shell (m)

D_1 - diameter of thermocouple junction #1 (m)

D_2 - diameter of thermocouple junction #2 (m)

e - thermocouple junction emf (volts)

E - Young's modulus (Pa)

h - average heat transfer coefficient (W/m^2-K)

$\bar{h}$ - enthalpy kJ/kmol

h^* - enthalpy (kJ/kg) (unreferenced Gas Tables [15])

h' - enthalpy (kJ/kg) (referenced to Gas Tables [15])

k - ratio of specific heats

K - thermal conductivity (W/m-K)

m - mass (kg)

mw - molecular weight

M - modulus of rupture for glass (Pa)

Nu - Nusselt number

P - pressure (Pa)

q - heat flux (W/m^2)

Q - heat transferred from charge (kJ)

r - radius of pressurized glass area (m)

R - universal gas constant (0.28703 kJ/kg-K)

Re - Reynolds number

S - maximum allowable stress value of material (Pa)

t - glass window thickness (m)

t.c. - thermocouple

T - temperature (K)

${}^{j}Tair^{j+1}$ - temperature of charge based on t.c. #1 & t.c. #2 between time interval j and j+1 (K)

$T_1{}^{j}$ - temperature of thermocouple 1 junction at time j (K)

$T_2{}^{j}$ - temperature of thermocouple 2 junction at time j (K)

$T_s{}^{j}$ - isentropic temperature at time j (K)

$uair$ - internal energy of air (kJ/kg)

v - charge velocity (m/s)

v' - specific volume (m^3/kg)

V - cylinder volume (m^3)

W - work added to charge (kJ)

x - distance (m)

X - mole fraction of gas in air

GREEK LETTERS

δ - glass window deflection (m)

$\Delta\tau$ - time interval (s)

μ - charge viscosity (kg/m-s)

μ^* - poisson's ratio for glass (0.21)

ρ - density (kg/m^3)

Φ - equivalence ratio

σ - stress (Pa)

θ - temperature

ω - internal cell pressure (Pa)

SUBSCRIPTS

$_i$ - inside diameter

$_k$ - outside diameter

$_o$ - ideal gas

$_s$ - isentropic process

SUPERSCRIPTS

^{j} - time

^{m} - average value

^{n} - Reynolds number exponent for forced convection flow

^{x} - Prandtl number exponent for forced convection flow

1. INTRODUCTION

1.1 Historical Review of Engine Starting Aids

Diesel engines have a reputation of being difficult to start in low temperature enviroments. This is a result of not having the proper thermodynamic conditions for autoignition of the fuel in the cylinder when the fuel is injected. To assist these engines, a variety of starting aids are available for use. Among these are items like electric block heaters which are used to warm the engine to improve cranking speeds.

In the mid 1940's Schweitzer [26]' experimented with introducing Diesel fuel vapors into the intake manifold to test the effect on startability of Diesel engines at room temperature. He found that it was not the vapour of the highest cetane fuel (shortest ignition delay) that produced the best starts but the most volatile. While the results were not spectacular, he found that introduction of the fuel during the intake process increased the time available for vaporization and therefore promoted ignition of the regular fuel. Carburetion of highly volatile hydrocarbons into the intake manifold as a starting aid was also tried. Here again, the qualification of a good starting fluid was that it was a highly volatile liquid. In the course of Schweitzer's study, Diethyl ether was used to assist starting. It was so effective an aid that the method of

---

'Numbers in square brackets refer to references.

introduction (injection, evaporation or carburetion) was inconsequential. The principle disadvantages with Diethyl ether are:

1. that it is a fire hazard.
2. the potential for violent explosions in the engine exists with improper use.

Nevertheless, at that time the introduction of Diethyl ether was the most effective way to start a Diesel in cold weather. It is still the most common starting fuel used today.

Austen and Lyn [4] later investigated the application of heating aids to the cold - starting phenomena in Diesel engines. Three main applications were tested on an automotive type 4-cylinder, 19 to 1 compression ratio diesel engine, they were:

1. Heating of the intake air
    (i) electrically at the air intake.
    (ii)electrically at the inlet port.
    (iii) using a fuel burner in the intake manifold.
2. Fuel injector line heating.
3. Use of a heater (glow) plug in the prechamber.

With the intake air being heated, starts down to -15°C in 45 seconds of cranking were recorded using 2 kW of power on average. The researchers found that "fuel line heating was found to be ineffective as a starting aid because of excessive heat loss both before the fuel enters the chamber and to the chamber wall due to impingement when it enters the chamber". Lastly, they also determined that "the main function of the heater plug was to provide a high temperature ignition source rather than a heat source" [4, p.111]

Each of these aids has advantages and disadvantages and they may be used to compliment one another on any particular engine.

1.2 Timed Spark Discharge as a Starting Aid

A new starting aid should show some advantages when compared with existing ones. The timed spark discharge system developed for this study is easily adapted to pre-chamber engines, produces rapid starts and requires less energy than the factory installed Bosch 955 glow plugs.

To evaluate the effectiveness of the timed spark discharge as a starting aid and to provide a basis for comparison, one would like to know for each system the lowest starting temperature possible for a given fuel, the time required to achieve the start, the energy consumed by the aid and for the timed spark discharge how critical is the timing, the spark location and the spark energy.

The timed spark discharge technique used in this study was originally used on an air cooled four cycle, single cylinder I.D.I. Onan diesel engine [22]. The engine was factory equipped with an electric glow plug in the pre-chamber and an electric air intake heater. The total electrical energy consumed by these aids was 480 W. This engine achieved starts at -40°C with the factory installed glow plug aids, but it would never warm up enough to run unaided at this temperature. However with the timed spark discharge the engine could be started at -55°C in 3 s cranking.

The spark timing and the location of the spark plug in the pre-chamber were both found not to be critical for starting this engine. A minimum stored energy of 2 J was necessary to achieve these starts.

The author is aware of only one other study that used a timed spark discharge as a starting aid, that of Atwell, Brumback and Manthey [3]. In this case, a low voltage ignition system (approximately 4500 v) with shunted surface gap spark plugs was tested in two diesel engines. One was a single cylinder, 4-stroke, air cooled I.D.I. engine, the other a 3-cylinder, 2-stroke, liquid cooled D.I. engine. Both used JP-4 fuel. Starts at -31°C were achieved in 8 s to 10 s of cranking. They found both the spark timing and plug location to be critical in the I.D.I., but neither in the D.I. model. They further stated that the same minimum amount of energy was required for both engines, although no details regarding stored spark energy or total energy were given.

With the success of the single cylinder starting tests [22], experiments were initiated to develop and study further the application of the timed spark discharge system to a multi-cylinder automotive type diesel engine.

A schematic of the electrical system used to produce the high energy spark discharge is shown in Figure 1.1. The discharge consists of two components, a high voltage spark (up to 30 kV) produced with an automotive ignition coil, and a low voltage (600 V) discharge from the storage capacitors. The high voltage breaks down the air in the external gap and the spark plug. The resistance of the ionized air then drops drastically allowing the charge stored in the main storage capacitors to discharge thereby producing a high current spark in the spark plug. The two discharges appear as a single spark. High energy (1J to 2J per firing) was used in this application instead of the low energy (50mJ) usually associated with automotive spark discharges for two reasons:

1. The spark volume increases as the stored energy increases.
2. The mobility of the spark kernel, from the plug electrodes into the charge increases as the stored energy increases.

The spark volume as well as its mobility are important in terms of enhancing the charge ignition. Nevertheless, for less severe conditions, i.e. at temperatures above -15°C, use of the high voltage (low energy) discharge alone should be adequate for starting purposes.

The primary objective of this investigation was to adapt a timed spark discharge to a four cylinder pre-chamber Diesel engine. In order to do so, knowledge of the pressure and temperature occuring in the cylinder during the

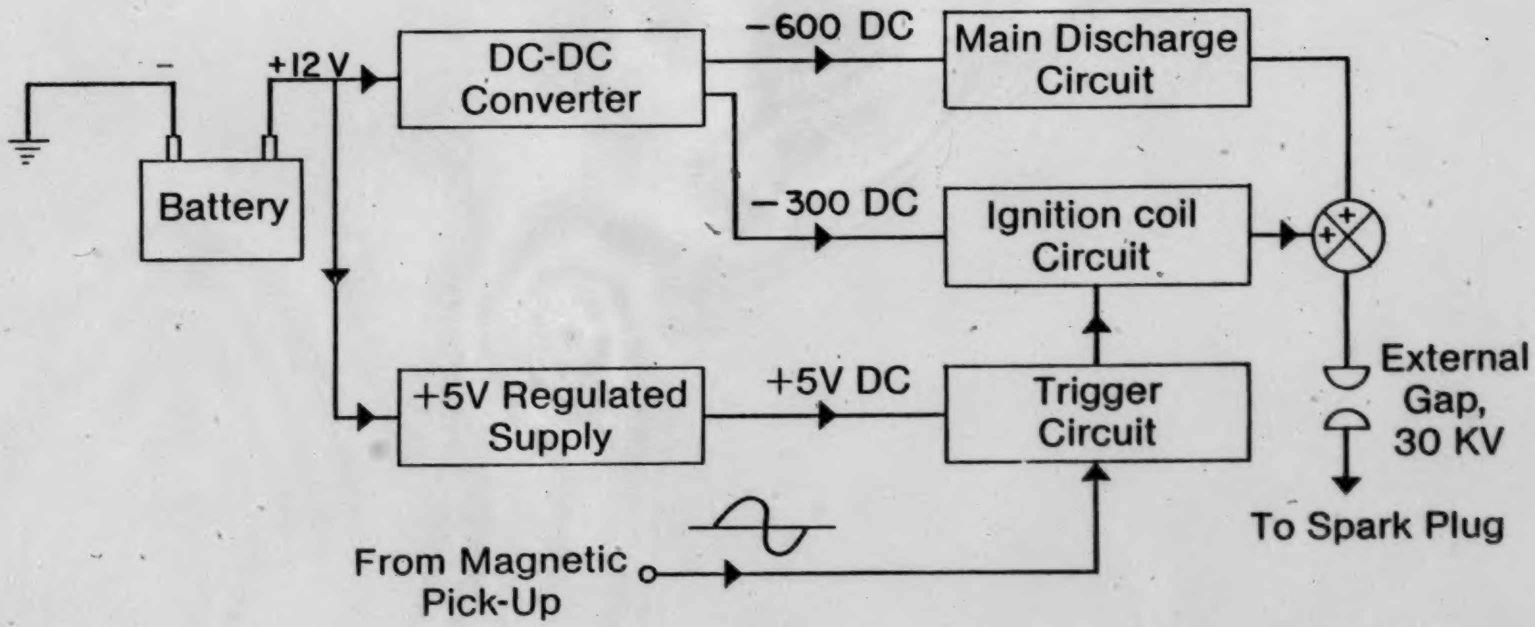

Figure 1.1 Block Diagram of Ignition Circuit

compression process (without any aids) is essential. Knowledge of charge history is necessary because spark plug breakdown voltage is a function of cylinder charge density, and cylinder charge density is in turn determined by its pressure, temperature and enclosed volume. These values of density can then be used to determine the relative breakdown voltage characteristics for spark plugs of various geometries and materials. These characteristics aid in the circuit design.

In order to have this plug testing capability, the design and construction of a high pressure cell was required, this is outlined in the first part of Chapter 3. The second part of Chapter 3 discusses the integration of the high pressure cell into a Schlieren system. This emphasizes another aspect of the problem of spark plug selection, this time regarding the potential influence on the ensuing combustion phenomena when energy is discharged across the electrodes. Here the effect of the energy discharged at the plug, is shown visually.

The main purpose of testing spark plugs for their breakdown voltage dependence on charge density, is to be able to choose the plug that has the lowest breakdown voltage requirement at any charge density. Testing and selection of appropriate spark plugs for the Mercedes-Benz engine are discussed in Chapter 4. A major advantage of using spark plugs with low breakdown voltage requirements is that the design of the discharge circuitry (used to generate these electrical potentials) is simplified, less expensive and inherently more reliable. This is because more commonly available components, operating at lower voltages can be used, probably with less shielding and grounding required throughout the entire system.

This study is the first known time a timed spark discharge aid has been adapted to a 4-cylinder, 4-stroke Diesel engine. The engine selected for this research was an OM636 Mercedes-Benz automotive type of 1950's vintage, yet quite representative of the general approach used in the 1980's. The current trend, being followed or set by many West German and U.S. automotive manufacturers is to use pre-chamber type engines for light vehicle use. The results of these starting tests will be covered in Chapter 5.

The secondary goal in this study was to obtain an appreciation for the heat transfer that occurs in the cylinder during motored operation. The point of this is to use these results as a baseline for future studies involving computer modelling of Diesel engine starting performance, with the assistance of starting aids. This is covered in Chapter 2.

As preparation of the charge for autoignition takes place during the compression process, and since this aspect of the cylinder heat loss phenomena was most important to the cold starting problem, the heat transfer analysis was limited to this stroke. In order to determine the cylinder volume, measurement of cylinder pressure, charge temperature and knowledge of piston location during the compression stroke with respect to TDC were required.

Lastly Chapter 6 contains a summary of the most important results of this investigation.

2. HEAT TRANSFER ANALYSIS

2.1 Analytical Approaches to Heat Loss Problem

One aspect to this study of starting a Diesel Engine at low temperatures, involved measuring the cylinder pressure and charge temperatures during cranking while the engine was being motored, in order to estimate the cylinder heat transfer.

Because this part of the study was of secondary importance, it was decided to use a simple approach. A common method used to measure heat transfer in an engine cylinder is with a heat flux probe. If heat flows in one direction only, then a temperature gradient is produced in the wall. The local wall heat flow can be easily calculated from the thermal conductivity, K, and the temperature gradient using Fourier's law as follows:

$$q = -K \left[\frac{\partial T_{wall}}{\partial x} \right]$$

where $\partial T_{wall}/\partial x$ is the local temperature gradient.

In most cases, however, heat flows in engines are not uni-dimensional due to construction characteristics and the measurement location in the cylinder, therefore a constant temperature gradient does not exist. However, some research facilities claim to make probes which simulate uni-dimensional flow [11].

An example of a study using a well instrumented engine that provided data requiring simple analytical tools is that of Annand's [2]. The test cylinder was in a D.I. engine and had a flat top piston and head.

A thin film thermocouple as well as conventional thermocouples, were inserted into the head to measure the cylinder head temperature and to provide evidence that the heat flux was one-dimensional and normal to the head. A fine wire platinum-iridium alloy transducer that could be used either as a hot wire anemometer or as a gas thermometer was also mounted in the head. Two quartz-crystal pressure transducers were fitted to the engine, one in the head and the other in the wall lining open to the crankcase to provide a known reference pressure. The experimental data was readily used to obtain a correlation of Nu for observed peak heat fluxes with the following expressions:

$$Nu = (D/K)Q/\Delta T$$

$$Re = \rho v D/\mu$$

The work of Greif et al. [8] is excellent for imparting an appreciation of the complexity of the cylinder heat transfer problem and the sort of detailed analysis that is sometimes required. Here a movable piston in a mock-up test cylinder was used. In the subsequent analysis the unsteady heat transfer to the sidewalls during piston compression of a single stroke was determined from the solution of the laminar boundary layer equation in the gas.

Faced with such an overwhelming selection of analytical techniques, tools and approaches, and as a result of the relative importance of this part of the study to the whole, it was decided to use the simplest method available. Therefore, the analysis followed by Mertz [19] will, for the most part, be used here. This desire to keep the analytical techniques as simple as possible was further solidified when the difficulty of adapting instrumentation to the cylinder, by modifying the head without weakening or affecting the operation of the engine, was realized. This was because of the limited space and complicated casting of the cylinder head.

2.2 Instrumentation

The engine used in this study was a Mercedes-Benz OM636, liquid cooled, I.D.I. Diesel, its specifications are listed in Table 2.1.

Table 2.1 Engine Specifications ([23])

Engine Type	4 Cycle
Number of Cylinders	4
Bore	75 mm
Stroke	100 mm
Displacement	1.767 L
Power output	38HP (Din) @3200rpm
Compression ratio	19:1
Clearance volume	23.5 cm^3
Pre-chamber volume	9.6 cm^3
Pre-chamber surface area	23.7 cm^2
Idling speed	1250 rpm
Half-throttle	1500 rpm

2.2.1 Charge Temperature Measurements

As there were only two existing access ports to the pre-chamber (and none to the main chamber), it was neccessary to install the charge measuring thermocouples where the fuel injector was normally fitted and the pressure transducer in the glow plug hole. The installations are shown in Figure 2.1.

The use of two thermocouples where each junction is different in size from the other, was one of many available techniques for measuring the charge temperature in an engine cylinder [19,21]. The thermocouple junctions were each made by first butt welding fine copper-constantan wires together. In one case 0.025 mm wire diameters were used, in the other 0.050 mm wire diameters. Spot welding of each junction onto two relatively robust (0.5 mm diameter) copper-constantan pins was then done as follows; copper onto copper and

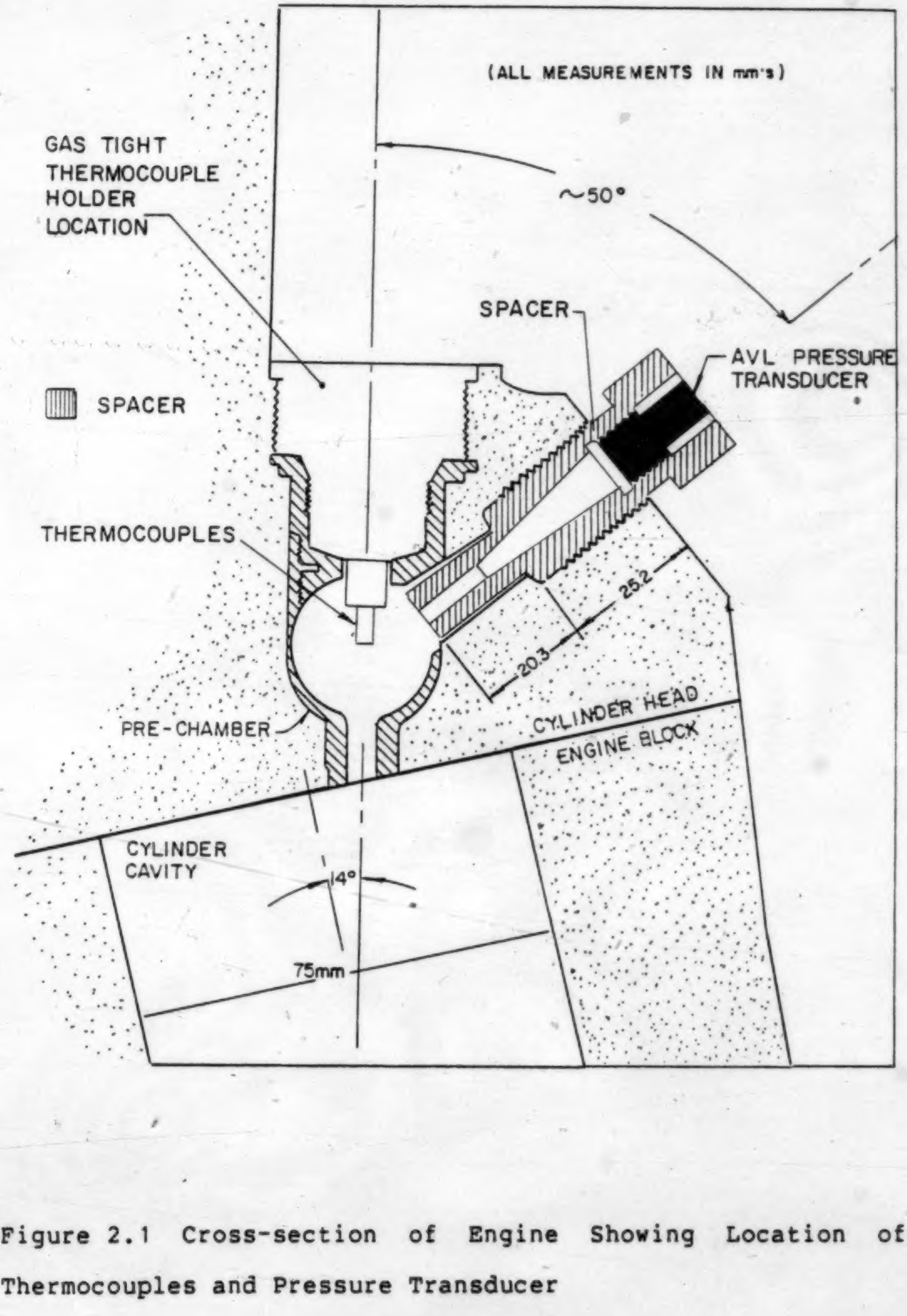

Figure 2.1 Cross-section of Engine Showing Location of Thermocouples and Pressure Transducer

constantan onto constantan. These pins were used to rigidly position the junctions in the center of the pre-chamber. It is worth noting here that although ideally the two junctions should have occupied the same point in space (a physical impossibility), in order to give more meaning to the measurements, the construction technique used resulted in a lateral separation between the junctions of about 2.5 mm.

Because these two thermocouple junctions were different in size, their mass and hence their time response would also be different. The measured temperature for each junction is used to estimate the actual charge temperature that would have been recorded by an ideal junction of zero mass and time response.

A quartic approximation to the NBS Type T (copper constantan) thermocouple data as a function of the measured thermoelectric voltage, was used to obtain the corresponding temperature[10]. The form of the expansion is:

$$T = a_0 + a_1 e + a_2 e^2 + a_3 e^3 + a_4 e^4$$

where e is in microvolts and T is in ° C. The maximum error incurred is approximately +/- 0.3 ° C. in the -200°C to 0°C range and +/- 0.17°C in the 0°C to 400°C range.

2.2.2 Pressure Measurement

A calibrated piezo-electric transducer, AVL Model# 12QP300CVK and Kistler Dual Mode Differential charge amplifier, Model #507, were used to measure the cylinder pressure.

2.2.3 Data Acquisition

Figure 2.2. shows the set up of the data acquisition system used for measuring the temperatures and pressures during the compression stroke. The procedure used for obtaining data at different temperatures and crankshaft positions was quite simple. First of all the engine was installed in a low temperature chamber. This room was maintained at the set point temperature for at least 24 hours. Then the D.E.C. LSI 11 data acquisition system was synchronized to the starter motor engaging, to begin sampling the first few seconds of engine cranking data, at 1KHz/channel.

Seven different signals from the engine were input to the computer. The pickup generating signals every 5° of crankshaft rotation was fed to two consecutive A/D channels. The A/D converter used in this D.E.C. LSI 11 system was a Data Translation DT2782 board, with 16 single ended input channels. Of the seven types of signals, four were used directly for analytical purposes. They were the two charge measuring thermocouples, the cylinder pressure and the engine rotational speed measured with a Servo Tek DC generator directly coupled to the flywheel. The remaining three signals were used for timing purposes. They were TDC of cylinder #1 (TDC1), TDC of cylinder #4 (TDC4), and pulses

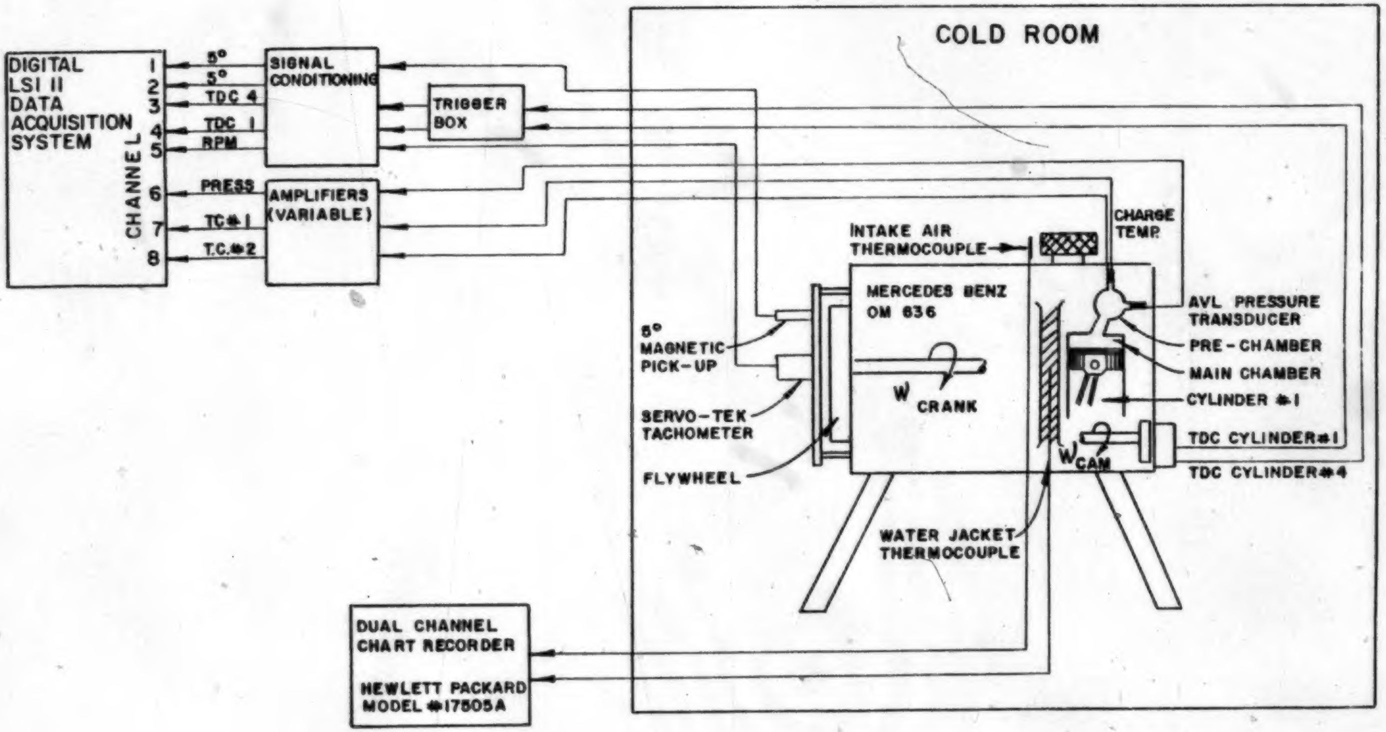

Figure 2.2 Schematic of Engine - Data Acquisition Set up for Heat Transfer

corresponding to every 5 degrees of crankshaft rotation (5°). TDC4 pulse was used for marking the beginning of the intake stroke on cylinder #1.

The 5° pulse was obtained with a magnetic pickup that sensed passing holes that were drilled into the flywheel. These holes were previously drilled in the fly wheel every 5° of crankshaft rotation. The pickup was separated from the flywheel by about 0.15 mm.

A significant amount of hardware and software conditioning was needed to produce usuable timing marker signals. On the hardware side, output signals for all three timing magnetic pickups TDC1, TDC4 and 5° were fed into a Schmidt trigger which produced a square pulse of magnitude 9.6 V and length 1.05 ms for each of these inputs. This magnitude was chosen as the acceptable signal, since the input range to the A/D was 0 V to 10 V. The sampling rate of 1 kHz was chosen as a reasonable time frame for obtaining more data than the minimum needed without running out of memory space. Because of this sampling rate, 1 kHz/channel, the timing signal pulse length required, had to be greater than 1 ms in order that the A/D would not miss any pulses. However, to take into account the effect of rapid acceleration of engine speed particularily at warm ambient temperatures when the time between the end of a pulse and the beginning of the next tends to decrease, possibly to the point of pulses overlapping, the pulse length had to be kept to a minimum. A pulse length of 1.05 ms was chosen as a moderate solution to this problem. Although the problem of pulses overlapping applies only to the 5° pulses, for design simplicity the other two timing pulses TDC1 and TDC4 were both fixed at the same value as the 5° pulse.

Double tracking of the 5° pulse to the computer was done to minimize the effect of a problem common to many A/D boards, that is the tendency to randomly assign a digitized count of zero when the input was greater than zero volts (i.e., the correct count should have been greater than 0). However, sometimes both channels were assigned a count of zero corresponding to the same input pulse. This was unfortunately unavoidable under the present experimental set-up and fortunately rare. At worst ±1 pulses out of the seventy-two 5° pulses were missed (or 1 per engine revolution). The number of missed 5° pulses/revolution could have been further reduced by triple tracking the 5° pulse to the A/D, however, because of the complication involved in changing the software to handle these modifications, it was decided to live with the situation.

Conditioning of t.c. signals was also required in the form of high gain (due to low signal strength) and effective shielding from starter motor noise (rather than filtering which tends to distort fast signal components) to get meaningful signals to the computer.

Although data was sampled at 1kHz/channel, only data that was associated with a known cylinder volume was retained, i.e. at each 5° pulse occurence.

This increment in crank angle of 5 degrees in fact determined the resolution that could be expected from the subsequent analysis. Ideally it should have been as small as possible, typically 1° or less [11], but practically for this system 5° was the minimum. This was because of the minimal space between drilled holes on the flywheel, and the type of pickup used.

Using known engine specifications (stroke, crank radius etc.), TDC1,TDC4 and the 5 degree pulses for timing markers, a volume array was generated as a function of crankshaft rotation.

A time base was easily extracted from the data as the sampling rate was fixed at 1KHz/channel.

The use of software with the D.E.C. LSI 11 Data Acquisition System is shown in Figure 2.3. The system was used for recording raw data, sorting out the data in time (using the timing markers), doing the analysis during each compression stroke and plotting the results.

The intake air temperature and the water jacket temperature were both continuously recorded with a dual channel chart recorder, Hewlett Packard Model #17505A. In this way, the engine core temperature history with respect to the ambient temperature could be monitored and the period of time the engine was maintained at the cold room temperature measured. Also the effect of the heat added to the block during the data acquisition, by the cranking action, could be assessed.

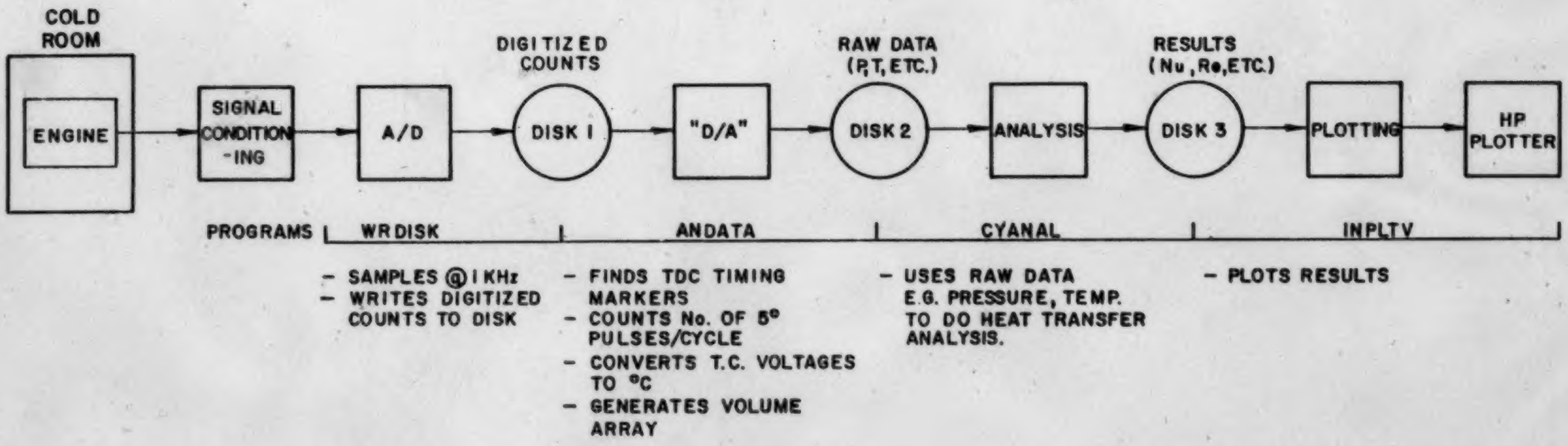

Figure 2.3 Flow Chart for D.E.C. LSI 11 Data Acquisition System Showing Software Use

2.3 Calculation of Charge Temperature using Two Thermocouples with Different Junction Sizes

It is well known that the larger the thermocouple (t.c.) junction mass the longer its response time. This principal is used with the two t.c.s (with different masses) located in the center of the pre-chamber, to calculate the charge temperature that would have been observed if a single t.c. of zero mass was used.

To do so apply the general heat exchange equation to a t.c. junction (1).

$$Q_{conduction} + Q_{radiation} + Q_{convection} = Q_{stored} \qquad (1)$$

For the conditions occuring during cranking, the radiation error in the measured t.c. readings should be less than 1K, [21]. Similarily, depression of the maximum measured temperature due to conduction losses should be around 1%, [21], therefore both $Q_{radiation}$ and $Q_{conduction}$ can be neglected. Equating the convective heat transfer to the change in internal energy of the t.c. junction and then expressing in finite difference form one obtains:

$$mC(T^{j+1} - T^{j})/{}^{j}\Delta\tau^{j+1} = hA({}^{j}Tair^{j+1} - 1/2\,(T^{j+1} + T^{j})) \qquad (2)$$

where: C = specific heat of junction

m = mass of junction

A = surface area of junction

h = film coeficient of heat transfer

${}^{j}Tair^{j+1}$ = temperature of air (charge) based on t.c. #1 and t.c. # 2 values for time interval $\Delta\tau$ j to j+1

T^{j}, T^{j+1}=junction temperatures at the beginning and end of time interval $\Delta\tau$

In order to simplify equation (2) an expression for the mass to surface area ratio for the thermocouple is now determined. Because the actual junction shape was somewhere between that of a cylinder and a sphere, the analysis will be done first based on the assumption that the junction is a cylinder then it will be assumed it is a sphere.

If one assumes that the cylindrical thermocouple junction (of diameter $D_{junction}$) occupies the same total volume and has the same length as the two pieces of wire (of diameter D_{wire}) from which it was made, then conservation of volume requires

$$2\left[\frac{\pi(D_{wire})^2 L}{4}\right] = \frac{\pi(D_{junction})^2 L}{4}$$

from this

$$D_{junction} = D = \sqrt{2}\, D_{wire}$$

Neglecting the surface areas of the cylinder ends, an expression for the mass to surface area ratio is then found as shown:

$$m/A = \rho D/4 \tag{3}$$

substituting (3) into (2) produces :

$$(\rho DC/4)(T^{j+1} - T^{j})/\Delta\tau = h({}^{j}Tair^{j+1} - 1/2(T^{j+1} + T^{j})) \tag{4}$$

Applying equation (4) to two t.c.'s of different junction diameters 1 and 2 and dividing one by the other results in:

$$\frac{D_1(T_1{}^{j+1} - T_1{}^{j})}{D_2(T_2{}^{j+1} - T_2{}^{j})} = \frac{h_1[Tair - 1/2(T_1{}^{j+1} + T_1{}^{j})]}{h_2[Tair - 1/2(T_2{}^{j+1} + T_2{}^{j})]} \tag{5}$$

- in this case $Tair$, h_1 and h_2 are unknowns

Assuming the junctions are sufficiently close to each other to claim that the charge properties are the same then McAdams' correlation [17] of the average heat-transfer coefficient for heating or cooling of air flowing perpendicular to the axis of a single cylinder can be used. This is in the following form:

$$Nu = (Re)^{n}(Pr)^{x}$$
$$hD/K = (\rho Dv/\mu)^{n}(Cp_{0}\mu/K)^{x} \tag{6}$$

Dividing the above expressing for junction 1 by that of junction 2 one obtains:

$$\frac{h_1}{h_2} = \left[\frac{D_2}{D_1}\right]^{1-n} \qquad (7)$$

Substituting (7) into (5) and solving for Tair:

$${}^{j}Tair^{j+1} = \frac{1/2\left[(T_1^{\,j+1}+T_1^{\,j})\left[\frac{D_2}{D_1}\right]^{2-n}\left[\frac{T_2^{\,j+1}-T_2^{\,j}}{T_1^{\,j+1}-T_1^{\,j}}\right]-(T_2^{\,j+1}+T_2^{\,j})\right]}{\left[\frac{D_2}{D_1}\right]^{2-n}\left[\frac{T_2^{\,j+1}-T_2^{\,j}}{T_1^{\,j+1}-T_1^{\,j}}\right]-1} \qquad (8)$$

Here it should be noted that all the parameters in (8) are known except for n. This represents the average slope of McAdams' correlation of Nu for flow over a single cylinder (see Figure 2.4), over the range traversed during the compression stroke. Nevertheless, even though the actual operating conditions are not as yet known, this analysis was done in an iterative fashion on the computer where a guess of the average slope can be made and later checked against the actual slope based on calculated junction heat-transfer coefficients using equation (7).

The correlation of Nu for the flow of air over a single cylinder (6), is shown in Figure 2.4, and can be subdivided into five sections for better accuracy. The usual form is to write:

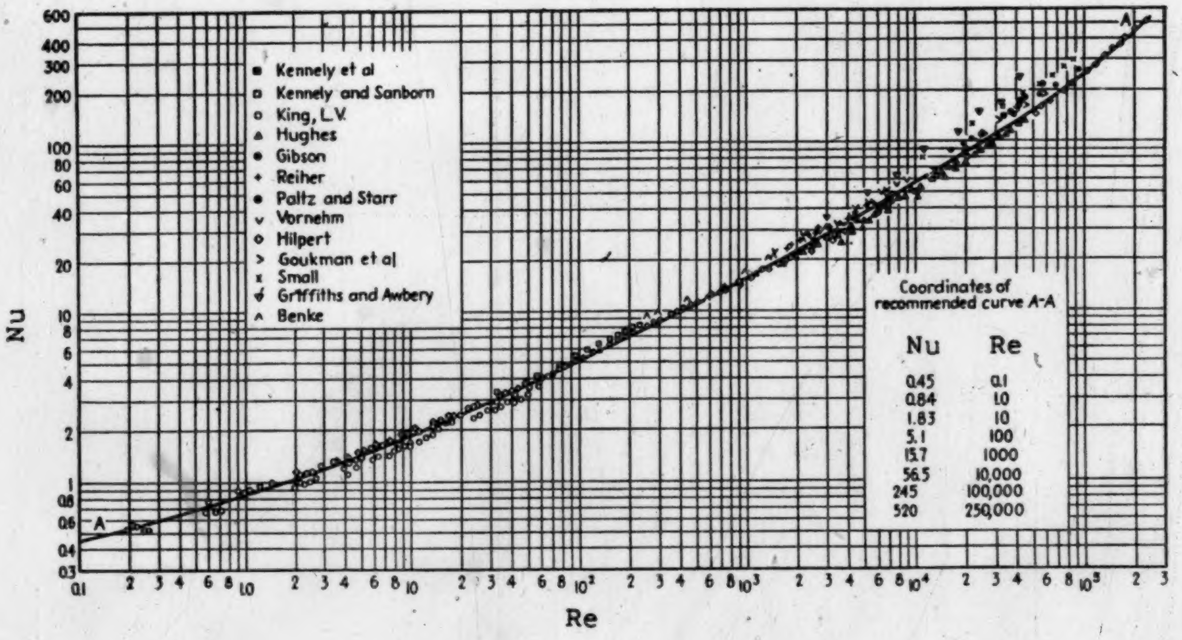

Figure 2.4 Average Nusselt Number for Heating or Cooling of Air Flowing across a Single Cylinder (from McAdams [17])

$Nu = c_1 Re^{n1} Pr^{1/3}$

taking Pr into consideration, assuming it remains constant throughout the compression stroke. This can be expressed as:

$$Nu = c\ Re^{n} \qquad (9)$$

where the values of the constant c and exponent n are listed in Table 2.2. This assumption has little effect on the subsequent analysis, typically less than 1/2 of a percent. The properties in equation (9) are to be evaluated at the film temperature of the fluid (in this case air) as follows:

$$T_{film} = (T_{junction} + T_{air})/2$$

Table 2.2 Coefficients for Calculation of Heat Transfer on a Circular Cylinder with Air Flowing Normal to its Axis ([17])

Nu	Re	C*	n
0.65 - 1.41	0.4 - 4	0.891	0.330
1.41 - 3.42	4 - 40	0.821	0.385
3.42 - 29.3	40 - 4000	0.615	0.466
29.3 - 121	4000 - 40,000	0.174	0.618
121 - 773	40,000 - 400,000	0.0239	0.805

* taking into account Pr

Here because the t.c. junction mass is so small it is assumed that the response time is negligible, and as a result, the junction temperature is the same as the fluid temperature, or,

$$T_{film} = T_{air}$$

It was estimated that this assumption on average caused a 10% reduction in charge velocity, as yet to be determined at each point in the compression stroke.

Using the above assumed value of n, a value of T_{air} can now be determined during each time interval j to j+1 throughout the compression stroke, using the measured readings from t.c. #1 and t.c. #2 both at the beginning and end of these time intervals.

The results of T_{air} obtained from (8) were found to be the "litmus" test for the quality of the rest of the analysis. By this, it is meant that if T_{air} did not meet certain criteria to be discussed later, the subsequent analysis would be obviously in error, necessitating taking more data. A possible explanation for this involves the origin of the raw data, P, T and V, from which the subsequent analysis is performed. While a high degree of confidence is placed in the accuracy of the pressure and volume measurements, this is not necessarily the situation with the charge temperature results. This is for several reasons:

1. This method of estimating the charge temperature was only done in one chamber, the pre-chamber, and the assumption was then made that the calculated T_{air} is

representative of the entire cylinder volume.

2. The sizes of both t.c. junctions may have been too large. In this case 0.025 mm diameter wire was used to make one junction and 0.05 mm diameter wire was used for the other, while Meyer [21] suggests using a maximum wire diameter of less than 0.025 mm.

Smoothing of the raw t.c. measurements was required before evaluation of the charge temperature. This was because each change in slope for both t.c. #1 and t.c. #2 as functions of time (C.A.) would cause a corresponding change in slope for the T_{air} curve, and as such cause a ripple effect throughout the rest of the analysis. To some extent, the method proposed here to determine the dimensionless heat transfer in the cylinder during the compression stroke, is analogous to repeatedly taking the derivative of a curve (due to the number of steps involved). Consequently smoothing was used to control these intermediate states from "blowing up". The coarseness of each time interval, 5°C.A., (instead of the 1°C.A. maximum suggested [11]), probably also contributed to the amount of smoothing required for all measured and derived parameters. Although this technique of data manipulating was not desirable, it was necessary. Further justification is offered for its use with the observation that general trends, which are the end results here did not seem to be greatly affected by this amount of smoothing.

2.4 Cylinder Pressure Measurement

The following is an analysis of a compression stroke from the intake valve closing (@130°BTDC) to TDC in cylinder #1 of the test engine, at an ambient temperature of -26.5°C.

The cylinder pressure measured throughout the compression stroke is shown in Figure 2.5. The measured cylinder peak pressure was 2200 kPa (gauge) for this test, while showing some variability from test to test, was not significantly different from the manufacturers suggested value of 2400 kPa considering that the test sites is 700 m above sea level. One would conclude from this that the blowby losses are probably as low as other references have suggested [9,13].

2.5 Determination of Isentropic Charge Temperature

The temperature history of the charge assuming an isentropic process, using the measured pressures was then generated as follows. Here an iterative process was used as the determination of T_s required knowledge of the ratio of specific heats k; k is unknown but is a function of T_s. Therefore initially all values of k were assumed equal to 1.40, and

$$T_{s\,@130^{\circ}BTDC} = Tair_{@130^{\circ}BTDC}$$

Using (10) an array of values for T_s was calculated.

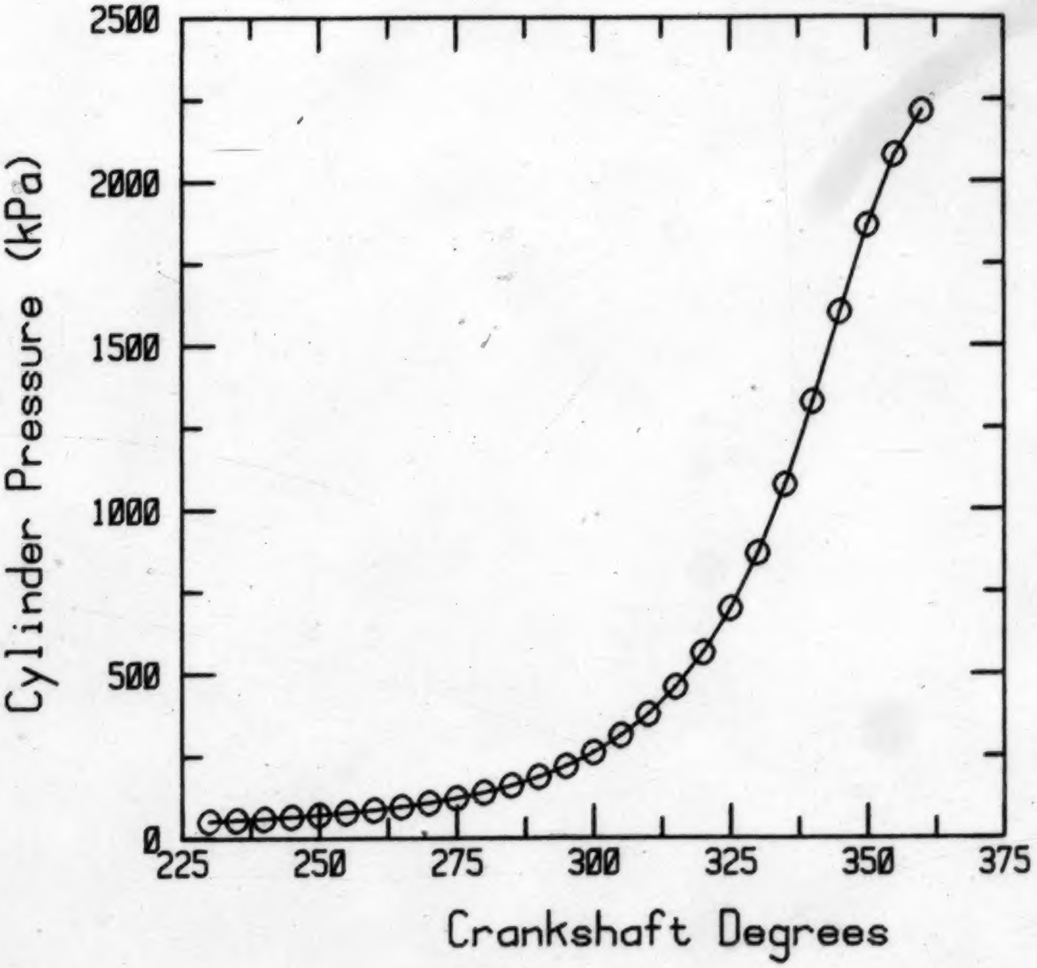

Figure 2.5 Measured Cylinder Pressure During Compression Stroke

$$T_s^{j+1} = T_s^j \left[\frac{P^{j+1}}{P^j}\right]^{\frac{{}^jk^{j+1}-1}{{}^jk^{j+1}}} \qquad (10)$$

Using an expression for the internal energy of air as a function of temperature, derived from ideal gas relationships, see Appendix A, the internal energy of the charge at each point in the isentropic compression was evaluated. An average value of $Cp_o air$ for each 5° interval of crankshaft rotation was then obtained using the previously calculated isentropic temperatures and the associated internal energy corresponding to the beginning and end of each interval. A corresponding array of average values of k in each 5° interval was then generated, using these new $Cp_o air$ values, also shown in Appendix A, as follows.

$${}^jk^{j+1} = \frac{{}^jCp_o air(T)^{j+1}}{{}^jCp_o air(T)^{j+1} - R} \qquad (11)$$

Experience revealed that four iterations were required to produce convergence of k and T_s to their final value. Figure 2.6 shows the charge temperature measured with t.c. #1 and t.c. #2, calculated using t.c. #1 and t.c. #2 to obtain T_{air}, and calculated using the measured pressures (assuming an isentropic compression) to obtain T_s. Here one observes

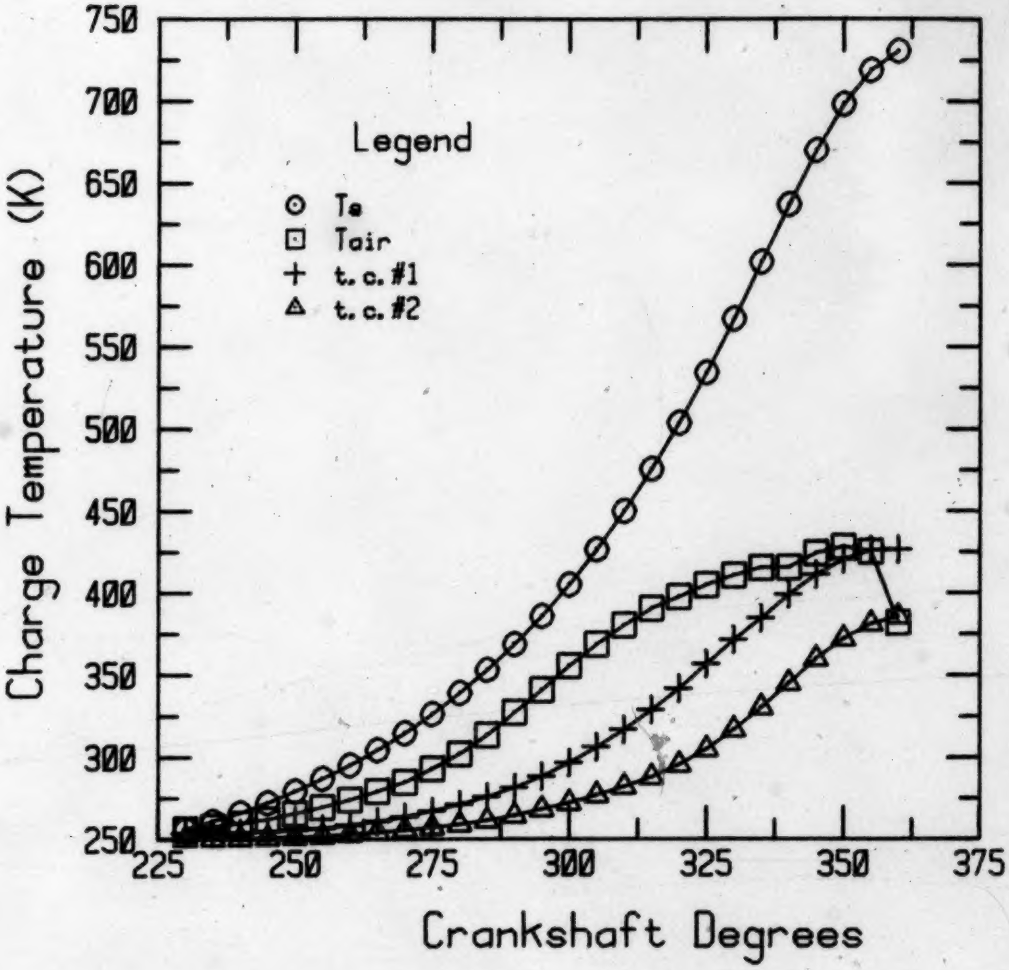

Figure 2.6 Measured and Calculated Charge Temperatures during the Compression stroke

that all curves are basically smooth and increasing and that in general

$$T_s > Tair > t.c.\#1 > t.c.\#2$$

Theoretically this should always be the case. This was the criteria for *Tair* previously referred to as the "litmus" test for acceptability of subsequent analysis. In fact, this proved very reliable, by simply observing the relative values and shapes of the temperature records the type of results could be anticipated.

2.6 Charge Density Determination

The charge density was derived based on the measured pressure, known volume and calculated *Tair* assuming no mass leakage from 130°BTDC to TDC, using the ideal gas law. This was obtained as follows:

$$\rho = \frac{m}{V} = \frac{P}{R\ Tair}$$

where:

m = charge mass (kg)
P = measured cylinder pressure (kPa)
V = known cylinder volume (m^3)
R = universal gas constant (0.28703 kJ/kg-K)
Tair = calculated charge temperature (K)

This is shown in Figure 2.7.

2.7 Isentropic Work added to Charge

With the values for T_s array the corresponding internal energy can again be obtained, and used to determine the incremental isentropic work added to the charge as follows.

$$ {}^{j}W^{j+1} = m_{@130^{\circ} BTDC} \left(u_s^{\,j+1} - u_s^{\,j}\right) \qquad (12) $$

In this case the mass is assumed constant throughout the compression process, although in fact there will be blowby losses through the intake and exhaust valves and past the piston rings to the crankcase. This was done here for simplicity, although initially it was hoped that the pressure and temperature sensors would have been sufficient to continuously monitor the cylinder mass at each step in the compression stroke. During the experimental design stage it was expected to be able to place at least one t.c. in the main chamber via the pre-chamber as well as two in the pre-chamber. This would have given a better representation of the charge temperature in both chambers. However, due to the small diameter of the pre-chamber orifice, locating a t.c. in the main chamber was not possible. The resulting instantaneous cylinder mass based solely on the pre-chamber t.c.s, were found to vary sinusoidally throughout the compression stroke. Due to the small amount of blow-by expected, the cylinder mass should have virtually been

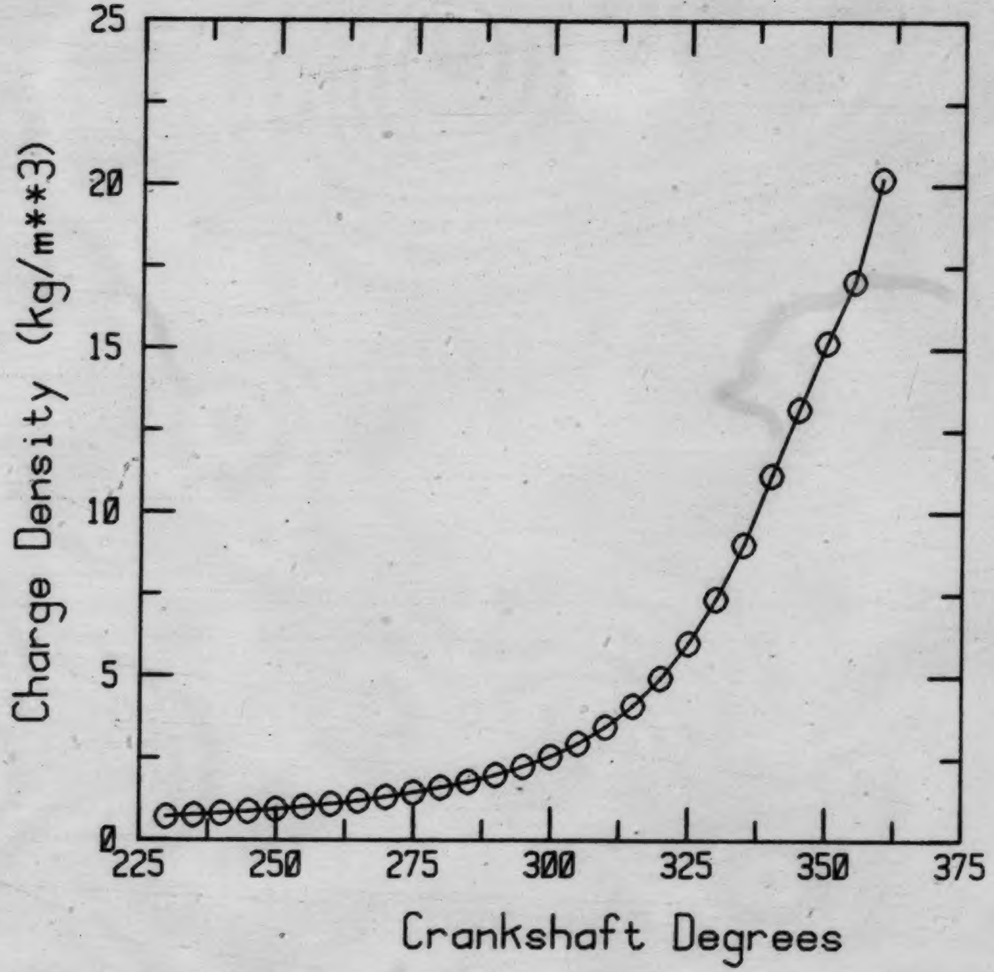

Figure 2.7 Charge Density during Compression

constant. As it was, this was taken as an indication that the charge temperature was not as representative of the entire cylinder volume as would have been hoped. This assumption was not crucial to the results as "blowby losses should not exceed 1/2 % of the engine swept volume under any particular operating conditions."[13].

2.8 Heat Lost from Charge

The incremental heat loss from the charge to the cylinder wall can now be determined, by using the first law of thermodynamics as follows:

$$dQ = du + dW$$

By subtracting from the incremental isentropic heat added to the charge, the actual amount of heat added, the heat loss is determined (13), see Figure 2.8.

$$ {}^{j}Q^{j+1} = {}^{j}W^{j+1} - m_{@130^{\circ}BTDC} \left(uair^{j+1} - uair^{j} \right) \qquad (13)$$

In order to get an idea of what percentage of the total energy added to the charge is actually lost to the cylinder walls, the cumulative isentropic work added and the cumulative heat lost from the charge at each point in time is plotted in Figure 2.9. From this it appears that 75% of the heat that was added is lost to the walls under these test conditions, a fairly substantial amount to lose

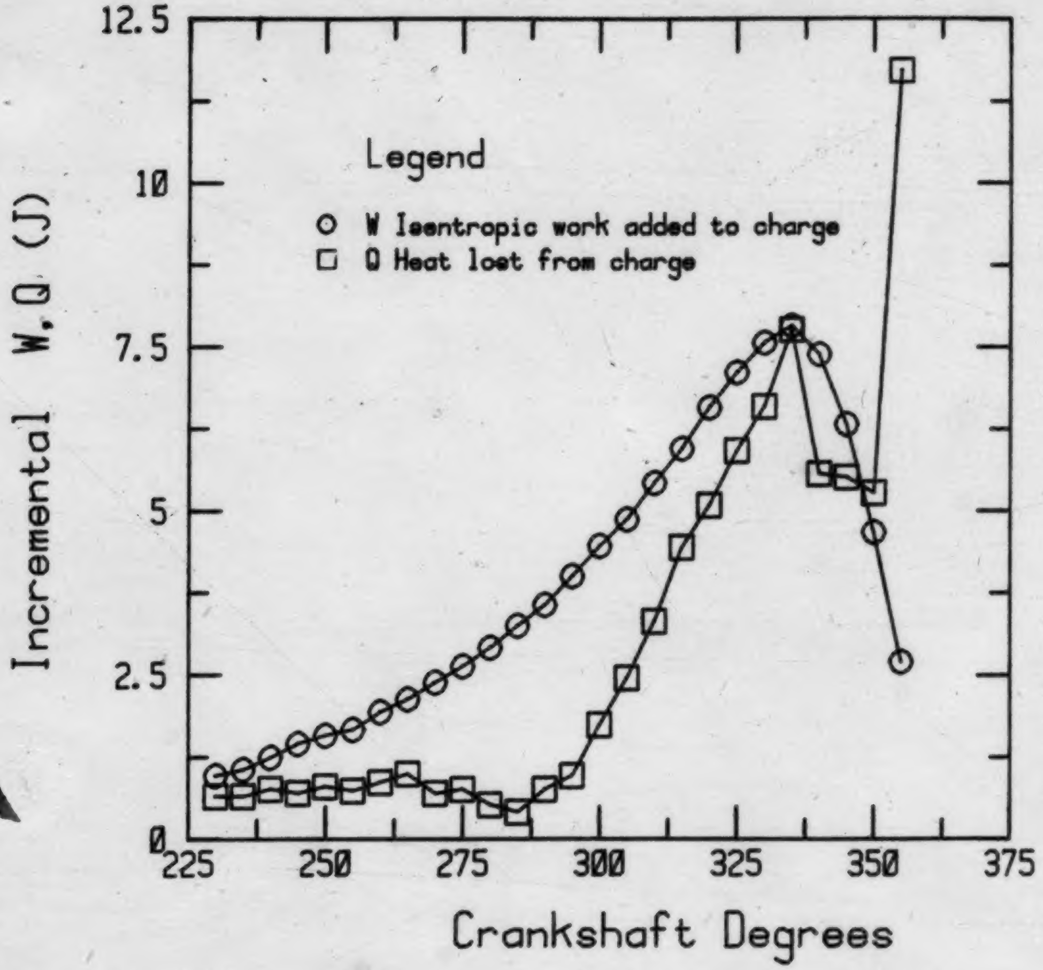

Figure 2.8 Incremental Isentropic Work Added to Charge and Incremental Heat Lost from Charge during each Interval throughout Compression Process

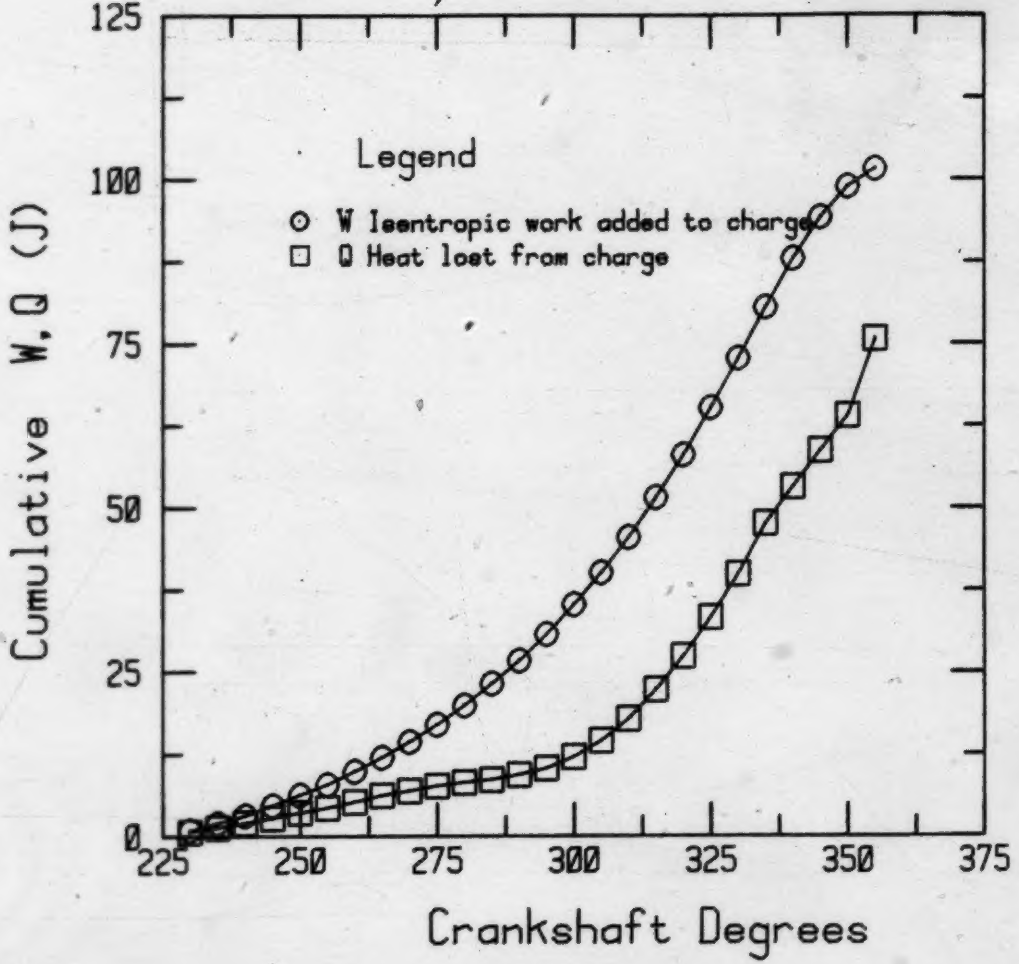

Figure 2.9 Cumulative Isentropic Work added to Charge and Cumulative Heat Lost from Charge during each Interval throughout Compression Process

considering the difficulties involved in producing autoignition conditions.

The heat loss from the charge to the cylinder as a whole is actually comprised of many components

$$Q_{cylinder} = Q_{wall} + Q_{piston} + Q_{head} + Q_{pre\text{-}chamber} \qquad (14)$$

As there was no provision made for determining what proportion of the total heat loss went to each sector, the assumption will be made that it was uniform throughout the cylinder (this includes all enclosing walls). If it is further assumed that the heat flux is constant and the charge temperature is representative of the entire enclosed chamber then is follows that:

$$T_{wall} = T_{head} = T_{piston} = T_{pre\text{-}chamber} = T_{cylinder} \qquad (15)$$

Furthermore, several researchers, [2,9], have found that the cylinder wall temperature remains more or less constant under these sort of test conditions, i.e., when the engine is cranked for only a few seconds. Monitoring of the Mercedes-Benz's cooling water temperature showed that a minute of cranking resulted in a temperature increase of only a few degrees celsius. From this it is inferred that the wall temperature should remain virtually constant during the 3 seconds of cranking when data is being sampled. Therefore equation (15) becomes:

$$T_{cylinder}=T_{wall}=T_{head}=T_{piston}=T_{pre\text{-}chamber}=\text{constant}$$

2.9 Average Cylinder Heat Transfer Coefficient

Using Newton's law of cooling and solving for h_{cyl}, the average cylinder gas film coefficient can readily be obtained on an incremental basis.

$$ {}^{j}h_{cyl}^{\,j+1} = \frac{{}^{j}Q_{cyl}^{\,j+1}}{{}^{j}\Delta\tau^{j+1}\;{}^{j}\left[\sum_{i}\left(A_i\,\Delta T_i\right)\right]^{j+1}} \tag{16}$$

or

$$ {}^{j}h_{cyl}^{\,j+1} = \frac{{}^{j}Q_{cyl}^{\,j+1}}{{}^{j}\Delta\tau^{j+1}\;{}^{j}A_{cyl}^{\,j+1}\left({}^{j}T_{air}^{\,j+1} - T_{cyl}\right)}$$

where:

$$ {}^{j}A_{cyl}^{\,j+1} = {}^{j}A_{wall}^{\,j+1} + A_{head} + A_{piston} + A_{pre\text{-}chamber} \tag{17}$$

These results are shown in Figure 2.10. The general shape of the average cylinder heat-transfer coefficient curve for the Mercedes-Benz engine used in this study was found to resemble that obtained by Greif [8] in an analytical study of heat losses from a compressed charge to a cylinder wall.

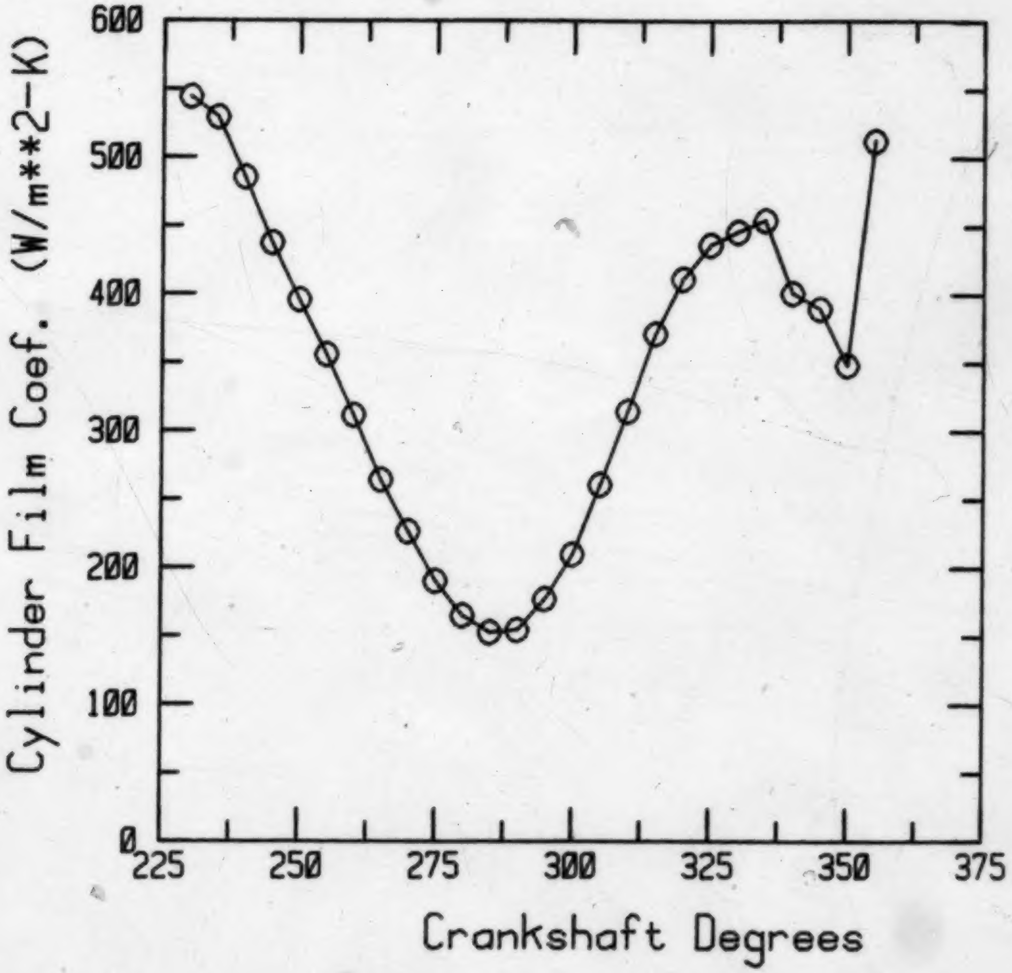

Figure 2.10 Average Cylinder Heat-Transfer Coefficient at each Point in the Charge Compression

2.10 Cylinder Nusselt and Reynolds Numbers

One would then like to express the results in a non-dimensional form of Nusselt and Reynolds number, which are defined to be:

$$Nu_{cyl} = h_{cyl} D_{cyl} / K$$

$$Re_{cyl} = \rho v D_{cyl} / \mu$$

Where h_{cyl} was just determined, and K, ρ and μ are properties of the charge [1,2]. Expressions for the thermal conductivity, K, and the absolute viscosity, μ, for air as functions of temperature were obtained using reference [30] as follows:

$$K = \frac{0.6325(10^{-5})\sqrt{T}*418.68}{\left[1 + \dfrac{245.4*10^{-(12/T)}}{T}\right]} \qquad (18)$$

where:

K = thermal conductivity (W/m-K)

T = Temperature (K)

and:

$$\mu * 10^8 = \frac{145.8\ T^{3/2}}{T + 110.4} \tag{19}$$

where:

μ = absolute viscosity (kg/m-s)

T = Temperature (K)

Therefore only Dcyl, some characteristic length of the cylinder, and v (the charge velocity) are unknown. In some studies Dcyl is set equal to the cylinder bore. However for this case as both the Nu and the Re will be determined on a step by step basis throughout the compression stroke where the cylinder volume changes with time it was thought best to use a characteristic length that also varied representatively with time.

$$Dcyl^j = \left[\frac{\text{Cylinder Volume}}{\text{Cylinder Surface Area}}\right]^j \tag{20}$$

$$Dcyl^j = \left[\frac{Vcyl}{Acyl}\right]^j$$

This leaves only the charge velocity as unknown. As mentioned earlier, because of the space limitations of the cylinder head, hot wire probes were not installed for charge velocity measurements. Therefore, in order to obtain some sort of representation for the magnitude of charge velocity, an analysis of the flow over the thermocouple junctions using Nusselt's expression for forced convection over a single cylinder (and later for a sphere as well) was done.

Here it was assumed that the junction flow conditions can be modelled by flow normal to the axis of a single cylinder. Equation (9) is again expressed as follows:

$$(hD/K)_{junction} = c(\rho vD/\mu)^{n}_{junction} \tag{21}$$

where both the values for c and n depend on the range of $Re_{junction}$ being used.

Using (4) the film coefficient for a particular junction is obtained.

$$h = \frac{\rho CD/2(T^{j+1} - T^{j})}{{}^{j}\Delta\tau^{j+1}(2\,{}^{j}Tair^{j+1} - (T^{j+1} + T^{j}))} \tag{22}$$

where the above parameters refer to the thermocouple junction.

The gas film coefficient for each junction was then evaluated throughout the compression stroke. From these, an average film coefficient value for each junction over the entire process was determined. These results, while important in determining the charge velocity, can also be used to check the validity of the value of n in equation (21). This was previously assumed as an input to the charge temperature (8). Using equation (7) n is obtained as follows:

$$n = 1 - \frac{\log(h^{m}_{\mathit{junction1}}/h^{m}_{\mathit{junction2}})}{\log(D_{\mathit{junction1}}/D_{\mathit{junction2}})} \qquad (23)$$

If the assumed and actual values of the slope n differed, then the process was repeated with another guess into equation (8) until good agreement was achieved. This was one of the checks used to judge the validity of assumptions made and hence the overall analysis.

After this the Nu_{junction} was determined making use of both junctions again throughout the stroke as follows:

$${}^{j}Nu_{\mathit{junction}}^{j+1} = \frac{1/2^{j}[(h^{m}D)_{\mathit{junction1}} + (h^{m}D)_{\mathit{junction2}}]^{j+1}}{{}^{j}K^{j+1}} \qquad (24)$$

With the known Nu_{junction}, the corresponding Re_{junction} can be determined and the flow velocity over the junctions extracted, see Figure 2.11. The assumption is then made that this velocity of the charge flowing over the thermocouple junctions was representative of the charge flowing throughout the cylinder as a whole. For this test at -26.5°C, the assumed average slope of the correlation of Nu for flow over a cylinder, see Figure 2.11, over the range anticipated was $n = 0.37$, while the actual calculated slope was $n = 0.39$.

If there was good agreement between the assumed n and the actual n, then another check for the validity of this

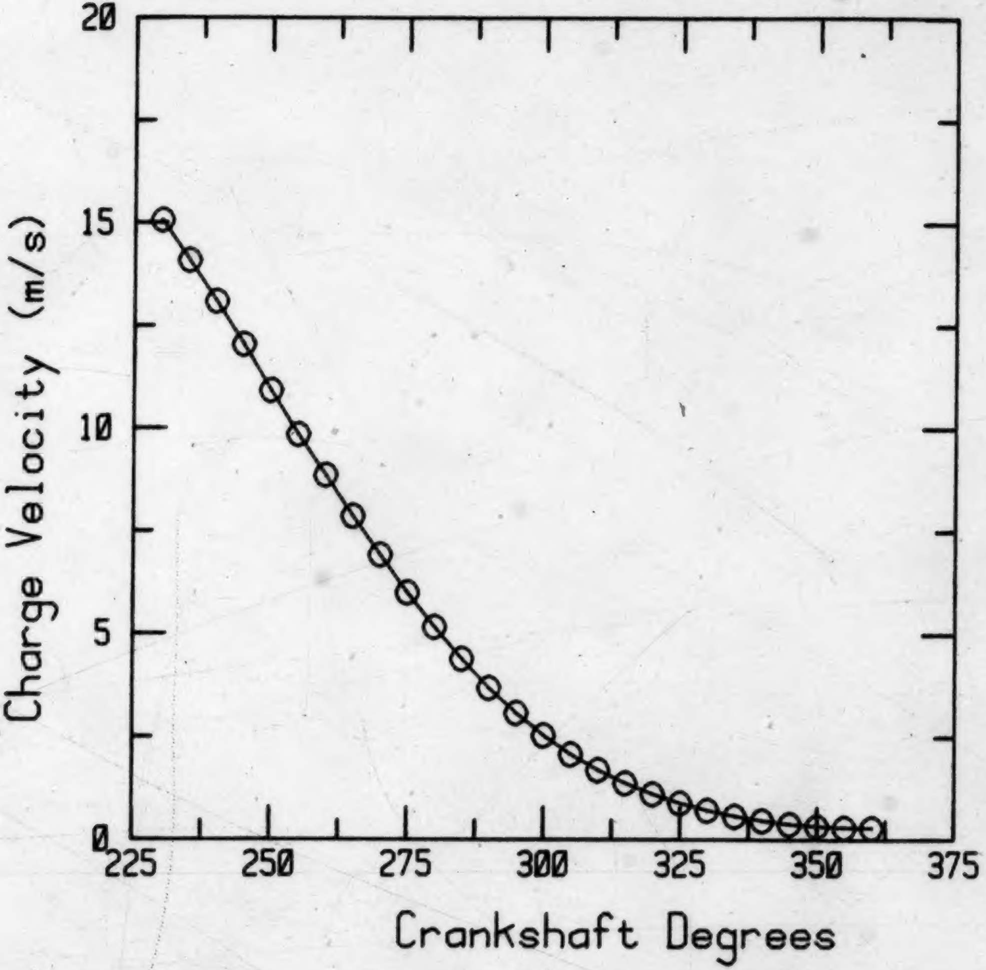

Figure 2.11 Charge Velocity Extracted from Flow Conditions over Thermocouple Junctions (assuming cylindrically shaped junctions)

process was to see if the actual (or assumed) n (they should be roughly the same at this point) occurred around the average $Nu_{junction}$ calculated for the entire compression stroke. Here the calculated average Nu for the entire compression stroke was $Nu^m = 2.65$. This is more or less in the middle of the range $1.40 \le Nu < 3.4$ having an average slope of 0.385, which is roughly what was guessed.

Because the t.c. junction was shaped somewhat like a sphere and somewhat like a cylinder, the analysis was done using both approaches. It should be noted that the heat transfer analysis done assuming the t.c. junction resembled a sphere, followed the same method as outlined above. The required correlation of Nu for flow over a sphere and the corresponding coefficients for the relationship are listed in Appendix B. The major impact of these methods to the results obtained, was on the charge velocities that were extracted. In general it seemed that the velocities obtained using the cylindrical junction approach may have been too high, for example v_{max} (@ 130°BTDC, T=27°C) = 66 m/s. Mertz [19] performed a similar analysis on an I.D.I., 19:1 compression ratio Diesel engine at an ambient temperature of +13°C. Here he found that the maximum velocity obtained, just after the intake valve closed was around 20 m/s. On the other hand, when a spherical junction was assumed the resulting velocities seemed low. For the test conducted at T=-33°C, the average $Re_{junction}$ obtained placed the entire test in the region of $1 \le Re_{junction} \le 3$, of Figure 2.12

(from McAdams [17]), i.e., heat conduction of a sphere in a stagnant environment. This is clearly not true as the engine cyclic speed, from which the charge motion in the cylinder is generated, is reduced by a factor of 3 from that at room temperature (+22°C), and not reduced to 0 rpm.

Nevertheless, it seems that the calculated Nu for flow conditions in a cylinder (while the charge is being compressed) was not greatly affected regardless of which flow conditions are assumed for the t.c. junction. This is observed in Figure 2.13 and 2.14, where the shapes of both curves are shown to be very similar. Furthermore, the order of magnitude for the Re_{cyl} at each point in the process, with either assumption, is roughly the same.

Engine cranking data was collected for ambient temperatures of @ -33°C, -26.5°C, and +27°C. The results for the flow conditions at T = -33°C and T = +27°C assuming the t.c. junctions are cylindrical in shape were compared to the predicted (25), see [1,2] and shown in Figures 2.15 and 2.16 respectively.

$$Nu = 0.3\ Re^{0.7} \tag{25}$$

While the experimentally generated curves for the three test temperature, shown in Figures 2.13, 2.14, 2.15 and 2.16, do not precisely follow the predicted, the scatter of the data is more or less symmetric about it, with the exception for data taken at +27°C. Furthermore, the shapes

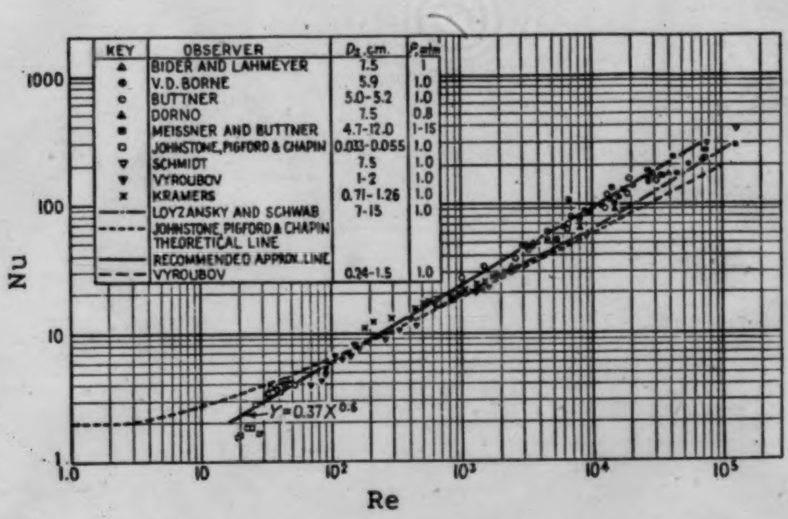

Figure 2.12 Average Nuselt number for Heating or Cooling of Air Flowing across a Single Sphere (from McAdams [17])

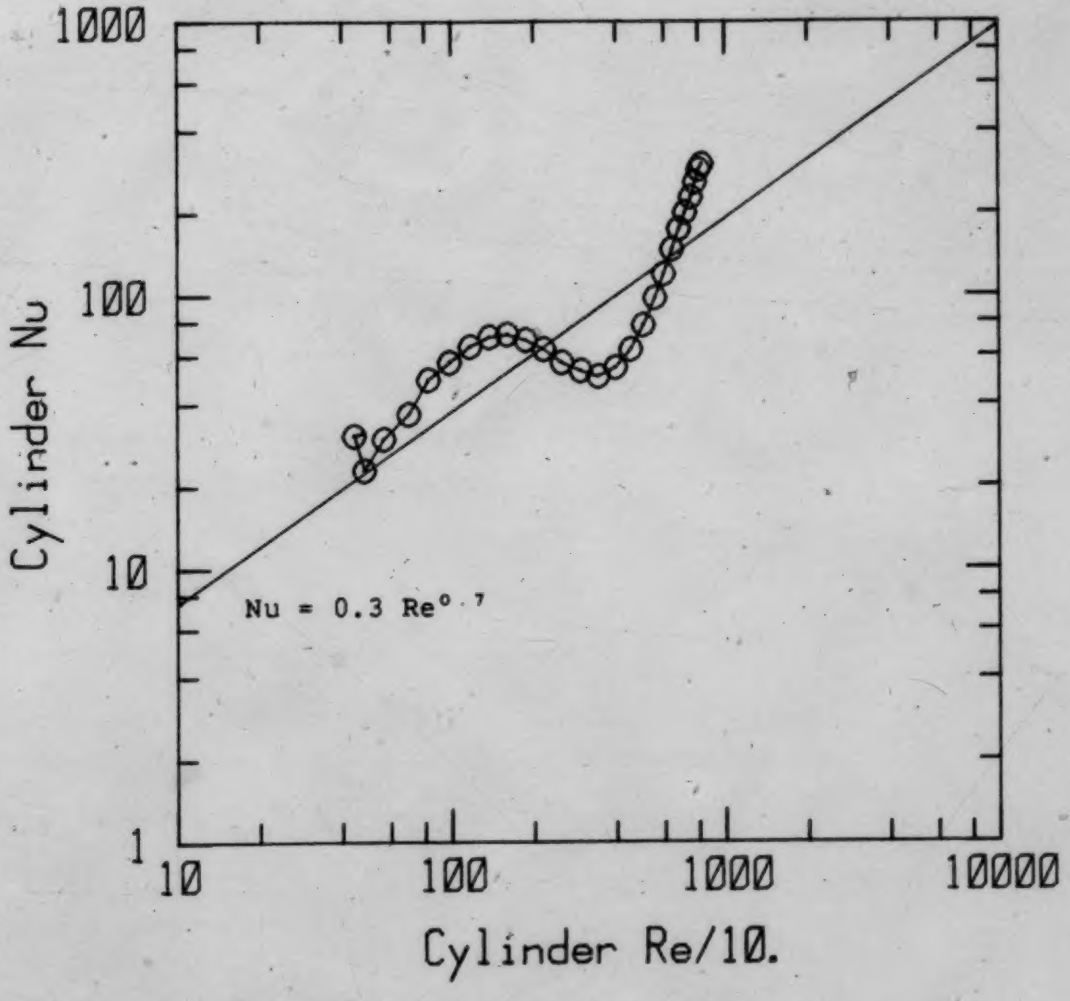

Figure 2.13 Average Cylinder Nusselt Number for Heating of Air (charge) during Compression Stroke @ T = -26.5°C (assuming t.c. junction is a cylinder)

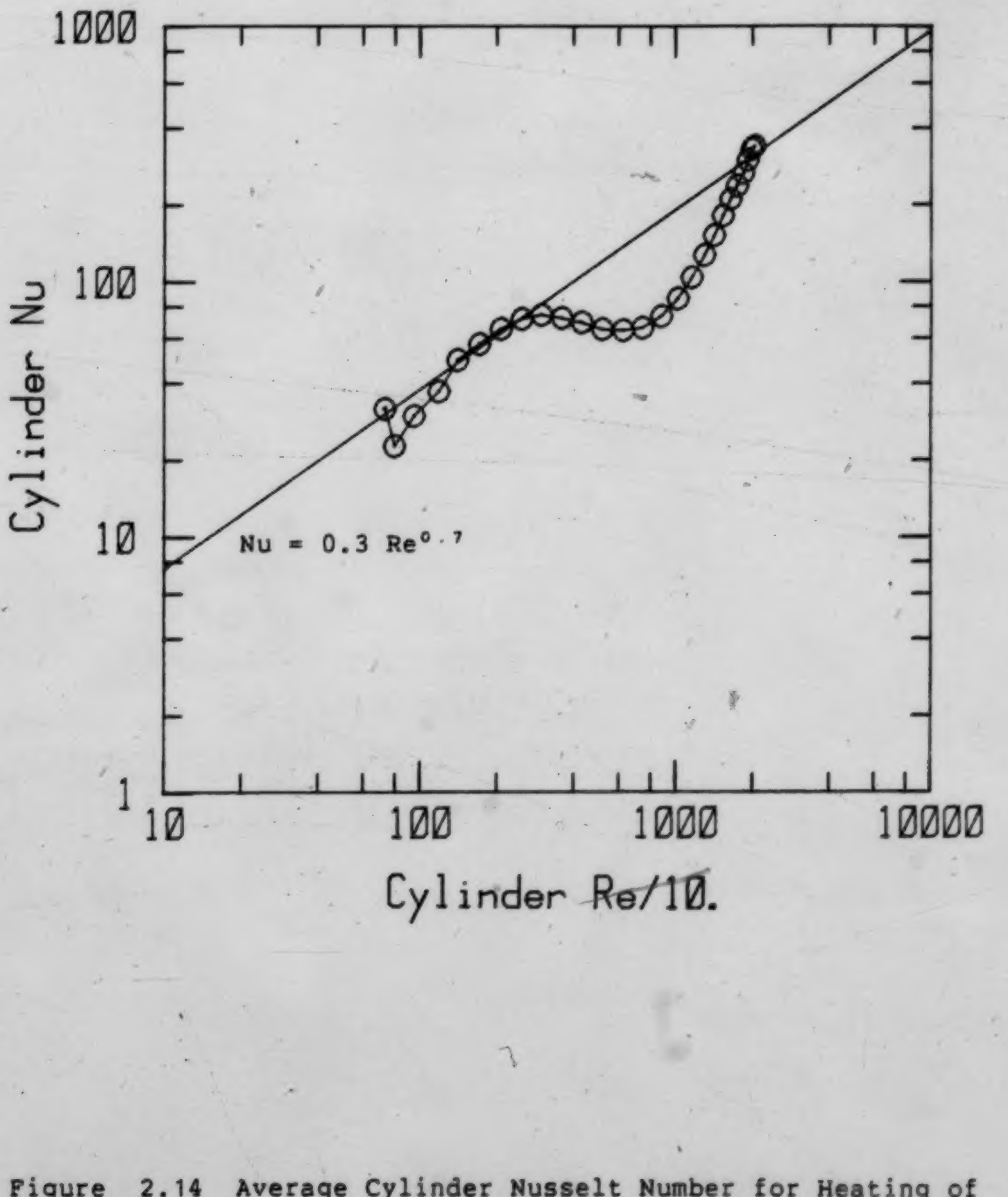

Figure 2.14 Average Cylinder Nusselt Number for Heating of Air (charge) during Compression Stroke @ T = -26.5°C (assuming t.c. junction is a sphere)

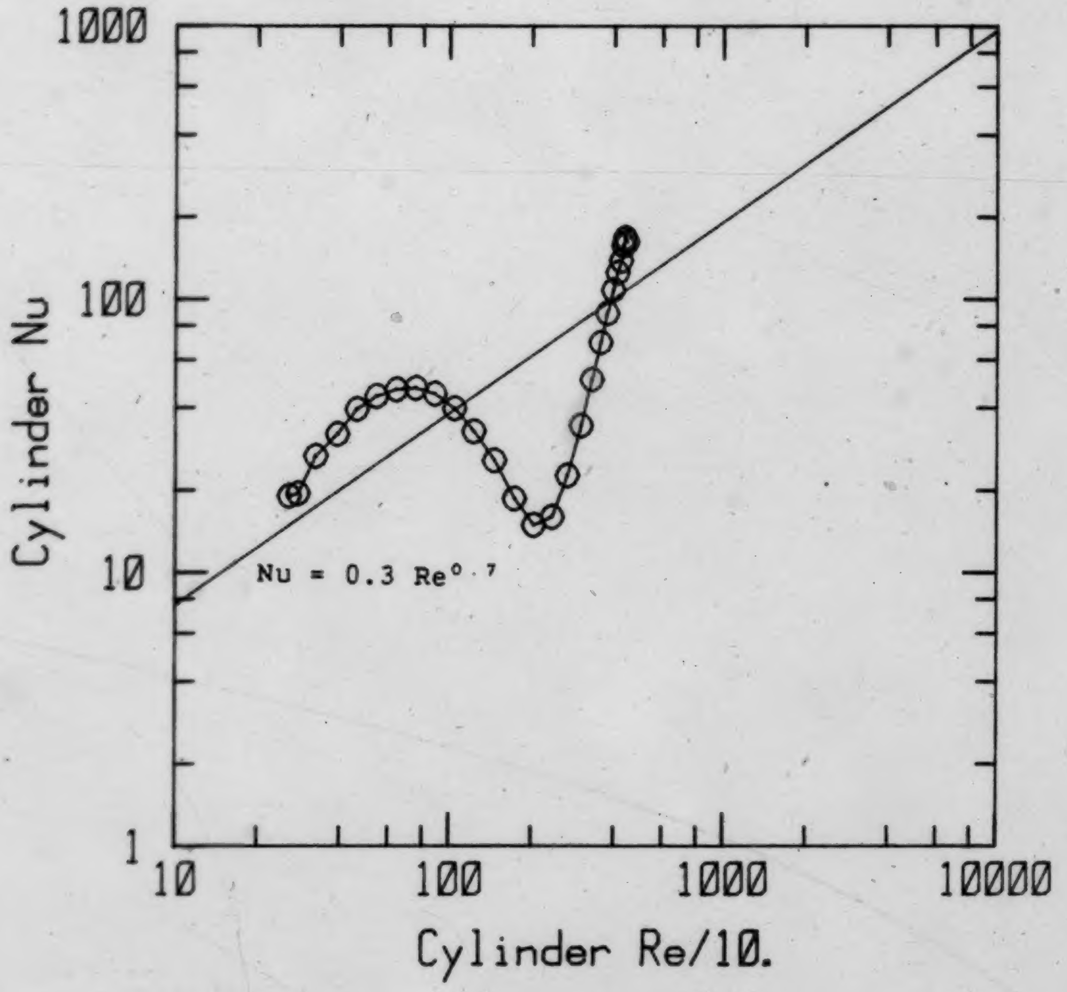

Figure 2.15 Average Cylinder Nusselt Number for Heating of Air (charge) during Compression Stroke @ T = -33°C (assuming t.c. junction is a cylinder)

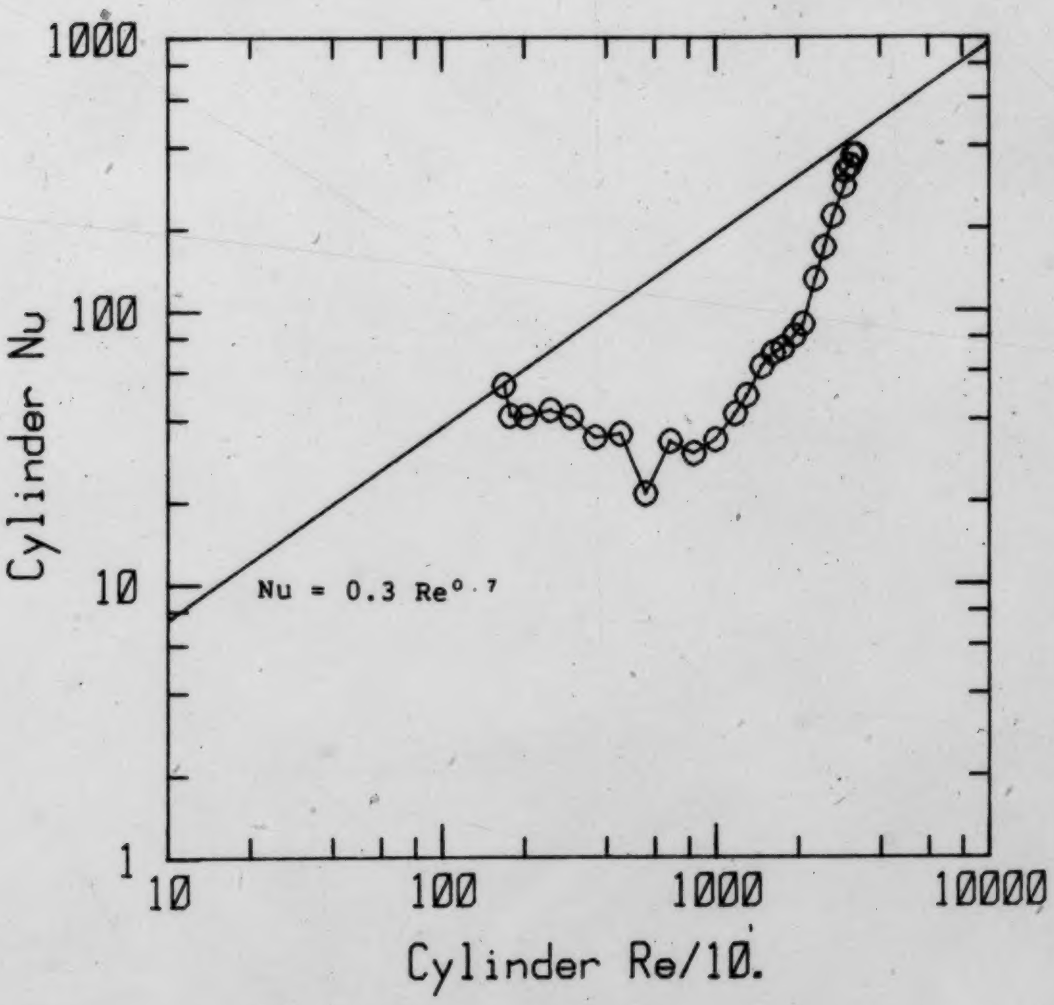

Figure 2.16 Average Cylinder Nusselt Number for Heating of Air (charge) during Compression Stroke @ T = +27°C (assuming t.c. junction is a cylinder)

of the curves shown for tests conducted at -33°C and -26.5°C are very representative of the results obtained for most tests.

Since the charge measuring thermocouples were located in the pre-chamber, and their results assumed to describe characteristics of the charge throughout the entire cylinder, it seems reasonable to expect the Nu_{cyl} and Re_{cyl} results derived to more closely match the expected at the beginning and end of the compression stroke. This is because at these two point in the process, the measured temperatures would be more representative of the charge as a whole than during the intermediary points. At the closing of the intake valve a uniform temperature distribution should exist throughout the cylinder, i.e., $T_{air} \cong T_{wall}$ as only the induction work was added to the charge up to this point in time. Similarily at TDC, because the t.c.s would be more centrally located in the charge than at any other time in the process, their resulting temperature, T_{air}, should be fairly representative of the overall charge. For most tests this was found to be the case.

A listing of the computer program used in the heat transfer analysis, is found in Appendix C.

3. HIGH PRESSURE CELL

3.1 Cell Design

3.1.1 Design Criteria

In order to successfully match spark plugs and circuitry to the engine it was necessary to have the capability for testing the effect of ambient charge density on breakdown voltage requirement. To acomplish this a combustion cell was designed and built.

The design criteria set down for the cell were:

1. the ability to withstand an internal pressure of 1 MPa to 3 MPa,
2. to permit installation of standard 18mm spark plugs for breakdown voltage and combustion testing,
3. to be integrated into an existing Schlieren set up,
4. to incorporate maximum diameter Schlieren quality windows on both ends for producing a large photographic image,
5. to accept a pre-mixed gas/air stream for combustion studies and a port to exhaust the wastes,
6. to have quick assembly capacity,
7. to have minimum cost.

3.1.2 Cell Performance

The cell design interior dimensions were 8.0 cm diameter, 10.2 cm long with the window glass blanks being 15.2 cm diameter and 2.44 cm thick on each end, this is shown in Figure 3.1. The recommended working pressure is 2 MPa, although higher pressures can be sustained for short durations. The maximum initial charge density should be less than seven times the atmospheric density. This assumes that combustion of a stoichiometric mixture of methane and air, $\Phi=1.0$, initially pressurized to 700 KPa, does not cause the peak pressure to be more than 2.8 MPa and to be held at that value for more than a few seconds. Appendix D discusses this more fully.

3.1.3 Cell Features

The cell body was machined out of type 304 stainless steel for strength and corrosion resistance reasons. The wall thickness of the cell was nominally chosen to be 1 cm This was done to allow the firing end of a standard 18 mm spark plug, with a short reach, to slightly project into the cell. Here it was thought that having the plug end visible in the Schlieren photographs would be a good viewing aid for doing subsequent analysis. The cell body was then mounted onto an aluminum cradle, which was fastened to a table fixed to the ground. This sort of care was required to maintain the cell's alignment in the Schlieren system in the event it was accidentally jarred. Aluminum was used for the glass

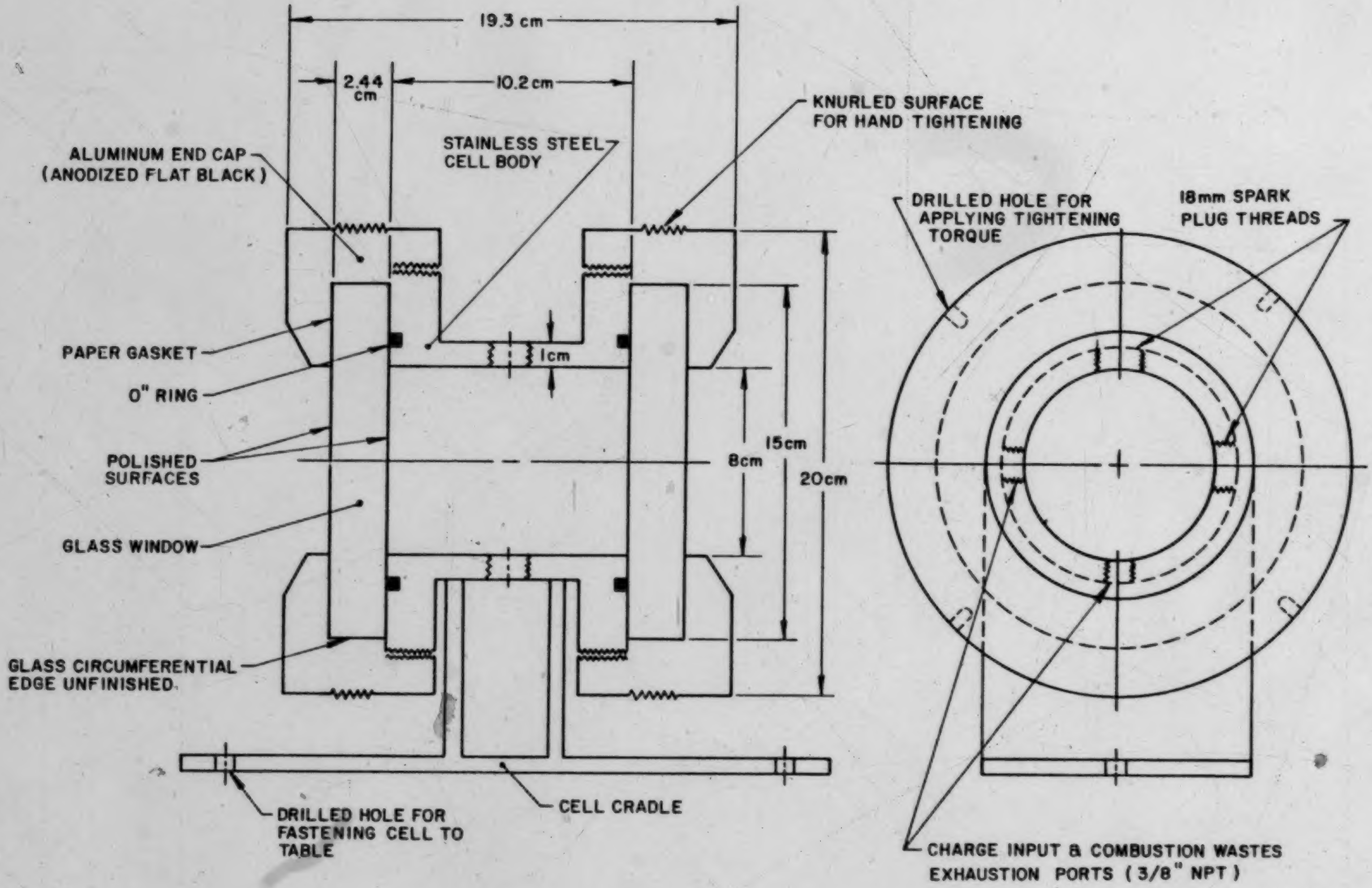
19.3 cm
2.44 cm
10.2 cm
STAINLESS STEEL CELL BODY
KNURLED SURFACE FOR HAND TIGHTENING
ALUMINUM END CAP (ANODIZED FLAT BLACK)
PAPER GASKET
0" RING
1cm
POLISHED SURFACES
8cm
15cm
20cm
GLASS WINDOW
GLASS CIRCUMFERENTIAL EDGE UNFINISHED
DRILLED HOLE FOR FASTENING CELL TO TABLE
CELL CRADLE
DRILLED HOLE FOR APPLYING TIGHTENING TORQUE
18mm SPARK PLUG THREADS
CHARGE INPUT & COMBUSTION WASTES EXHAUSTION PORTS (3/8" NPT)

Figure 3.1 High Pressure Cell

retaining end caps because of its moderate cost as well as being dissimilar to the cell body. This is often used to prevent binding, when one side of the mating threads is made of stainless steel. The caps were then anodized flat black to reduce light reflection off its exterior surfaces.

The thread on clamping technique was chosen for two reasons:

1. to reduce the time required for cleaning combustion products off glass and cell interior surfaces, that would distort the Schlieren images,

2. to provide a consistent method of applying clamping torque in order to reduce the likelihood of local stress concentrations. Glass windows retained with bolted connectors require special care because of this.

An "O" ring was located between the glass and the cell to seal in the cell's gases. On the other side of the glass a 0.3 mm thick paper gasket helped distribute the clamping force from the end caps uniformly over the glass and to minimize scratching of the clamped surface of the glass..

There were four access ports to the cell, not including the glass ends. Of these two were 18mm spark plug threads cut into the side of the cell while the two other ports designated for charge input and for combustion products exhaustion, were drilled and tapped for 1/4" N.P.T.

3.1.4 Pressure-Deflection Testing

Of the entire glass blank surface area only 28% is subjected to direct internal cell pressure, the remaining 72% is used for supporting this pressurized part. Each end cap, used to clamp the glass blanks onto the cell was custom machined to a specific blank. This resulting tight fit, typically less than 0.025 mm along the blank's diameter, coupled with the large amount of supporting surface area should have provided a securely clamped situation.

Pressure-deflection tests were done on the newly machined cell. Grashof's formulas for the maximum deflection in circular plates, obtained by the theory of flexure for ideal, elastic materials [27], was used to determine the expected behaviour for both the simply supported edge (25) and the fixed edge (26) cases with uniform load.

EDGE SIMPLY SUPPORTED:

$$\delta max = 3/16\ (1-\mu)\ (5+\mu)\ \omega r^4/Et^3 \tag{25}$$

EDGE FIXED:

$$\delta max = 3/16\ (1-\mu^2)\ \omega r^4/Et^3 \tag{26}$$

where:

E = Young's modulus for glass, $69(10)^3$ MPa

μ = Poisson's ratio for glass, 0.21

r = unsupported radius, 4 cm

t = glass thickness, 2.44 cm

ω = uniform internal pressure, MPa

After performing these tests, the results suggested that the glass may not have truely been fixed after all. In this case it appears that there may have been some bulk movement of the entire glass window outward along the cell's longitudinal axis, compressing the paper gasket. The results then are open to many interpretations, depending on the assumptions made regarding the clamping conditions. However, as it was desirable to compare the measured experimental deflections to some theoretical standard, the bulk movement of the glass was assumed to take place and the deflection of the centre of the glass measured relative to the inner clamped edge.

The results plotted in Figure 3.2, show the measured glass deflection closely following the fixed end configuration rather than the simply supported end case. This was important to know, as the type of clamping situation dramatically affects the pressure-deflection behaviour of the glass and the maximum safe working pressure in the cell. A factor of safety of 2 was used to account for the average expected loading time, clamping conditions, mechanical surface treatment of glass and temperature boundary conditions. Details of the cell glass design are found in APPENDIX B.

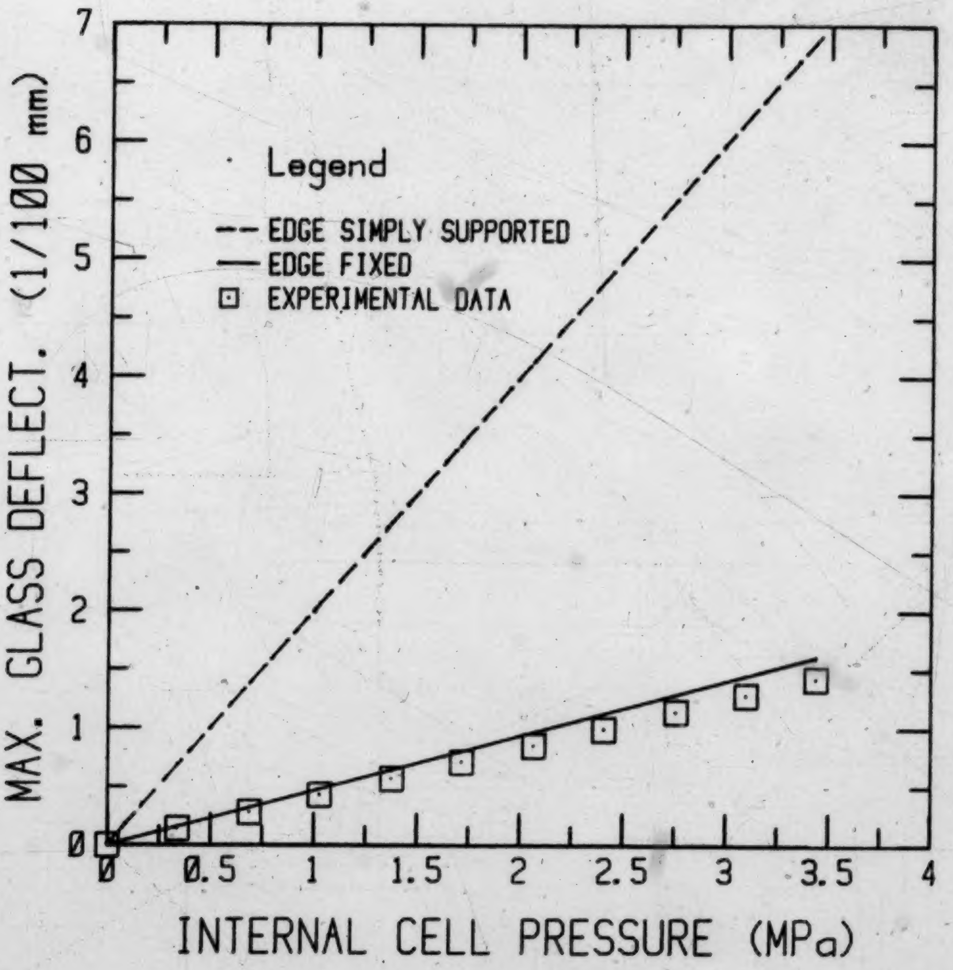

Figure 3.2 Load-Deflection Test of Glass Window

3.2 Cell - Schlieren System

3.2.1 Schlieren Technique

Many methods have been developed for making fluid flows visible. Merzkirch [20] describes many of these. In a gas, local changes in density, especially the abrupt changes occurring across a shock wave, may be made visible because of an accompanying change in refractive index n. Of the three principle techniques utilizing this property, the Schlieren method was used here. In this system, Figure 3.3, light is collected by a lens and focussed onto a pinhole. The emerging light beam is then collimated by concave mirror, CM_1, passed through the gas in the cell, brought to a focus by concave mirror, CM_2, and then projected onto the camera photographic plate. The He-ne laser was used for initial alignment of the system. At the focal plane of CM_2 where an image of the pinhole is formed, a knife edge is introduced to cut off part of the light. If the gas density is uniform within the beam, the illumination on the screen, although reduced by the knife edge is also uniform. If, however, in any part of the gas a density gradient exists in a direction perpendicular to both the light beam and to the knife edge, more or less light is intercepted by the knife edge. Corresponding parts of the image of the test section on the screen are therefore darker or brighter. The change in brightness is proportional to the density gradient.

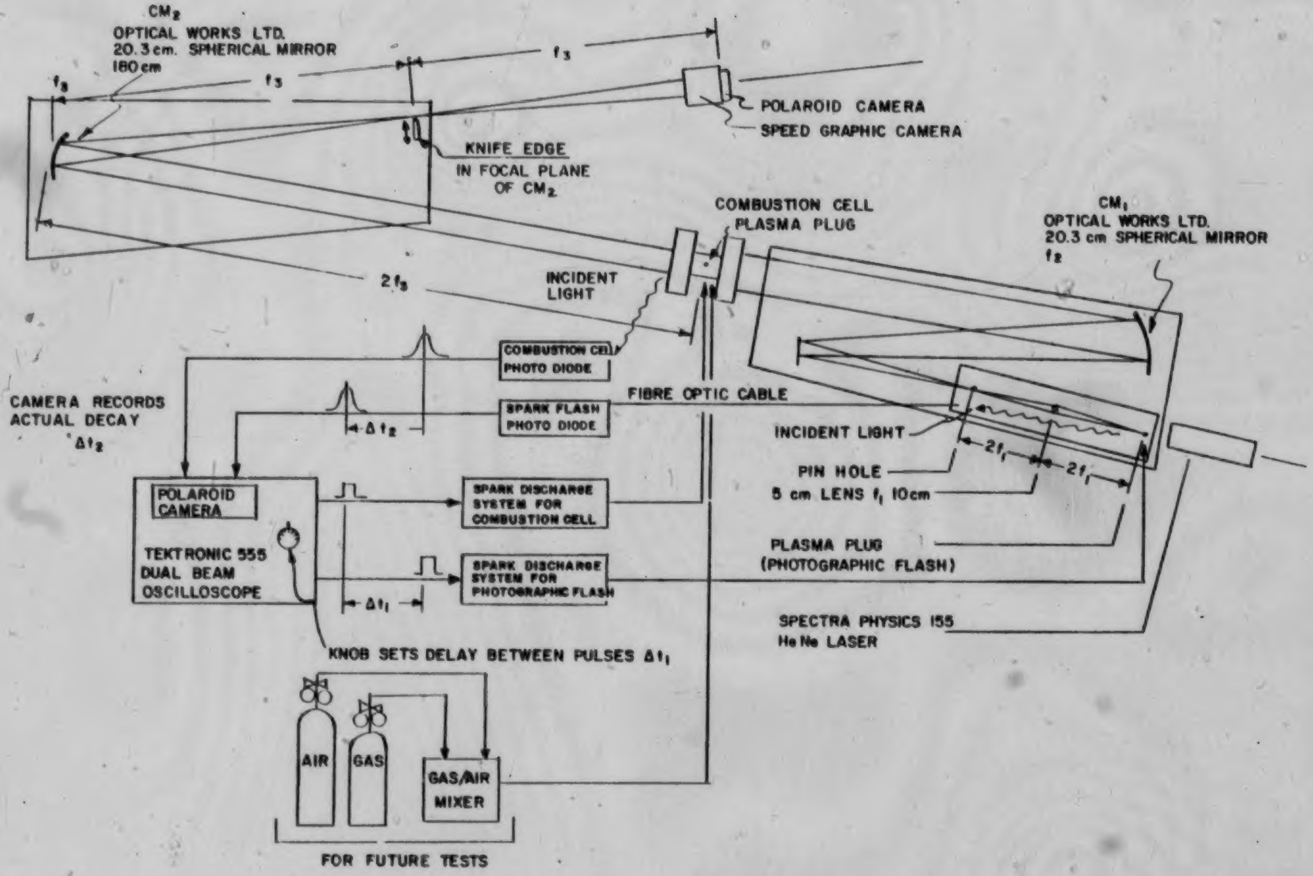

Figure 3.3 Cell-Schlieren System

One of the main purposes for this system was to study spark kernel motion and jet penetration as a function of plug geometry, ambient conditions and combustion cell spark discharge circuitry parameters. Therefore, by ensuring the plume path was oriented in the same direction as the movement of the knife edge, sensitivity to density gradients in this direction was achieved and adequate Schlieren photographs obtained. If radial sensitivity is required, the knife edge can be replaced with a dot.

3.2.2 Cell-Schlieren System Integration

Two spark plugs were used in this system, one as a microsecond light source for flash photography and one for producing the observable event in the cell. There were also two corresponding spark discharge systems. Schlieren photographs were taken of a modified champion plasma plug discharging into air at atmospheric pressure. These photographs were taken at different time delays after the initiation of the event, i.e. pulsing the cell spark plug. Ideally it would have been nice to follow the development of each event in time with a high-speed cine-camera, however, the existing equipment was capable of taking only single photographs of high speed events. Hence for each photograph with a particular time delay, a corresponding discharge of the cell spark plug was required. Nevertheless, the process was so consistent that this approach was very acceptable for the type of results required. It should be recalled that the initial ambient conditions in the cell can easily be altered. Air and/or gas in various combinations and at different initial pressures can be obtained using an available gas/air mixer.

3.2.3 Operation of the System

The procedure used to obtain instantaneous flash photographs of events in the cell are as follows.

A time delay between the event and the flash occurences was dialed into the Tektronics 555 Dual-Beam oscilloscope which then sent the two pulses, correspondingly spaced in time, to the two spark discharge systems. Although the same circuit design principles were used for both spark discharge systems the requirements and capabilities of each were quite different. As a result the components and subsequent operational characteristics of these discharge systems were also different. This is shown as follows. Using the oscilloscope to repetitively trigger both discharges with a fixed time delay between the pulses results in time delay measurements that are neither the dialed in amount nor consistent. Therefore, in order to take this into account, photodiodes were used in the measuring of the delays, and the scope/camera setup used to record them.

Recording the timing of the cell spark plug firing was accomplished simply by placing the corresponding photodiode close to the spark source. However, the amount of electromagnetic radiation from the photographic flash plug required moving the photodiode several feet from the flash. Since the flash source was enclosed in a box and its photodiode located outside, a fibre-optic cable was used to transport the light signal.

The flash and event spark discharge durations were approximately 30μs and 20μs respectively. Here the shorter duration discharge was used for the event and not for the flash where it would have added approximately a 30% improvement in shock wave resolution. This was done because the high and low voltage settings for the event discharge were adjustable, which is important for testing purposes, whereas those of the flash were fixed.

About 1.45 J of stored energy was discharged for each event spark plug firing whereas around 14 J was required for the flash.

3.2.4 Photographic Results

The photographs shown in Figures 3.4 and 3.5 are representative of the sort of quality and resolution produced by this system. The 115μs delay print, Figure 3.4, clearly shows the shock wave propagating from the event spark plug on the right side. The spark plug used in these photographs is a plasma jet plug with an orifice fixed to its end. The plasma plug's internal cavity volume was 30.2 mm^3 while the orifice was 1.4 mm in diameter. Note that as previously mentioned the system is sensitive to density gradients in the direction of the plume path, i.e., from

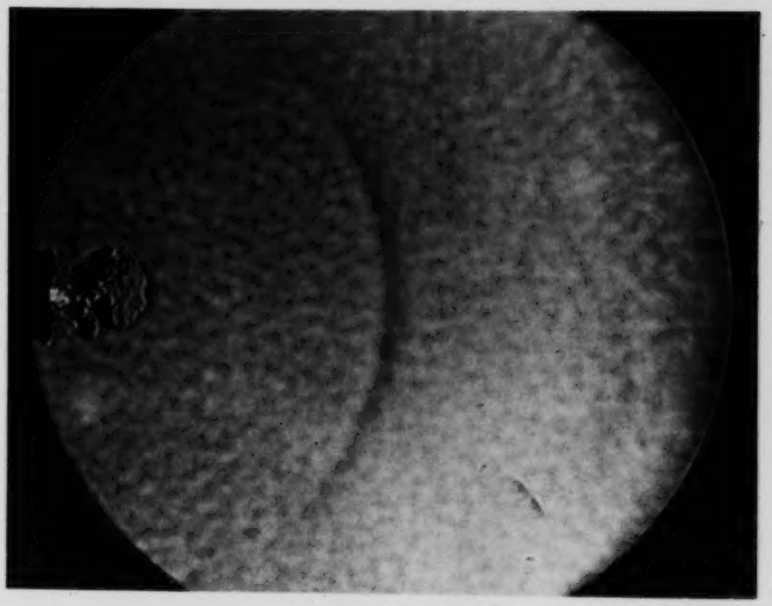

Figure 3.4 Plume Penetration at Ambient Pressure after 115 μs

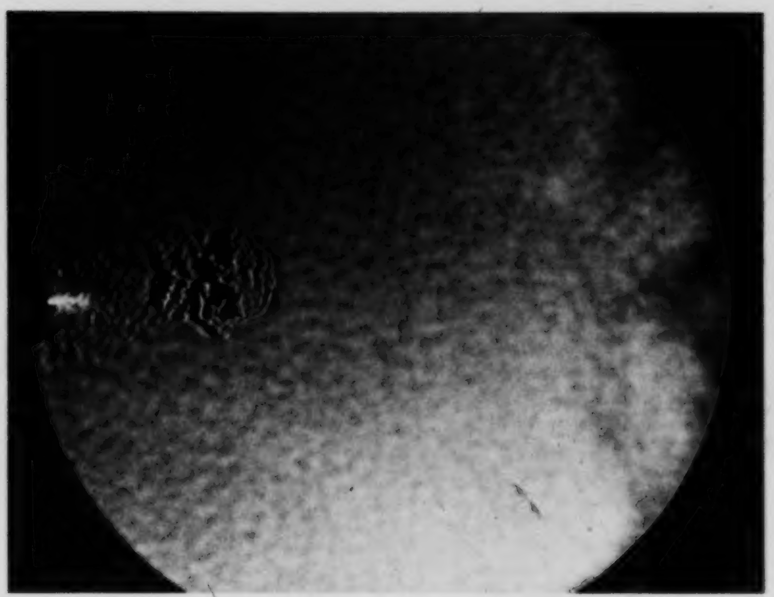

Figure 3.5 Plume Penetration at Ambient Pressure after 1065 μs

side to side. If further improvement in the system is desirable, for example, if resolving the shock wave becomes important, the flash will have to be shortened by a factor of 10 to about 3μs in duration.

The second photograph, Figure 3.5, shows a much more developed plume, taken 1065μs after the discharge of the event plasma plug. Here the advancing plume has penetrated one third the distance across the cell after only 1 ms. This is the main feature of plasma jet igniters, the ability to propel a kernel of highly ionized gases into a dense medium. This will be discussed in more detail in Chapter 5.

These figures illustrate the usefulness of the cell-Schlieren as designed. The cell's main use in this study however was for measuring voltage breakdown characteristics of various spark plug configurations for use in the Mercedes-Benz Diesel engine.

4. SPARK PLUG SELECTION AND CIRCUIT DESIGN

4.1 Influence of Charge Density and Plug Geometry on Breakdown Voltage

A thorough study of the voltage requirements for increasing ambient air density was necessary in order to select an appropriate plug type and geometry for discharging in the high pressures in the Diesel engine, during cold cranking. Measurements on the engine during these cranking conditions showed that, as the ambient temperature decreased, the cylinder density at the peak of the compression stroke increased, meaning that it would be more difficult to discharge a spark across the gap as the ambient temperature was lowered. The cylinder density measured during cranking at -33°C is shown in Figure 4.1.

There are two basic types of spark plugs for use in engines, the air gap and the surface gap types. Figure 4.2 shows cross-sections of both types of spark plugs. With the air gap type, the spark jumps from the centre metal electrode through the compressed charge to the ground electrode, while with the surface gap type the spark runs along the ceramic surface from the central electrode to the ground electrode. Two types of surface gap plugs are shown in Figure 4.2, the first, a so-called plasma jet plug has a recessed cavity through which the spark passes to ground, while with the second, the standard surface gap plug, the spark travels radially outwards. By using high energy

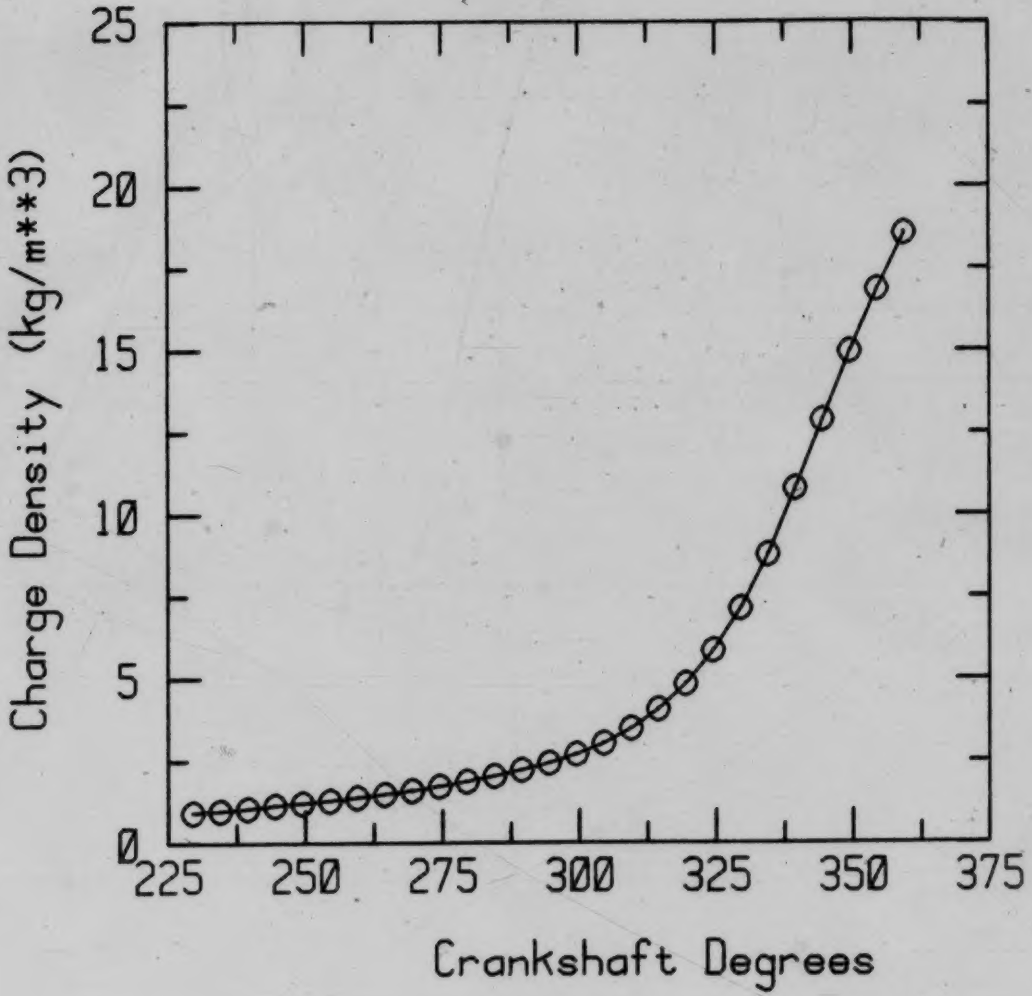

Figure 4.1 Charge Density during Compression Stroke @ -33°C

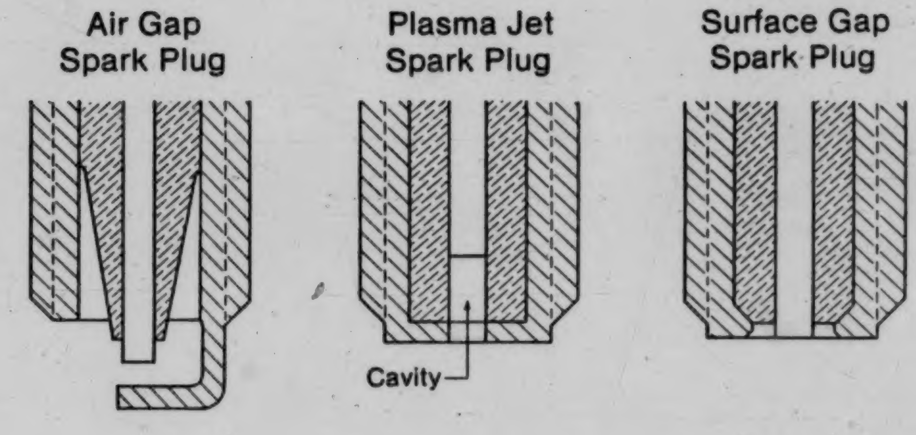

Figure 4.2 Cross-Sections of Spark Plug Types

discharges with plasma jet spark plugs, the gas in the cavity can be rapidly raised to high temperatures and thus create a significant over pressure which jets the ionized gases away from the plug as was illustrated in Figure 3.5. This type of action allows one to move the effective ignition source away from the spark plug. The surface gap spark plugs also exhibit some motion of the spark away from the surface during discharge but to a much lesser extent than the plasma jet plug.

For testing the breakdown characteristics of different plug geometries, the high pressure cell described in Chapter 3 was employed.

Each of the three types of spark plugs were tested for their voltage breakdown characteristics as the ambient gas density was increased over the range from 0 to 40 kg/m^3. Figure 4.3 shows the results of these tests for typical spark plugs. The air gap type show the steepest rise in the voltage required for breakdown with increasing gas density while the recessed cavity plasma jet plugs show a levelling off of the voltage requirement above gas densities of 10 kg/m^3. The breakdown voltage characteristics of the air gap plugs follow Paschen's empirical law [29]. That is, the breakdown potential of a gas is a function of the gas density and the electrode spacing only. Because the geometry of the surface gap plug differs from the air gap plug and the spark travels along the ceramic surface, Paschen's law does not apply to surface gap plugs. The standard surface

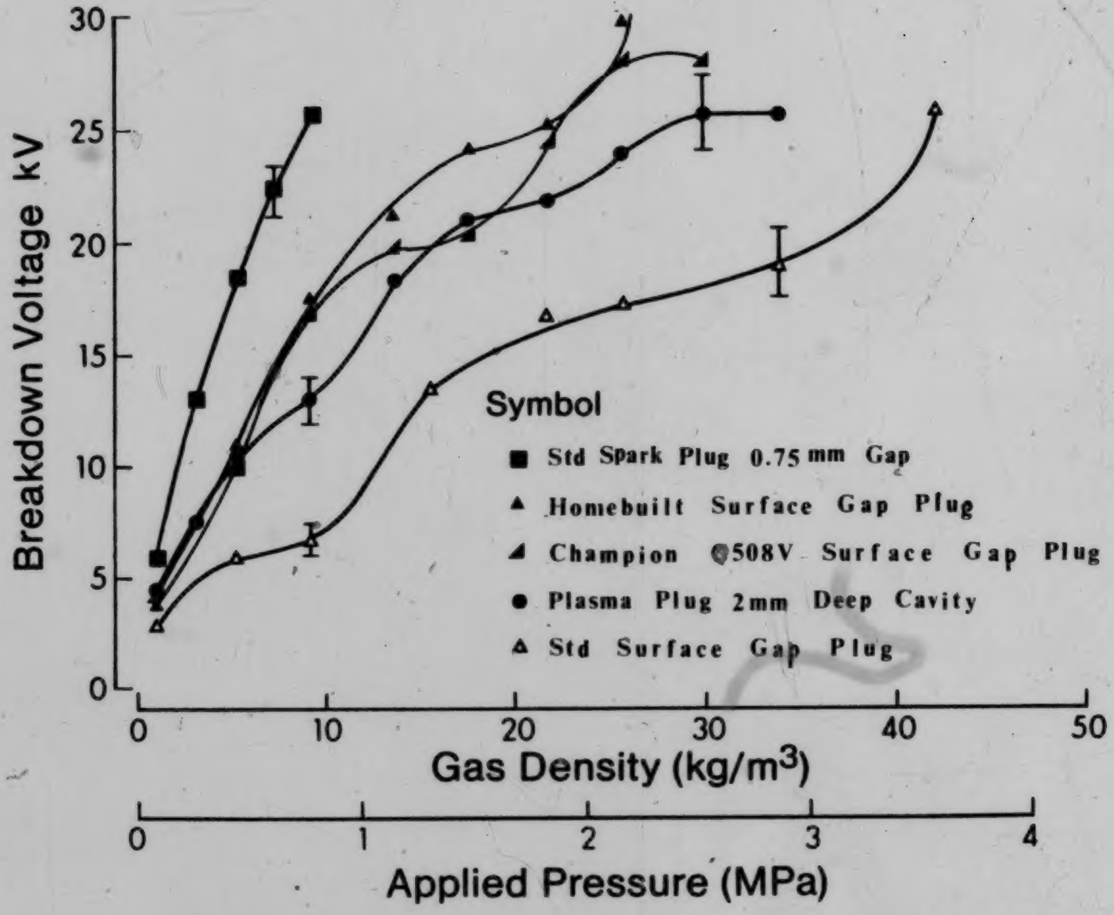

Figure 4.3 Spark Plug Breakdown Voltage Dependence on Ambient Air Density

gap plug exhibited the lowest breakdown voltage for a given applied gas density.

If the compression process in the engine cylinder is adiabatic, the maximum gas density in the cylinder is equal to the compression ratio multiplied by the intake gas density. For this Diesel engine and the ambient conditions used in this study, the cylinder air densities at the end of the compression stroke were estimated to be in the range of 20 to 30 kg/m^3. In practice, measurements of in-cylinder temperature and pressure showed that the peak cylinder densities were about 20% less than the theoretical maximum. This means that in order to have reasonable breakdown voltage requirements, only the plasma jet and the standard surface gap plugs would be suitable for use in a Diesel engine. Both types of plugs were utilized, but, because standard surface gap plugs have the lowest breakdown voltage and are very resistant to fouling when short duration sparks are used, they were used for most of the starting tests. Radial tracking of the spark along the annular region between the centre and ground electrodes tends to blow off any soot that collects during engine operation. A very desirable feature for Diesel engine application.

4.2 Problems with Pre-Chamber Access - Special Designs

At the start of this four cylinder engine study, it was decided to avoid any modifications to the engine. This was done partly for the future benefit of having the capacity to easily retrofit other engines, possibly in the field with a system that requires little modification and partly to simplify the experimental setup and avoid ruining the cylinder head.

With this very restrictive design criteria of avoiding any modification, the only option left for adapting spark plugs to the engine involved using the existing glow plugs installation hole. Access to the prechamber through this port was so limited, in terms of the hole size and shape, and distance from the head exterior to the pre-chamber, that no commercially available surface gap plug was adequate. As a result of this, surface gap plugs were designed and built using industrially available material. This approach was ultimately discarded after much futile effort, as the resulting manufacturing problems and poor performance characteristics created more problems than it solved.

After consultation with the Champion Spark Plug Company [6], an experimental surface gap plug was suggested for these particular requirements. Appendix C shows both the homebuilt plug and the unmodified Champion G508V. Because of the small diameter of the G508V spark plug, only minor modifications were required to allow installation in the engine. Here, the main body of the plug was machined just enough to allow it to slip down the existing glow plug location, (18 mm spark plug threads) a retaining nut was then threaded in after the plug. Figure 4.3 also shows the breakdown voltage requirement as a function of ambient density, for the homebuilt as well as the Champion G508V plugs. Here it is seen that both the homebuilt and the G508V surface gap plugs performed intermediate to the air gap plug and the plasma plug. However, the G508V plug required less voltage than the homebuilt plugs at a given charge density and more importantly, the G508V flattens out at about 27 kg/m^2 whereas the homebuilt plug after a short levelling off period continued to exhibit air gap characteristics. This figure does not present all the factors which are important in overall performance, though. As far as operating reliability, breakdown consistency, centre electrode erosion rate, ruggedness of construction materials etc. was concerned, the G508V was far superior. It was used in the engine for all of the results reported here.

4.3 Ignition System

4.3.1 Introduction

The ignition system for the four cylinder Diesel engine basically consists of four single cylinder ignition units. Each single unit is a typical system previously described in Chapter 1 and capable of discharging up to several joules of energy to each spark plug. A schematic diagram is shown in Figure 4.4. Individual magnetic pickups are used to synchronize ignition system firing to cam gear rotation.

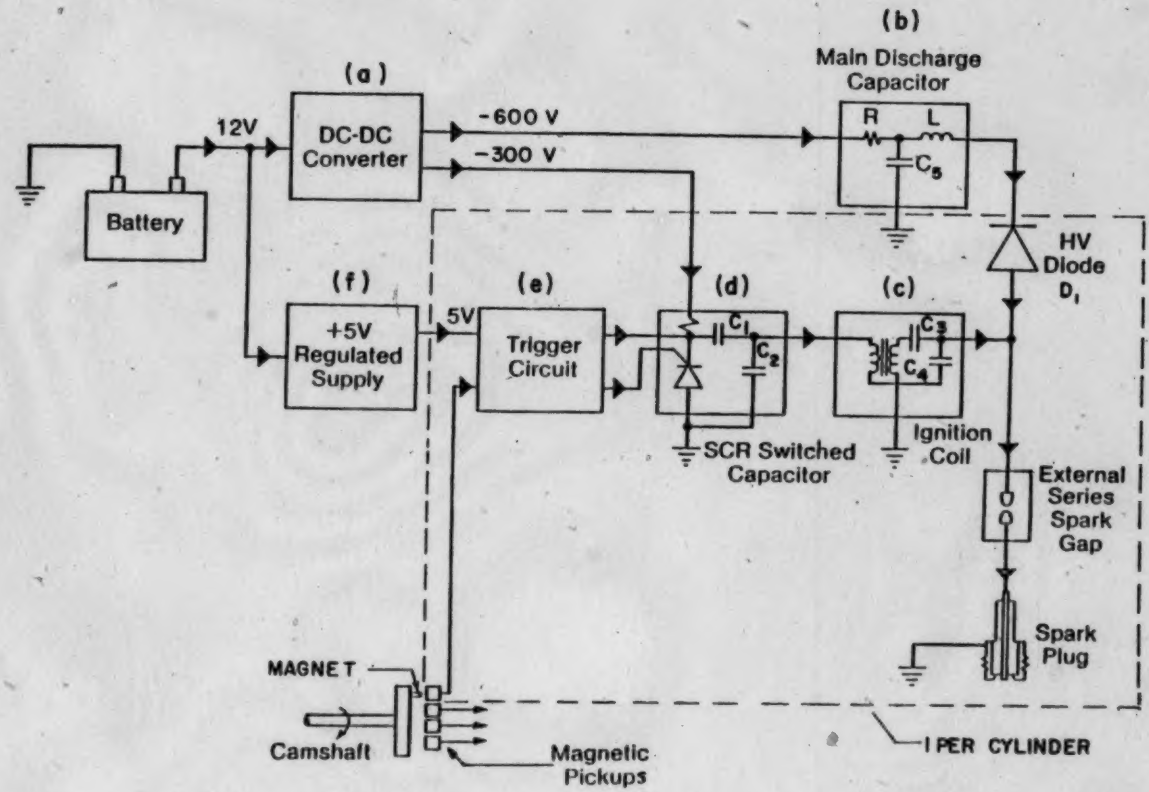

Figure 4.4 Schematic of the Four Cylinder Ignition System Driving External Gaps and Spark Plugs

4.3.2 Power Supplies

Figure 4.4 also shows the three power supplies providing outputs of -600 V dc, -300 V dc and +5 V dc from a 12 volt battery. The -600 V and -300 V supplies are typical DC-DC inverters using toroidal Hammond transformers, while the +5 V output was obtained from an IC regulator. The -600 V dc and -300 V dc powers the high voltage (low energy) and the low voltage (high energy) circuits whereas the +5 V supply powers the electronics of the ignition units. This is shown in more detail in Appendix E, Figure E.1.

4.3.3 Trigger Circuits

Four identical trigger circuits were used. Circuit triggering was obtained in the following way. When a signal from a magnetic pickup (Figure 4.5) reaches a certain level a square pulse is produced that turns on an optically isolated SCR that in turn switches the main SCR on. Appendix E, Figure E.2 shows a schematic of this. Clipping of large input signals, pulse stretching to eliminate the possibility of multiple trigger signals (if the input signal is noisy or full of spikes), and two optical isolating stages were incorporated to reduce the chances of signals coming back from the output of the trigger circuit.

4.3.4 SCR Switched Capacitor and Ignition Coil

When the main SCR is switched on charge stored in C_1, shown in Figure 4.4, is discharged into the primary of a

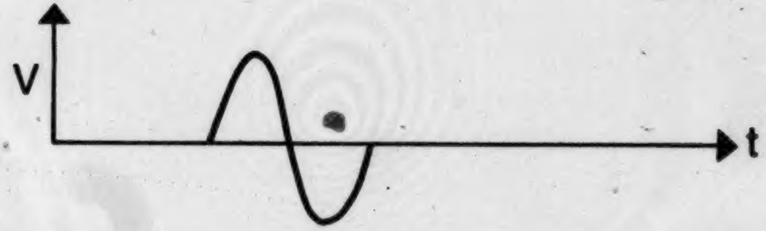

Figure 4.5 Typical Ignition Circuit Input Signal

standard automotive ignition coil, generating a high voltage discharge. C_2 filters out spikes coming back from the coil. An important modification to the high voltage side of the simple circuit, Figure 1.1, involves using the capacitor C_4 in the locations shown in Figure 4.4. C_4 serves as a temporary storage of energy from the coil as the voltage builds up before being dumped in the plug gap when breakdown occurs. Using C_4 in this way greatly increases the energy delivered from the coil to the spark plug.

If C_4 is typically 0.0002μF and charged to 30 kv then it delivers about 90 mJ to the spark plug. A standard automotive ignition system delivers around 50 mJ spark plug.

4.3.5 Main Discharge Capacitor

When the high voltage (low energy) discharge from the coil occurs, the main discharge capacitor, C_5, charged to -600 V also discharges, producing a high current arc. Both this discharge and that from the voltage circuit appear as a single spark at the plug because D_1, a special high voltage, high current diode, and C_3, a blocking capacitor, are used to protect the respective circuits from discharges in the wrong direction. For these starting tests a value of 8μF was used for the main discharge capacitor C_5 at 600 V, which produced a discharge energy of around 1.45 J/plug. Therefore the total spark discharge energy per plug, adding in the contribution from the high voltage (low energy) discharge of 90 mJ, was a little over 1.5 J.

The present multi-cylinder circuit design consumes about 50 watts per cylinder. This is typical of factory installed glow plugs used on similar engines.

5. STARTING EXPERIMENTS

5.1 Low Temperature Chamber

Figure 5.1 is a schematic of the Mercedes-Benz engine installed in a low temperature chamber (interior volume 20 m^3) capable of maintaining temperatures down to -60° celsius, ±1° celsius. The controls for starting the engine were set up outside the low temperature chamber, with an umbilical cord used to carry signals back and forth between the control panel, the engine and the dual channel chart recorder, Hewlett-Parkard Model #17505A.

5.2 Engine Modifications

There were two modifications to the Mercedes-Benz engine. The first was fitting the timing mechanism to the engine. This was accomplished by attaching a circular flat plate with a magnet pressed into it on to the end of the camshaft. Four magnetic pickups, set at 90° apart, were mounted in the camshaft housing parallel to but separated from the rotating plate and magnet by about 0.05 mm. This mechanism was designed in such a way that the spark timing could be varied ±30° of crankshaft rotation on either side of TDC.

The second modification involved installing a Validyne pressure transducer (0 → 21 MPa FS) in the high pressure fuel delivery line to the injector of cylinder #1. This was done at the start of the study when there were questions of

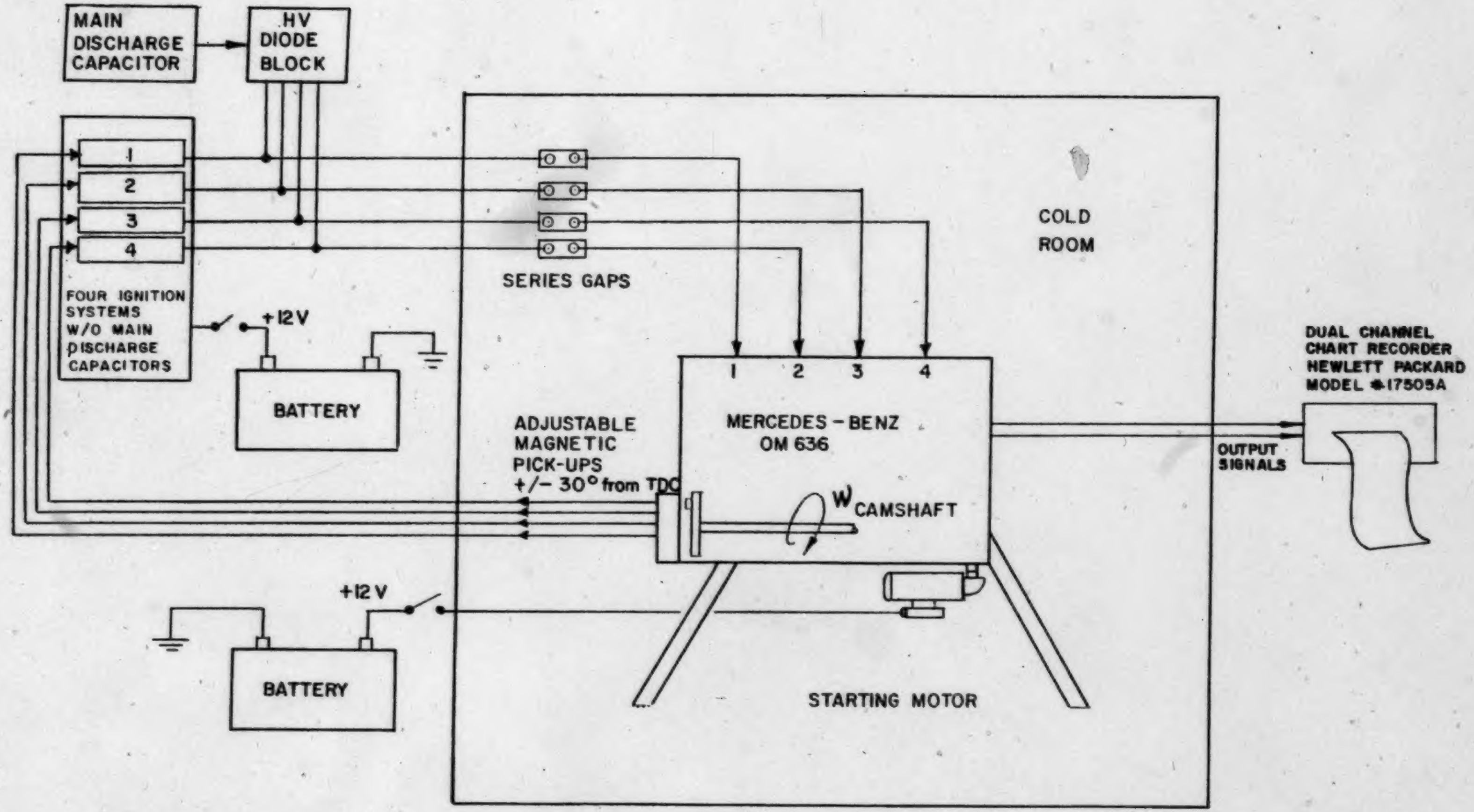
MAIN DISCHARGE CAPACITOR
HV DIODE BLOCK
1
2
3
4
FOUR IGNITION SYSTEMS W/O MAIN DISCHARGE CAPACITORS
+12V
BATTERY
SERIES GAPS
COLD ROOM
DUAL CHANNEL CHART RECORDER HEWLETT PACKARD MODEL #17505A
1
2
3
4
MERCEDES - BENZ OM 636
ADJUSTABLE MAGNETIC PICK-UPS +/- 30° from TDC
$W_{CAMSHAFT}$
OUTPUT SIGNALS
+12 V
BATTERY
STARTING MOTOR

Figure 5.1 Schematic of High Energy Ignition Adapted to Engine in Cold Room

whether or not the fuel injection pump was operating properly, when did the fuel spray begin and for how long?

The spark plugs were installed in the glow plug locations, as shown in Figure 5.2 which is a cross section of the engine cylinder-prechamber. Here the axis of the spark plug intersects the fuel injector axis at an angle of about 50°. This means that the surface where the spark occurs on the surface gap plug is not directly exposed to the fuel spray. It is felt that not having control over this one parameter, the orientation of the spark plug with respect to the fuel spray, probably limited the success of the study.

5.3 Power Supplies, Fuel and Lubrication

Two 12 V batteries were used for these starting tests. One was used to power the starting motor and solenoid, while the other was used to energize the fuel solenoid and to run either the glow plugs or spark discharge system, depending on which aid was installed in the engine. Both batteries were kept outside the cold chamber in the +22°C room environment.

Over the course of this three year study the fuel acquired for these starting tests was Artic (AA) Diesel. Because of the time scale involved, the physical specifications changed somewhat from sample to sample. The cloud points and pour points ranged from -45°C to -51°C. These as well as other fuel specifications are listed in

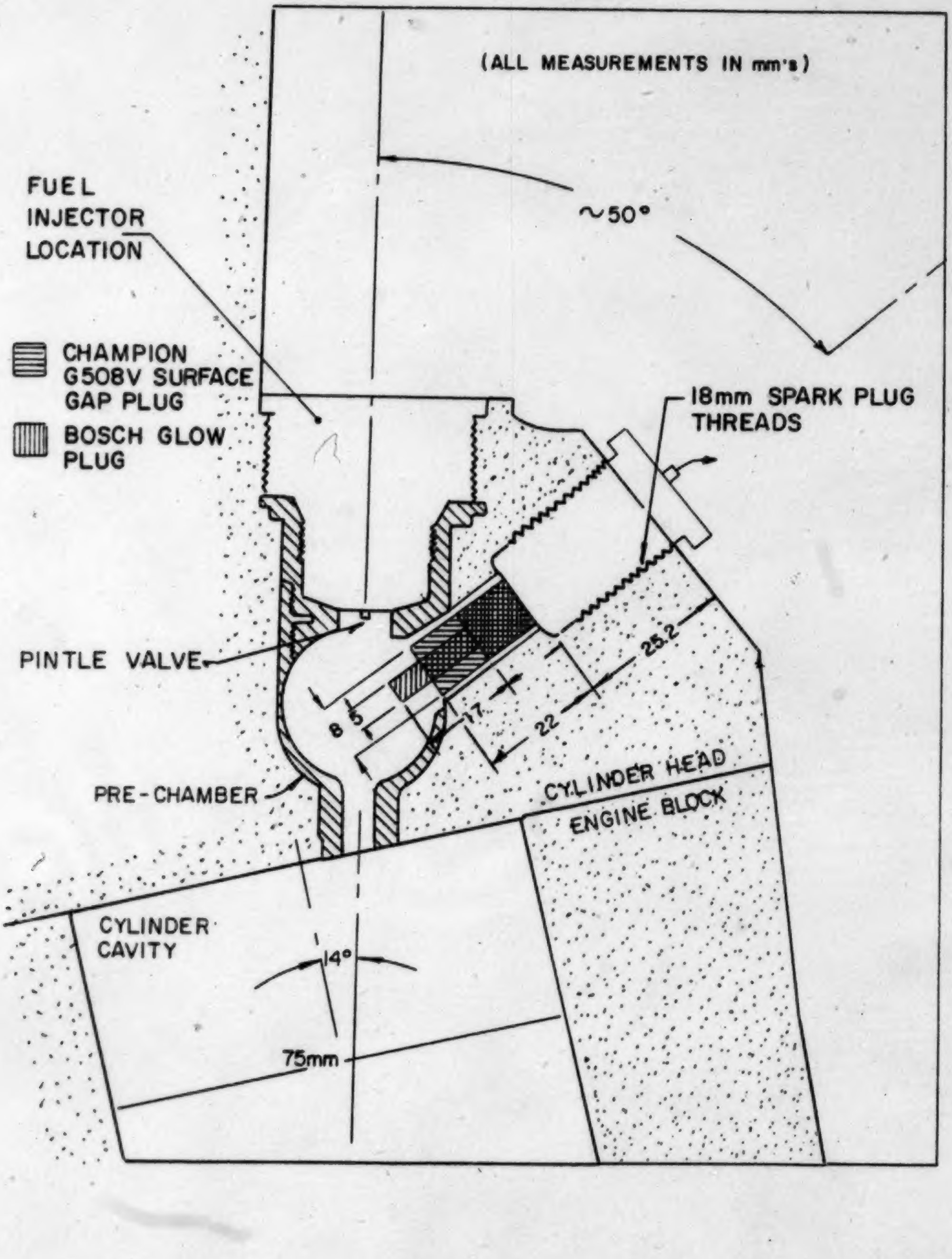

Figure 5.2 Cross Section of Engine Showing Fuel Injector and Starting Aid Location

Appendix D. For all starting tests the fuel was cold soaked with the engine. The crankcase oil used in the engine was Artic OW-30.

As part of a regular preventative maintenance program, once every two weeks or so, the engine was warmed up to room temperature (+22°C) and run for 30 minutes to ensure proper functioning.

5.4 Starting Procedure

The starting procedure followed was simply to crank the engine until it started, or for a maximum of 60 seconds. Extensive cranking tests revealed that the engine responded best with the Champion G508v surface gap plugs when a plug depth of 22 mm, measured from the sealing surface to the firing end, (see Figure 5.2) in combination with a 1/2 throttle setting was used.

In performing these starting tests, a simple definition of a start emerged. It was observed that if and when the engine cyclic speed reached 460 rpm, the starter motor solenoid could be disengaged and the engine would continue to accelerate to the governor speed. This was found to be a reliable, unbiased criteria which was easy to implement. Furthermore, not once did the engine stall after it had attained this mark, either with the factory installed glow plugs or the timed spark discharge. A 60 second pre-heat was used for the glow plug starts, at temperatures above -34°C and 90 seconds below this point.

At each ambient temperature the engine was cold soaked for about 15 hours then a quick timing sweep done with starts every 2 1/2 hours to obtain the general dependency of the starting time on spark timing. Long duration soak periods (15 hours or more) were then used to more accurately define the engine starting time dependence on spark discharge timing. The total amount of stored energy discharged per spark plug was kept around 1.5 J.

5.5 Results

The experiments with the 4-cylinder I.D.I. Mercedes-Benz engine were done to demonstrate the application of the timed spark discharge starting to such an engine and to compare it with the factory glow plug aid under identical conditions.

This engine did not respond to the timed spark discharge aid as well as had been anticipated. Previously, this aid had been adapted to two single cylinder Diesel engines, one a direct injection type, the other an indirect injection model. With these engines starts at the fuel pour point temperature (about -50°C) were obtained with only 3 seconds cranking. Nevertheless, with the 4 cylinder engine, improvements in the starting times were obtained with the timed spark discharge aid over the factory installed in-cylinder glow plugs.

At temperatures down to -20°C almost instantaneous starts resulted with use of either aid. This is shown in

Figure 5.3. However, below this point the engine took around 2 1/2 to 3 times longer to start with the Bosch 955 glow plugs than with the timed spark discharge aid. A certain amount of variability existed in the starting test results. One notable example of this involved a 6 1/2 s start after the engine was cold soaked at -35°C for 50 hours. This represented a substantial improvement over the previous timed spark discharge starts under identical conditions.

Figure 5.4 shows the effect of ambient temperature on the cranking time as the spark timing is varied. This shows that it takes longer to start the engine as the ambient temperature decreases. However, one can also see that the timing region where reasonable starts are obtainable, i.e. cranking time less than 20 s, shrinks as well as becomes more retarded in time, as the temperature drops. This can be seen by noting that for starts at -20°C (with the engine soaked at this temperature for 10 hours on average) this region spanned 27° from TDC to 27°ATDC, while at -35°C (for 15 hours or more) it was 4° in duration from 13°ATDC to 16°ATDC. From this it is easy to see how little chance there is of any starts below -35°C under the present experimental set-up.

Figure 5.5 shows a start representative of the engine behaviour when aided by glow plugs, after being at -34°C for 18 hours. For this test a 90 s pre-heat period prior to the initation of cranking, and a 67 s post-heat period, also measured from the start of cranking, were used. In the

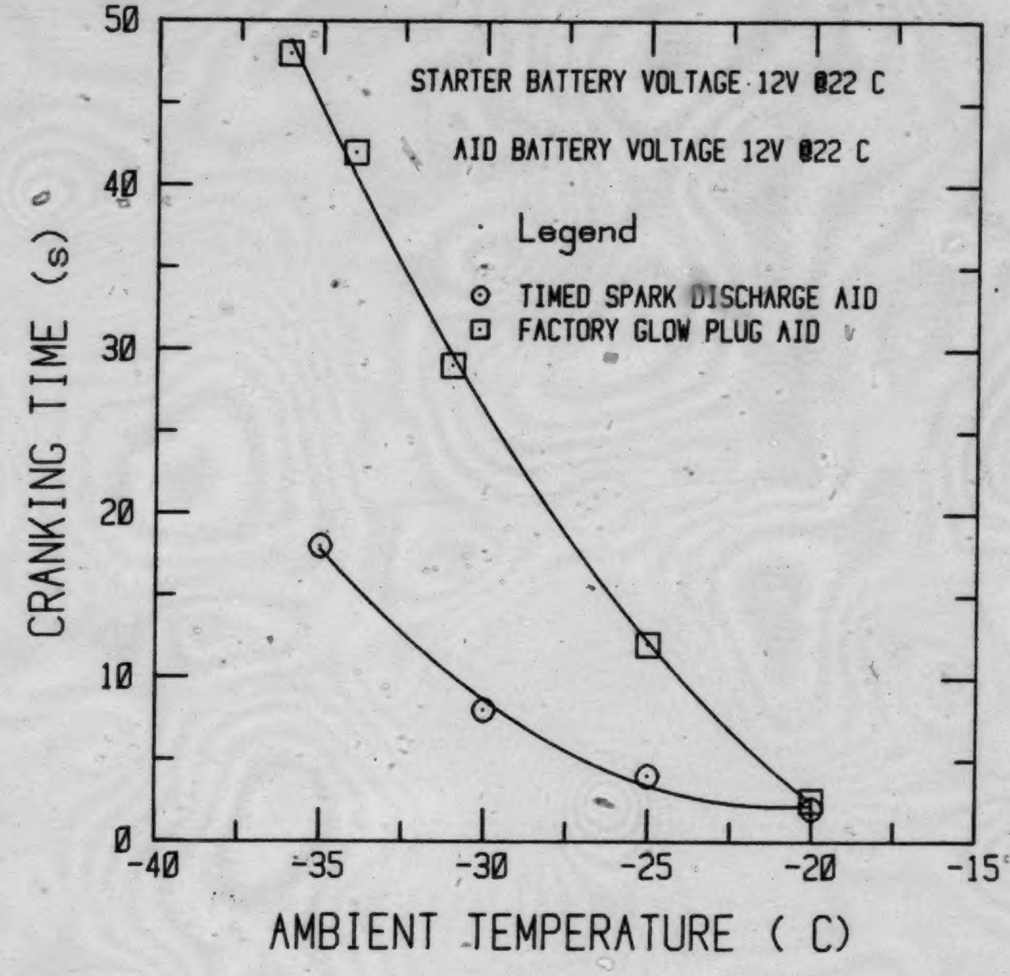

Figure 5.3 Cranking Times for Engine with Starting Aids

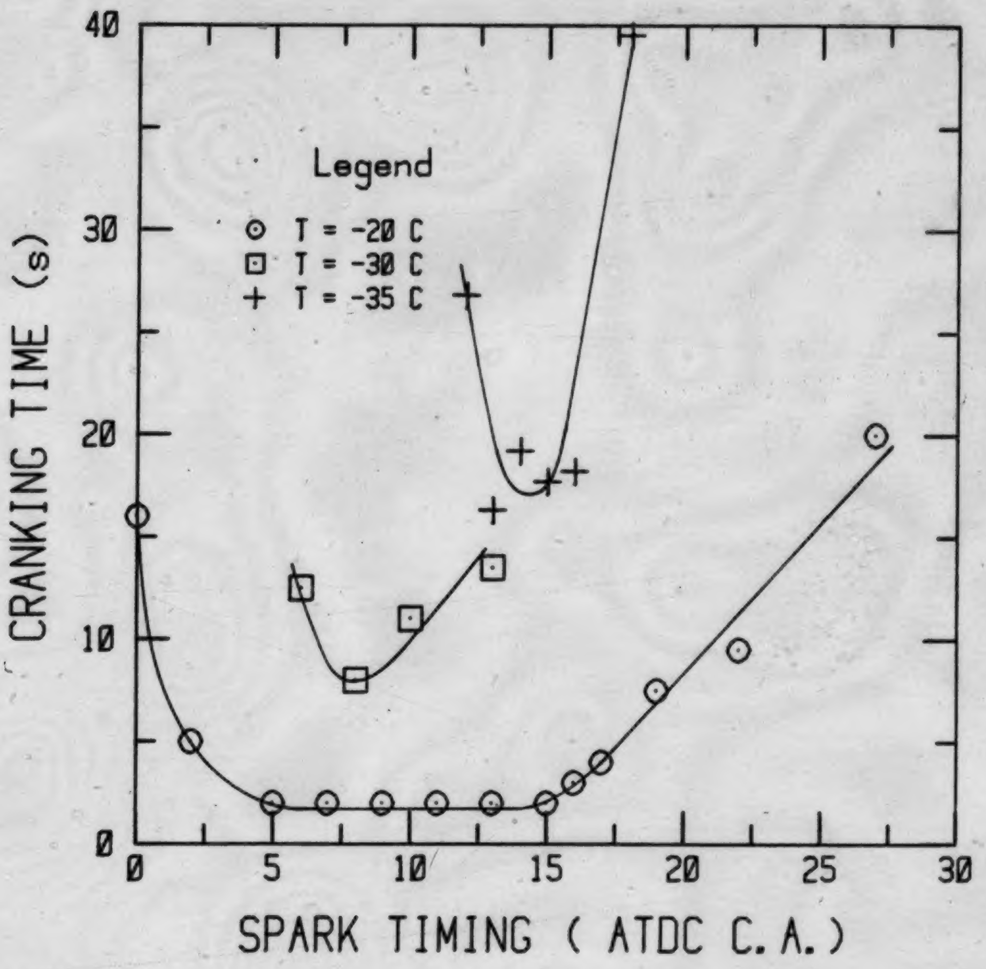

Figure 5.4 Effect of Ambient Temperature on Spark Timing Window

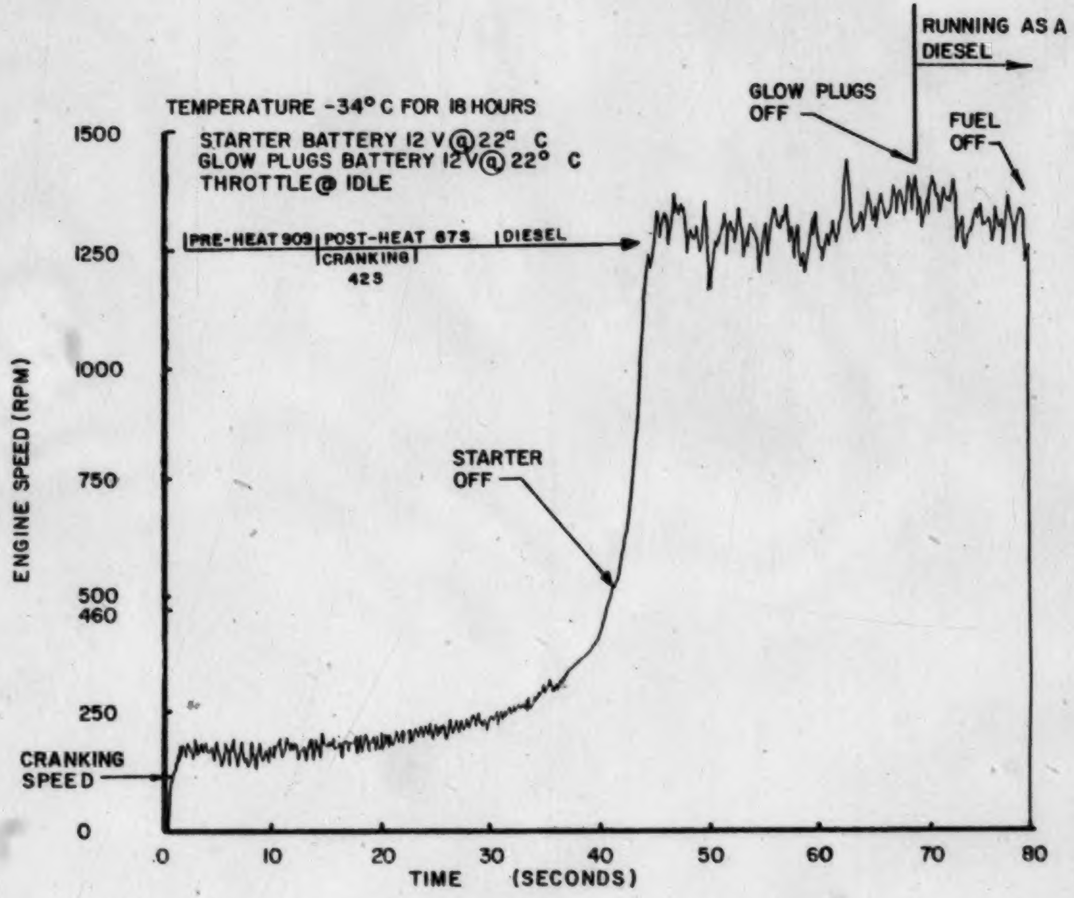

Figure 5.5 Mercedes-Benz Starting - Running Characteristics with Factory Installed Glow Plug Aid

period of cranking, which lasted for 42 seconds, the engine speed quickly rose to around 150 rpm, whereas the engine cranking speed for this temperature without any aid is close to 100 rpm (see Figure 5.6). The engine cyclic speed then increased slowly to about 350 rpm then quickly accelerated across the 460 rpm mark, where the starter motor is disengaged, to the idling speed of 1250 rpm.

A comparable starting - running trace with the spark discharge aid fitted to the engine is displayed in Figure 5.7. It is seen from this that the engine speed for the first few seconds was very close to that measured without any aid, 100 rpm. Quick acceleration to around 300 rpm followed by a matching decelleration to slightly above the 100 rpm mark. After a few seconds, the engine speed began to increase, sometimes quite rapidly, to the running speed of 1500 rpm. The starter motor solenoid was disengaged when the engine speed was close to 650 rpm. Two subsequent attempts were made to turn off the spark discharge aid at the 42 s and 55 s points in the start. These were both unsuccessful as the engine was not warmed up sufficiently to run unaided. At about the 70 s mark into the test the spark discharge aid was finally turned off and the engine left to run as a Diesel. A 350 rpm drop in engine speed then ensued, which required about 45 s of running time to regain.

The engine takes substantially less time (a factor of 2 1/2 to 3) to start with the timed spark discharge aid than with the glow plugs. The tendency to accelerate quicky, a

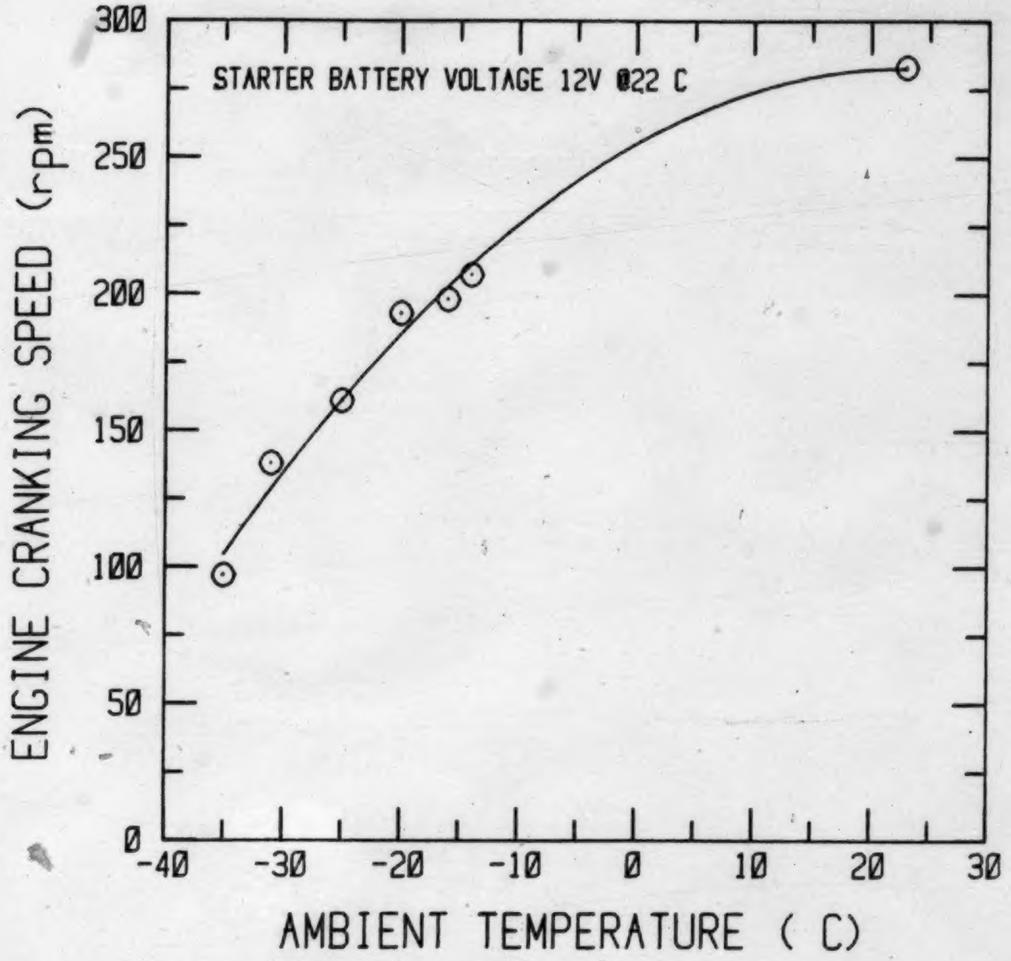

Figure 5.6 Effect of Ambient Temperature on Engine Cranking Speed

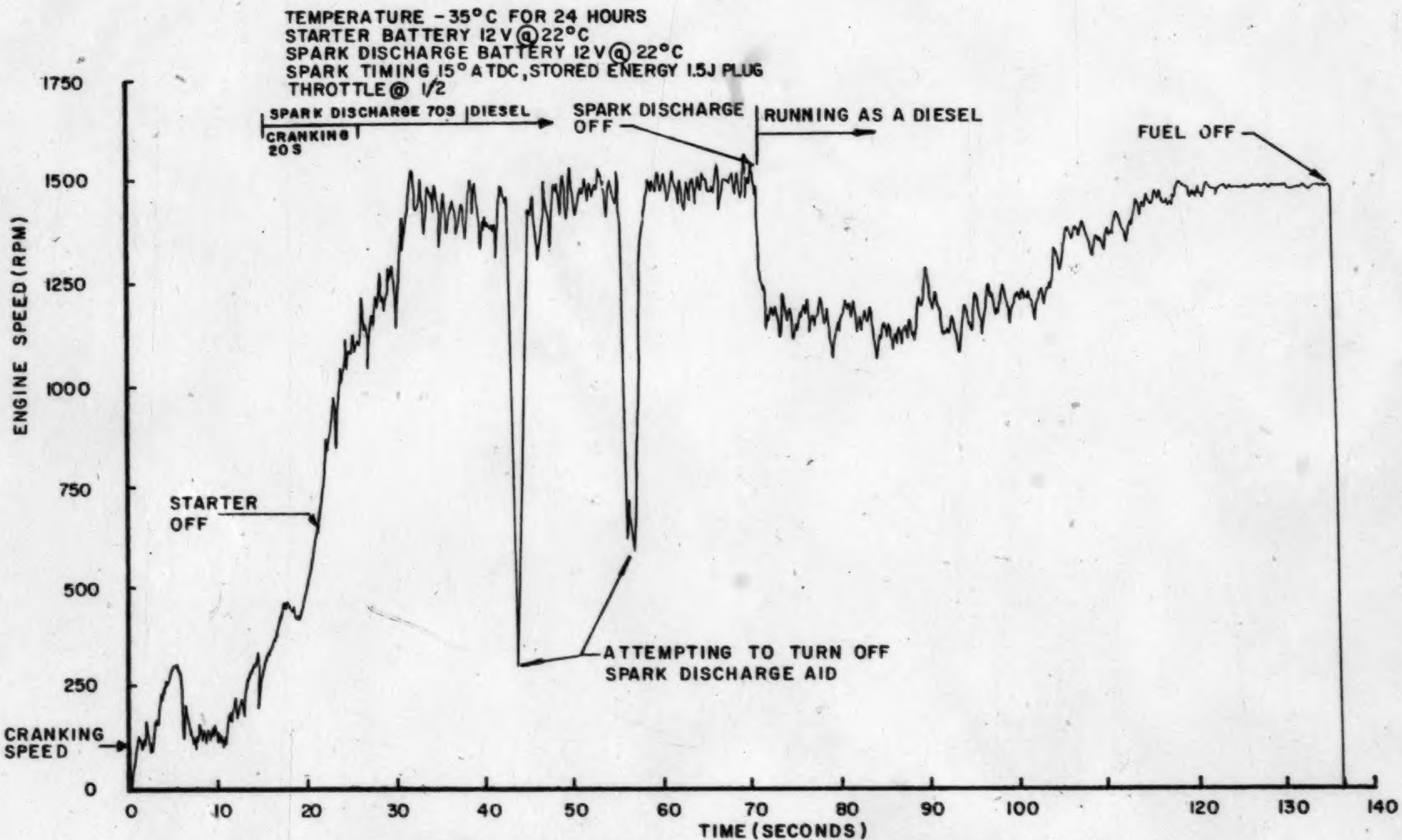

Figure 5.7 Mercedes-Benz Starting - Running Characteristics with Timed Spark Discharge Aid

few seconds into the start, is taken as evidence of the presence of partial combustion. Further substantiation of this is offered by the fact that starts in the order of 6 s at -35°C for long durations were recorded with the timed spark discharge aid. These were not representative, though, of normal engine starting behaviour.

One other point to note is the rapid and smooth acceleration of the engine when aided by the glow plugs, as opposed to the more sluggish response when aided by the timed spark discharge aid. A trend similar to this was noticed when performing starting tests with the timed spark discharge. It was the tendency of the engine to accelerate faster and smoother as the required cranking time increased. It was also observed that as the spark timing was advanced the rate at which the engine sped up to its running speed also increased. However, for this study, minimizing the starting time was much more important than optimizing the engine behaviour as it accelerated to governor speed.

5.6 Effects of Fuel Injection Timing on Ignition Delay

Figure 5.8 shows a pressure-time trace for fuel in the injection pump delivery line to the injector for cylinder #1 during cranking at -34°C. Here it is seen that at this temperature the fuel delivery from the pump starts at about 28°BTDC, the pintle valve then opens when the line pressure is around 14 MPa (@ about 8°ATDC) spraying fuel into the pre-chamber and closes at about 20°ATDC. In a sense the

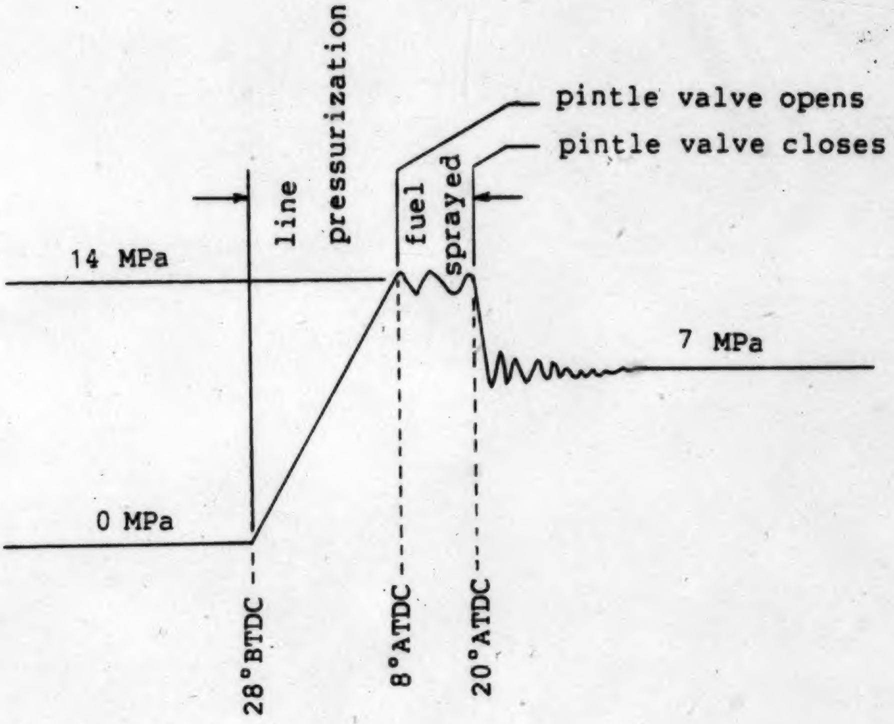

Figure 5.8 Typical Pressure Buildup in Fuel Injector Line during Cranking for Cylinder #1, Temperature -34°C

starting behaviour of the engine at -35°C shown in Figure 5.4 maps out the timing and duration of the fuel spray. This should not be very surprising as optimum starting conditions (from 13°C ATDC to 16°C ATDC @ -35°C) should be related to optimum fuel spray conditions (from 8° ATDC to 20° ATDC @ -34°C).

Figure 5.9 shows a pressure-time trace during the compression and combustion expansion strokes for a mechanical injection C.I. engine running at full load [21]. The four stages in the ignition process indicated in Figure 5.9 are shown in a little greater detail in Figure 5.10.

The period from the start of fuel injection until the initiation of ignition is called the ignition delay. This delay period is comprised of two parts, the physical delay and the chemical delay.

In the physical delay period disintegration of the fuel spray, by high pressure atomization (ΔP across orifice=14 MPa) shown in Figure 5.11, followed by turbulent mixing of vaporized fuel droplets and then the raising of the mixture temperature takes place.

During the period of chemical delay the reactions start slowly then accelerate until ignition starts. Unlike the homogeneous charge S.I. engine, there is no orderly propagation of a flame along a definite frame front, but flames appear in many areas where combustible mixtures form and auto-ignition occurs.

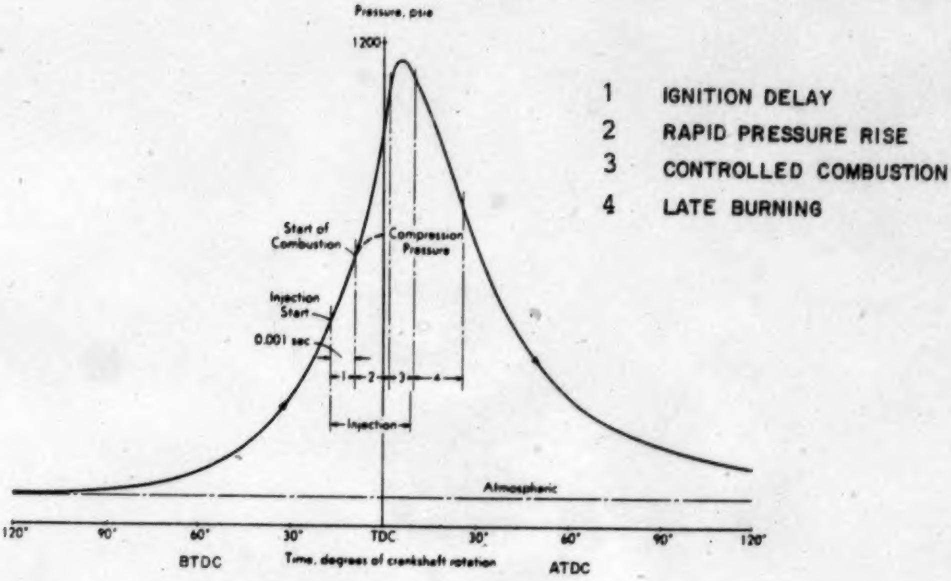

Figure 5.9 Pressure - Time Diagram for Mechanical-Injection Engine Running at Full Load

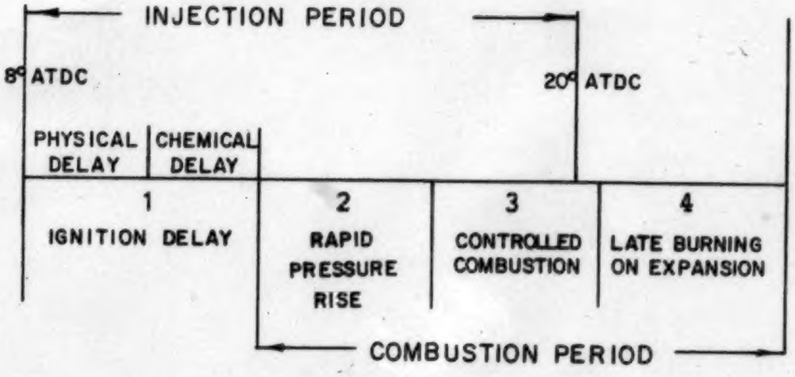

Figure 5.10 Four Stages of Diesel Combustion (Mercedes-Benz Fuel Injection Period measured @ -34°C)

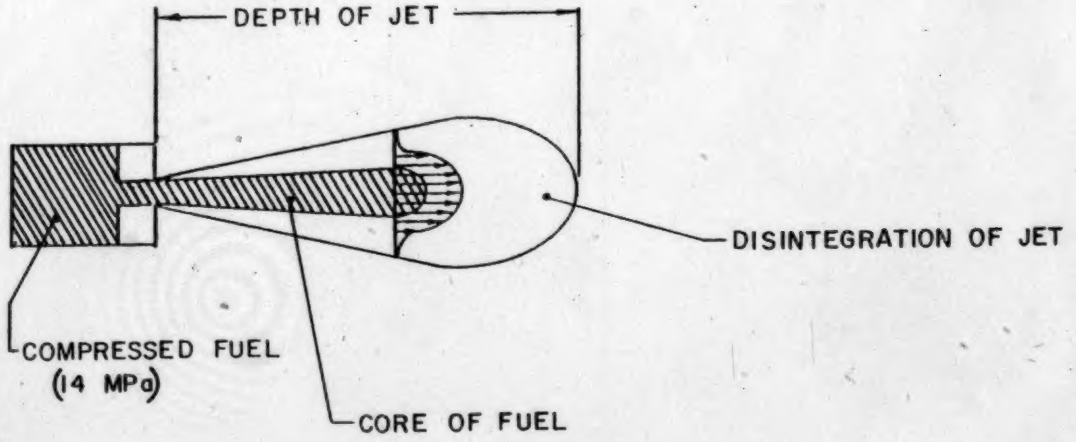

Figure 5.11 Schematic of Disintegration of a Fuel Jet

Instead of relying on the conventional factory installed glow plugs as a starting aid, this study implemented a timed spark discharge system. Here, the initiation and propagation of combustion is directed to the initial stages of ignition. This is possible because in discharging the energy stored in the capacitors across the surface gap plug electrodes, a high temperature plasma is created. The concentration of active species present in the plasma is sufficient and/or hot enough to promote chain branching reactions at a rate which will maintain and extend the flame [7]. Because of the heterogeneous nature of the charge in C.I. engines, regions exist with droplets of fuel alone, with fuel vapor but not air, with air alone and with fuel and air mixtures. When ignition begins in a region that contains both fuel and air, the flame will propagate if the region of mixture is continuous [24]. However, heat transferred from burning regions to adjacent ones, on the verge of self-ignition, may cause ignition. This points out the difficulty in being able to distinguish between flame propagation and self-ignition which is aided by adjacent high temperature regions. Therefore, in order to enhance the ignition process, a system that can generate high energy discharges to produce the plasma as well as a means to distribute the ignition nuclei throughout the charge is required. Ideally the plasma jet spark plug should be used in this application because over-pressurization of the plasma generating cavity causes significant charge penetration by the plasma. However because plasma jet igniters are succeptible to fouling problems, the surface gap plug which does not foul yet produces some motion of the plasma away from its end was chosen for this application. This has a two pronged effect, firstly the movement of ignition nuclei into the charge reduces the need for the mixture region, where ignition began, to be continuous in order to promote flame propagation. Secondly, because the number of points of ignition has increased, more areas close to self ignition are adjacent to more burning regions. The net effect is that more of the charge will be burned and in less time than without any aid. This is very desirable as the more energy liberated close to TDC the greater the amount of work that can be done throughout the expansion stroke.

This mechanism for enhancing ignition in a Diesel engine is what is thought to have occurred in the engine cylinder during cold starts. The best evidence to support this are the facts that in general, starts with the timed spark discharge aid took only 30% to 40% of the time required with the glow plugs. More than twice as much energy was consumed with the glow plugs than with the timed spark discharge (as a pre-heat period was required with the glow plugs). Also the starter motor consumed about twice as much energy when the glow plugs were used than with the timed spark discharge, as a result of the longer cranking periods required.

6. SUMMARY

The results of this study indicate the degree to which the timed spark discharge aid was sucessfully adapted to the Mercedes-Benz 4-cylinder, 4-cycle, I.D.I. automotive-type Diesel engine. The starts obtained with the timed spark discharge took on average 30% to 40% of the time required with the glow plugs, and the electrical energy consumed by the aid was less than 1/2 of that of the glow plugs. Furthermore the starter motor used twice as much energy when the engine was being aided by the glow plugs compared with the timed park discharge. Therefore for the overall starting process with the engine equipped with the timed spark discharge, the total energy consumed was only half of that normally used when starting with the factory installed glow plugs.

The timing window where the quickest starts were obtained was found to shrink and become more retarded in time as the ambient temperature decreased. Below -35°C this window had more or less disappeared altogether. This was interpreted to show the effect of ambient temperature on the physical delay period during the ignition process. That is, because of the adverse conditions at these temperatures the time required to properly prepare the fuel for autoignition in this engine is so long that starting is virtually ruled out. At one point in the study it was determined that 75% of the total heat added to the charge during the compression stroke at an ambient temperature of -26.5°C, was lost to the cylinder walls. Nevertheless, the improvements in starting times at ambient temperatures down to -35°C are attributed to the way in which the ignition process in the engine was enhanced. For this study, initiation and propagation of combustion was directed to the initial stages of the ignition process, particularly the chemical delay period. A plasma was generated by discharging a high energy across the plug electrodes and in the process was propelled somewhat into the charge. This method of aiding Diesel engines during the starting process exhibited partial combustion early in each start. The reasons for the absence of further initial combustion activity and quick acceleration to the governed speed is open to speculation. However, the following explanation was put forward. Because of the limited access to the pre-chamber, the spark plugs were installed in the existing glow plug locations. In this position the spark plugs were oriented in such a way that the firing end of the plug was not directly exposed to the fuel spray. Not having control over this variable, in this study, is felt to be at least partly responsible for limiting its success.

A thorough study of the voltage requirements for increasing spark discharges in ambient air densities was necessary in order to appropriately select a plug type and geometry for discharging in the high pressure environment in the Diesel engine cylinder. It was found that plasma plugs were ideal for creating a high volume spark kernel and for being able to effectively move the ignition source away from the spark plug into the charge medium. However, because plasma plugs are succeptible to fouling during engine operation, surface gap spark plugs (which are non-fouling) were best suited for this application. Champion G508V surface gap plugs were the only plugs tested that were reliable and small enough to be installed in the engine. These plugs required up to 30 kV to breakdown under simulated engine cranking conditions.

The ignition system used to develop the 30 kV, required to breakdown the gap under these adverse conditions, was designed as the spark plug testing and selection process was underway. This was because of the interdependence of these two aspects of the system. The final version of the system was found to be very reliable and consistently effective for cold temperature starting. The circuitry would discharge several joules of energy per firing at up to 60 Hz (1800 rpm). This was the maximum rate at which the circuitry would operate, fortunately by this time the engine would have been warmed up and not have any further use for this aid. Both aids used energy at approximately the same rates, 50 W per cylinder.

A high pressure cell was designed and built primarily to faciliatate breakdown voltage testing of various spark plug designs. The purpose of this exercise was for aiding in the appropriate selection of spark plugs to be used in adapting the timed spark discharge aid to the engine.

This cell was designed with the following criteria in mind.

To:

1. have a working pressure of 2 MPa.
2. permit installation of standard 18 mm spark plugs for breakdown voltage and combustion studies.
3. be integrated into an existing Schlieren set up.
4. accept a pre-mixed gas/air stream.
5. have quick assembly capability.

Several methods were used to determine the glass window dimensions needed, in order to withstand the expected stresses set up in the pressurized cell. The results of these indicated that a circular glass window 15 cm in diameter and 2.44 cm thick, where the inner 8 cm diameter section would be subjected to the internal cell pressure, would be adequate.

Pressure-deflection tests were done on the glass window and these values compared with theoretical predictions. Although, ideal clamping conditions of the glass was not possible in practice, the measured deflection showed good agreement with predicted deflections.

Additionally the cell was used, in conjunction with the Schlieren set up, to show how spark kernel motion and jet penetration are affected by plug geometry, ambient conditions and discharge circuitry initial conditions. The Schlieren system set-up for this and future studies is a simple way of photographing a single image, high speed event where density changes occur. It was further found to be very reliable, consistent and exhibited good photographic resolution.

The secondary aspect of this study involved estimating the heat loss from the engine cylinder during the compression stroke at various ambient temperatures. Here cylinder charge pressure and temperatures were measured along with the associated known cylinder volume. From this raw data, charge density and the work added to and heat loss from the charge were determined. The charge velocity and an average cylinder heat-transfer coefficient for the air flow in the cylinder during the compression stroke were used to verify an accepted correlation of Nusselt's number, namely

$$Nu = 0.3\ Re^{0.7}$$

REFERENCES

1. Annand, W.J.D., Heat Transfer in the Cylinders of Reciprocating Internal Combustion Engine. Proc. Inst. Mech. Engs. Vol. 177, 1963.

2. Annand, W.J.D., Pinfold, D. Heat Transfer in the Cylinder of a Motored Reciprocating Engine. Society of Automotive Engineers, Paper, 800457, 1980.

3. Atwell, L.P., Brumback, W.P., Manthey, W.R. Cold Starting Diesel Engines with Low Voltage Ignition. presented at the 11th Annual Earthmoving Industry Conference, SAE Central Illinois Section, Paper S-241, April 1960.

4. Austen, A.E.W. & Lyn, W.T. Some Investigations on Cold-Starting Phenomena in Diesel Engines. Proc. Instn. Mech. Engrs. (A.D.), 1959.

5. Avner, Sidney H. Introduction to Physical Metallurgy, 2nd Edition. McGraw-Hill Book Company, New York, 1974.

6. Champion Spark Plug Company, Personal Communication, 1983.

7. Dale, J.D., Oppenheim, A.K. Ignition Studies. Review Meeting at Science Application Inc., La Jolla California, March 1981.

8. Greif, R. Namba,T., Nikanham, M.. Heat Transfer During Piston Compression including Side Wall and Convection Effects. International Journal of Heat Mass Transfer Vol. 22: 1979.

9. Henein, N.A. Instantaneous Heat Transfer Rates and Coefficients Between the Gas and Combustion Chamber of a Diesel Engine. S.A.E. #969B, 1965.

10. Hewlett-Packard Practical Temperature Measurements. Application Note #290, Palo Alto, Ca., 1980.

11. Hohenberg, F. Günter. Advanced Approaches for Heat Transfer Calculations. S.A.E. Paper #790825, 1980.

12. Holman, J.P. Heat Transfer, 5th Edition. McGraw-Hill Book Company, New York, 1981, p. 536 (Table A-2).

13. Howarth, M.H. The Design of High-Speed Diesel Engines American Elsevier Publishing Company Inc., New York, 1966.

14. Kanury, A. Murty. An Introduction to Combustion Phenomena. Gordon Breach Science Publishers, New York, 1975.

15. Keenan, Joseph H., Chan, Jing, Kaye, Joseph. Gas Tables, 2nd Edition. John Wiley & Sons, Inc., New York, 1980.

16. Mantell, C.L. Engineering Materials Handbook. McGraw McGraw-Hill Book Company Ltd., New York, 1958: Section 27.

17. McAdams, William H. Heat Transmission. 3rd Edition. McGraw-Hill Book Company, Inc., New York, 1954.

18. Megyesy, E.F. Pressure Vessel Handbook, 3rd Edition. Pressure Valve Handbook Publishing, Inc., Tulsa, 1975.

19. Mertz, W.S. Jr. Gas Film Coefficient in a Diesel Engine Cylinder During Compression. M.Sc. Thesis, Department of Mechanical Engineering, Pennsylvania State University, 1960.

20. Merzkirch, Wolfgang Flow Visualization. Academic Press,New York, 1974.

21. Meyer, W.E., De Carolis, J.J. Compression Temperatures in Diesel Engines under Starting Conditions. SAE Vol. 70: 1962.

22. Morgenstern, B.; Dale, J.D.; Smy, P.R.; Clements,R.M. Low Temperature of a Diesel Engine Useng Timed Spark Discharge Presented at the Combustion Institute, Canadian Section, Annual Meeting Ottawa, Canada, May 1981.

23. Nitske, W. Robert. Mercedes-Benz Diesel Automobiles Motor Books International, Osceola, Wisconsin, 1981.

24. Obert, E.F., Internal Combustion Engines and Air Pollution. 3rd Edition. Intext Educational Publishers, New York, 1973.

25. Popov, E.P. Mechanics of Materials 2nd Edition. Prentice-Hall, Inc., Englewood Cliffs, New Jersey, 1978.

26. Schweitzer, P.H. Cold Starting of Diesel Engines. Diesel Power & Transportation, Vol. 24, p. 1190-1193,1230, Oct., 1946.

27. Seely, M.S., Smith, A.M. Advanced Mechanics of Materials, 2nd Edition. John Wiley & Sons, Inc. New York. 1952.

28. Shand, E.B. Glass Engineering Handbook. McGraw-Hill Book Co., New York, 1958.

29. Spreadbury, F.G., Electrical Ignition Equipment. Constable & Company Ltd, London, 1981.

30. U.S. Dept. of Commerce, National Bureau of Standards, Circular 564, Tables of Thermal Properties of Gases. p. 11, 12, Table 2-8 p. 69 & Table 2-9 p. 70., 1970.

31. Van Wylen, Gordon,J., Sonntag, Richard, E. Classical Thermodynamics. John Wiley & Sons, New York, 1974.

APPENDIX A: Internal energy of air and ratio of specific heats as a function of temperature

A.1 Determination of u = f(T)

A relationship for $u = f(T)$ was needed that could be used in the heat transfer analysis computer program. This was required in order to know the state of the charge during the isentropic compression. Using the thermodynamic relationship

$$u = h' - Pv' \qquad (A_1)$$

and substituting in the ideal gas law

$$Pv' = RT \qquad (A_2)$$

the following is obtained:

$$\begin{aligned} u = h' - RT,\ R &= \text{universal gas content} \\ &= 0.28703\ \text{kJ/kg-K} \end{aligned} \qquad (A_3)$$

Expressing the enthalpy of air on a molar basis, for each constituent as

$$\Delta\bar{h} = \sum_i X_i \Delta\bar{h}_i,\ i = 1,3\ (N_2,\ O_2,\ Ar) \qquad (A_4)$$

then on a mass basis by dividing by the molecular weight of air this becomes:

$$\Delta h^{+} = \Delta\bar{h}/mw \qquad (A_5)$$

Equation (A_4) can be expanded to

$$(\bar{h}_2-\bar{h}_1) = XN_2(\bar{h}_2-\bar{h}_1)N_2+XO_2(\bar{h}_2-\bar{h}_1)O_2+XAr(\bar{h}_2-\bar{h}_1)Ar \qquad (A_6)$$

The physical properties of air used are listed below.

Table A.1 AIR COMPOSITION ([31])

GAS	MOLECULAR WEIGHT WEIGHT (mw)	% BY VOLUME	MOLE FRACTION (X)
N_2	28.0134	78.03	0.7803
O_2	31.9988	20.99	0.2099
Ar	39.948	0.98	0.0098

From the definition

$$Cp_o \equiv (\partial h/\partial T)p \qquad (A_7)$$

the enthalpy can be obtained by integrating (A_7), ideally with the pressure held constant; this results in:

$$d\bar{h} = \bar{C}p_o dT \qquad (A_8)$$

For this case the pressures during the compression process are not constant but are low (less than 2.8 MPa). The error incurred will be minimal because of these low pressures. Therefore, integrating out (A_8) produces

$$\bar{h}_2 - \bar{h}_1 = \int_{T_1}^{T_2} \bar{C}p_o\ (T)dT$$

and by defining

$$\theta = T/100,\ T \text{ is in Kelvin}$$

this becomes:

$$\bar{h}_2 - \bar{h}_1 = \int_{\theta_1}^{\theta_2} 100\ \bar{C}p_o(\theta)d\theta \qquad (A_9)$$

The constant-pressure specific heats for the ideal gases that constitute air [31] are listed below.

$$\bar{C}p_oN_2=f_1(\theta)=39.060-512.79\theta^{-1.5}+1072.7\theta^{-2}-820.40\theta^{-3} \qquad (A_{10})$$

$$\bar{C}p_oO_2=f_2(\theta)=37.432+0.020102\theta^{1.5}-178.57\theta^{-1.5}+236.88\theta^{-2} \qquad (A_{11})$$

$$Cp_oAr = 0.5203 \text{ kJ/kg-K} \qquad (A_{12})$$

Substituting for each constituent into (A_6) and dividing by the molecular weight of air as in (A_5), $\Delta\ h^{+}air$ is obtained. h^{+} was then referenced to the accepted datum (of h^{+}=300 kJ/kg @ T=300 K) as follows

$$h' = h^* - 946 \text{ kJ/kg} \qquad (A_{13})$$

however as h' was only valid for 300K ≤ T ≤ 3500K and as it was necessary to know h' for T < 300 K

$$h' \equiv T \text{ for } 0 \text{ K} \leq T \leq 300 \text{ K} \qquad (A_{14})$$

Values of enthalpy, h', for air, from 0 K to 3000 K were checked using reference [31], and they were found to be within ±0.5%. The internal energy of air, u, was then obtained using (A_{15})

$$u = h' - 0.28703T \qquad (A_{15})$$

These results were also in good agreement with reference [31].

A.2 Determination of k = f(T)

It was also required to know the ratio of specific heats, k, between any two temperatures during the isentropic compression process. However, these temperatures are initially unknown as they were to be determined based on the measured cylinder pressure values. Hence an iterative type of solution was invoked four times as follows:

1. An average value of the ratio of specific heats k^m was initially assumed to be

$k^m = 1.40$

between all values of temperature (as yet to be determined) in the isentropic compression.

2. The temperature history based on the measured pressure and the assumed values for k was then determined using

$$T_s^{j+1} = T_s^j \left[\frac{P^{j+1}}{P^j}\right]^{\frac{{}^jk^{j+1} - 1}{{}^jk^{j+1}}} \qquad (A_{16})$$

3. These T_s results were then used to determine a new set of values for k.

k is by definition the ratio of specific heats

$$k = Cp_o/Cv_o, \qquad (A_{17})$$

where:

$$Cp_o - Cv_o = R$$

or $$Cv_o = Cp_o - R \qquad (A_{18})$$

Substituting (A_{18}) into (A_{17}) produces:

$$k = Cp_0/(Cp_0 - R) \qquad (A_{19})$$

In order to work out the isentropic temperature at the beginning and end of each 5° interval of crankshaft rotation, it was necessary to obtain an average value of the ratio of specific heats for air, k^m, over each interval as follows.

$$k^m = Cp^m/(Cp^m - R) \qquad (A_{20})$$

where:

$Cp_0 \equiv Cp_0 air$

$Cp_0 air^m = \int_{T_1}^{T_2} Cp_0(T)dT \;/\; (T_2 - T_1)$

$$Cp_0 air^m = (h_2' - h_1') \;/\; (T_2 - T_1) \qquad (A_{21})$$

By substituting (A_5) into (A_{21}) $Cp_0 air^m$ can be determined. This in turn can be input into (A_{20}) and new values of k^m obtained. These updated values for k^m are then used in step 2 and the process repeated. This was done four times in total. After this further changes in T_s and k^m values were found to be minimal.

APPENDIX B: Correlation of Nu for Flow over a Single Sphere

Table B.1 Coeffecients for Calculation of Heat Transfer on a Sphere with Air Flowing over it (taken from Figure 2.12)

Nu	Re	C	n
2.0	1 - 3	-	-
2.0 - 3.3	3 - 18.5	1.45	0.284
3.3 - 6.0	18.5 - 100	1.0	0.410
6.0 - 100	100 - 10,000	0.37	0.6

APPENDIX C: Listing of Heat Transfer Analysis Program;CYANAL

```
C       ---------------------------------------------------------------
C              CYANAL cycle analysis
C       ---------------------------------------------------------------
C       13 December 84
C       John D. Wilson
C
C This program reads in data previously stored on binary data disk#9
C    by program ANDATA.
C This data is arranged in 8 columns /96 rows/ as follows :
C
C                                COLUMNS
C    1          2         3         4         5         6         7        8
C  Crank   Cylinder  Loc. of  5 deg.   Engine  Cylinder  T.C.#1   T.C.#2
C  Angle     Volume 5deg.pulse Pulses   Speed   Pressure
C  (deg.)   (c.c.)   (ms.*8)  (volts)  (rpm)    (psig.)  (deg.)   (deg.)
C
C The program stores the information in the arrays IBUF and ARRAY
C
C The Heat Transfer analysis is done on a cycle by cycle basis
C for the compression stroke.
C
C Data was sampled at 1KHz/Channel but only data at every 5 deg. C.A.
C was retained. For the first 360 deg.C.A. there are therefore 73 of
C these locations. Because the intake valve closes at 130 deg.C.A.
C BTDC the analysis is performed between 130 deg. BTDC (J=47) and TDC
C (J=73).
C
C To run this program link with Subroutines TCHARG, INENRG and RSMOT
C
C Subroutine TCHARG estimates the charge temperature that would have
C been recorded if a t.c. of zero mass was used for the measurements.
C This is done using two t.c.s of different mass and time response.
C
C Subroutine INENRG determines the internal energy of the charge,
C as a functions of charge temperature, using ideal gas relations.
C
C Subroutine RSMOT is smoothing function.
C
C After the analysis is completed the results are written to Binary
C Data Disk #10 for plotting by INPLTV.
C
        INTEGER*2 DIBUF1(129),IBUF(256),FHJ2,LHJ2,FHw,LHw,FHJ1,LHJ1
        INTEGER*2 Xa,Xb,Spaces,IDEL2(30),IDEL1(30)
        INTEGER*2 DBLK(4),DALT(3)
C
        REAL A(96),NUJAVE,REJAVE,RMIN(8),RMAX(8)
        REAL DIR(128),H(73),U(73),MUA,MUB,KAYA,KAYB,KAYC
C
        REAL MU(73),KAY(73),NUJ(73),NUw(73),KAVE(73)
        REAL Mass(73),HtFlux(73),Hw(73),HJ2(73),HJ1(73)
```

```
C
        REAL CpAVE(73),deltaW(73),cumW(73),Tair(96),Ts(73)
        REAL deltaQ(73),cumQ(73),Acyl(73),TIME(73)
        REAL ARRAY(8,96),Scale(8)
        REAL REJ(73),REw(73),RHO(73)
        REAL V(73),Dcyl(73),CYLVOL(73),CYLsa(73),deltaT(73)
C
        DATA DBLK/3RDY0,0,0,0/
        DATA DALT/3RDY0,3RDY1,3RDL2/
C
        EQUIVALENCE (DIBUF1(2),DIR(1))
C
 2      DO 3 J=1,73
        CpAVE(J)=0.0
        Hw(J)=0.0
        NUw(J)=0.0
        REw(J)=0.0
        HJ1(J)=0.0
        HJ2(J)=0.0
        NUJ(J)=0.0
        REJ(J)=0.0
        cumQ(J)=0.0
        V(J)=0.0
  3     KAVE(J)=0.0
C
        DO 4 I=1,8
        DO 4 J=1,96
 4      ARRAY(I,J)=0.0
C
        TYPE 5
  5     FORMAT(55('-')/20X'CYANL2 cycle analysis'/55('-'))
 10     TYPE 20
 20     FORMAT(' Enter input device name                    '/
     Z         '       0 = to read data from DY0:       '/
     Z         '       1 = to read data from DY1:       '/
     Z         '       2 = to read data from DL2:       >'$)
        ACCEPT 30,IDEV
 30     FORMAT(I4)
        IF (IDEV.LT.0.OR.IDEV.GT,2) GO TO 10
        DBLK(1)=DALT(IDEV+1)
C
        ICHAN=IGETC()
        IERF=IFETCH(DBLK)
        IERL=LOOKUP(ICHAN,DBLK)
        TYPE 40,ICHAN,IERF,IERL
 40     FORMAT('ICHAN='I3', IERF='I4', IERL='I4)
C
 50     PAUSE 'Insert Binary Data Disk #9 and press RETURN '
        DO 60 I=1,128
 60     DIR(I)=0.0
        IERR1=ISPFNW("377,ICHAN,0,DIBUF1,1)
```

```
      IF (IERR1.NE.0) TYPE 70,IERR1
C
 70   FORMAT(' ISPFNW ERR=' I7)
      IF (DIR(1)-9.) 50,80,50
C
C     Guessing an initial value ,'Guessn', for the correlation
C     of Nu for flow over a single cylinder.
C
 80   TYPE 75
 75   FORMAT(' Enter exponent n, from NUJ = c * (REJ)**n  >'$)
      ACCEPT*,GUESSn
      TYPE 77,GUESSn
 77   FORMAT(' Exponent Guess is : n='F7.3)
C
      TYPE 90
 90   FORMAT(' Enter 1st. Block to read (3 Blocks will be read)>'$)
      ACCEPT 100,IFBLK1
 100  FORMAT(I5)
      IF (IFBLK1.LT.0.OR.IFBLK1.GT.970) GO TO 80
      IFBLK2=IFBLK1
C
      DO 101 J=1,3
      NBLOCK=IFBLK1+J-1
      IERR=IREADW(256,IBUF,NBLOCK,ICHAN)
          DO 106 I=1,256,8
          DO 106 ICOL=1,8
          IROW=(256*(J-1)+I-1)/8+1
          K=(I-1)+ICOL
 106      ARRAY(ICOL,IROW)=IBUF(K)*0.1
 101  CONTINUE
C
 107  TYPE 108 ,IFBLK1,IFBLK1+2
 108  FORMAT(' Read accomplished from block # 'I4' to block # 'I4)
C
C     Because of max. integer allowed ~32,000 vector TIME
C     was attenuated by 10 during read/write to disk
C
      DO 109 J=1,73
      TIME(J)=ARRAY(3,J)*10.
 109  TIME(J)=TIME(J)/(8.*1000.)
C
C     Retrieving Patm and # of 5deg.pulses BTDC1 info:
C
      Pa=ARRAY(4,1)
      N5btdc=ARRAY(4,2)
      TYPE 110,N5btdc
 110  FORMAT(' 'I4'  5deg. pulses were recorded BTDC1 ')
C
      TYPE 112
 112  FORMAT(/' Enter Wall Temperature, Twall (deg.C.) >'$)
      ACCEPT*,Twall
      TYPE 114, Twall
 114  FORMAT(' Twall = 'F7.1'deg.C')
      Twall=Twall+273.15
C
C     The subroutine RSMOT (real smoothing) is called to smooth
C      the engine speed, cylinder pressure and temperature
C      histories of T.C.#1 and T.C.#2.
C
      NPP=96
      DO 116 I=5,8
      DO 117 J=1,96
 117  A(J)=ARRAY(I,J)
C
      CALL RSMOT(A,NPP)
C
      DO 118 J=1,96
 118  ARRAY(I,J)=A(J)
 116  CONTINUE
C
C
C     The subroutine TCHARG (charge temp.) is called with
C     T.C.#1(column 7) and T.C.#2(column 8) as inputs and
C     charge temp. Tair(96) as output.
C
      I1=1
      I2=96
C
C     Converting T.C.#1 and T.C.#2 readings from deg.C. to Kelvin
C
      DO 120 I=7,8
      DO 120 J=1,96
 120  ARRAY(I,J)=ARRAY(I,J)+273.15
C
      CALL TCHARG(ARRAY,I1,I2,Tair,GUESSn)
C
C     Smoothing Tair in from 0 to 360 (deg.)
C
      NPP=73
      CALL RSMOT(Tair,NPP)
C
C     Converting pressure from Psig. to Kpa.(abs.)
C
      TYPE 134,Pa
 134  FORMAT(' Patm = 'F6.1' mm. of Hg.      ')
      Patm=Pa*14.7/760.
      DO 139 J=1,73
 139  ARRAY(6,J)=(ARRAY(6,J)+Patm)*6.89476
C
C     Working out mass (kg) in cylinder at each 5 deg.location using
C     the ideal gas law m=P*V/(R*T) ; R=287.03 J/kg-K
C
```

```
      DO 140 J=1,73
 140  Mass(J)=ARRAY(6,J)*ARRAY(2,J)/(Tair(J)*287.03*1000.)
C
C     Determining charge density during compression stroke
C
      DO 145 J=1,73
      CYLVOL(J)=ARRAY(2,J)/(10.**6.)
 145  RHO(J)=Mass(J)/CYLVOL(J)
C
C     Working out theoretical temp. history Ts , during
C     isentropic compression process, using measured pressure
C     values.
C              Ts(J+1) = Ts(J) * ( P(J+1)/P(J) )**( (Kave-1)/Kave )
C
C     Starting with Ts(47) = Tair(47)/@130deg. BTDC/ and K(J) = 1.40
C     4 iterations are done on the temp. and the polytropic exponent
C     note:  between Ts(J) and Ts(J+1) Kave is used
C
      DO 150 J=47,72
 150  KAVE(J)=1.40
C
      DO 155 J=1,73
 155  Ts(J)=0.0
C
      ITER=1
 160  CONTINUE
C
      Ts(47)=Tair(47)
      DO 170 J=48,73
      Ts(J)=Ts(J-1)*(ARRAY(6,J)/ARRAY(6,J-1))**((KAVE(J-1)-1.)/
     ZKAVE(J-1))
 170  CONTINUE
C
C     Finding internal energy during isentropic compress. process
C      u - kJ/kg.
C
      CALL INENRG(Ts,H,U)
C
      DO 180 J=48,73
      IF (Ts(J).EQ.Ts(J-1)) KAVE(J)=1.40
      IF (Ts(J).EQ.Ts(J-1)) GO TO 180
      CpAVE(J-1)=(H(J)-H(J-1))/(Ts(J)-Ts(J-1))
      KAVE(J-1)=CpAVE(J-1)/(CpAVE(J-1)-0.28703)
 180  CONTINUE
C
      ITER=ITER+1
      IF (ITER.LT.5) GO TO 160
C
      TYPE 185
 185  FORMAT(/' Enter 0 = to go on                                   '/
     Z        '         1 = to print J,CA,TC#1,TC#2,Tair,TS,P,H,U >'$)
```

```
        ACCEPT 30,IGO
        IF (IGO.EQ.0) GO TO 240
C
        TYPE 190
 190    FORMAT(/'  J     CA        TC#1      TC#2      Tair      TS
     Z        P       H        U'/
     Z'         (deg)     (degK)    (degK)    (degK)    (degK)
     Z   (kpa)     (kJ/kg)  (kJ/kg)')
        DO 200 J=47,73
 200    TYPE 210,J,ARRAY(1,J),ARRAY(7,J),ARRAY(8,J),Tair(J),Ts(J),
     ZARRAY(6,J),H(J),U(J),
 210    FORMAT(I4,8(1X,F8.2))
C
C       For rest of analysis assume cyl. mass = constant
C                                              = mass (@130deg. BTDC)
C
C       Calculating the isentropic work added to the charge, w - (kJ)
C
 240    TYPE 241,Mass(47)
 241    FORMAT(/' Initial mass (@130deg. BTDC) = 'E10.3 'kg.')
C
        DO 245 J=48,73
 245    deltaW(J-1)=Mass(47)*(U(J)-U(J-1))
        NPP=26
        DO 252 J=47,72
 252    A(J-46)=deltaW(J)
        CALL RSMOT(A,NPP)
        cumW(46)=0.0
        DO 254 J=47,72
C       deltaW(J)=A(J-46)
 254    cumW(J)=cumW(J-1)+deltaW(J)
C
C       Obtaining the internal energy of the charge during the
C       actual compression process (using Tair), u - kJ/kg
C
        CALL INENRG(Tair,H,U)
C
C
C       Evaluating the heat loss from the charge, q - (kJ)
C
        DO  270 J=48,73
 270    deltaQ(J-1)=deltaW(J-1)-Mass(47)*(U(J)-U(J-1))
        NPP=26
        DO 272 J=47,72
 272    A(J-46)=deltaQ(J)
        CALL RSMOT(A,NPP)
        cumQ(46)=0.0
        DO 274 J=47,72
C       deltaQ(J)=A(J-46)
 274    cumQ(J)=cumQ(J-1)+deltaQ(J)
C
```

```
      Apist=44.179/10000.
      Ahead=Apist
      Apre=23.66/10000.
      DO 280 J=1,73
      Acyl(J)=(0.5333*(ARRAY(2,J)-24.54)+7.940)/10000.
 280  CYLsa(J)=Acyl(J)+Apist+Apist+Apre
C
C     Determining Heat Flux (W/m**2-sec) for each 5deg. increment
C             HtFlux = deltaQ / ( ave.CYLsa * deltaTIME )
C
      DO 283 J=47,72
 283  HtFlux(J)=deltaQ(J)*1000./((CYLsa(J)+CYLsa(J+1))*0.5*
     Z(TIME(J+1)-TIME(J)))
C
C     Determining driving potential for heat transfer
C             deltaT = Tair(ave.) - Twall
C
      DO 284 J=47,72
 284  deltaT(J)=Tair(J)-Twall
C
      TYPE 285
 285  FORMAT(/' Enter 0 = to go on                                    '/
     Z        '        1 = to print J,CA,deltaW,cumW,deltaQ,cumQ,Time'/
     Z        '                         HtFlux,deltaT                >'$)
      ACCEPT 30,IGO
      IF (IGO.EQ.0) GO TO 299
      TYPE 293
 293  FORMAT(/'    J  C.A.   deltaW      cumW        deltaQ
     Z  cumQ        Time    HtFlux   deltaT'/15X,'(KJ)',7X,
     Z'(KJ)',8X,'(KJ)',4X,'(KJ)',7X,'(sec)',3X,'(W/m**2)',1X,'(deg.K)')
      DO 295 J=47,72
 295  TYPE 297,J,ARRAY(1,J),deltaW(J),cumW(J),deltaQ(J),cumQ(J),TIME(J)
     Z,HtFlux(J),deltaT(J)
 297  FORMAT(1X,I4,1X,F5.0,4(1X,E10.3),1X,F7.4,1X,E10.3,1X,F6.1)
C
C     Determining the cyl. gas film coef. Hw (W/m**2-K)
C
C     Expressing cyl. surface area ACYL=ACYL(theta) in terms of cyl.
C     volume ACYL=ACYL(cylvol), (m**2)
C
 299  DO 300 J=48,73
      IF ((Tair(J-1)-Twall).EQ.0.0) GO TO 300
      Hw(J-1)=1000.*deltaQ(J-1)/((TIME(J)-TIME(J-1))*
     Z(Tair(J-1)-Twall)*((CYLsa(J-1)+CYLsa(J))/2.))
 300  CONTINUE
C
C
C     Determining the gas film coefs. HJ1 and HJ2 (W/m**2-K) of
C     pre-chamber t.c.#1 and t.c.#2
C             Junction density      RHOJ = 8,938. kg/m**3
C             Junction specific heat CpJ = 0.3966 kJ/kg-K
```

```
C       Using  Tair(J), T.C.#1/ARRAY(7,1)/ and T.C.#2/ARRAY(8,J)/
C
        RHOJ=8938.
        CpJ=0.3966
        DJ2=SQRT(2.)*(2./1000.)*0.0254
        DO 320 J=48,73
        IF (ARRAY(8,J-1).EQ.ARRAY(8,J)) GO TO 320
        HJ2(J-1)=1000.*0.5*RHOJ*CpJ*DJ2*(ARRAY(8,J)-ARRAY(8,J-1))/
     Z((TIME(J)-TIME(J-1))*(2.*Tair(J-1)-(ARRAY(8,J)+ARRAY(8,J-1))))
 320    CONTINUE
C
        DJ1=SQRT(2.)*(1./1000.)*0.0254
        DO 325 J=48,73
        IF (ARRAY(7,J-1).EQ.ARRAY(7,J)) GO TO 325
        HJ1(J-1)=1000.*0.5*RHOJ*CpJ*DJ1*(ARRAY(7,J)-ARRAY(7,J-1))/
     Z((TIME(J)-TIME(J-1))*(2.*Tair(J-1)-(ARRAY(7,J)+ARRAY(7,J-1))))
 325    CONTINUE
C
C       Evaluating absolute viscosity ,MU kg/m-sec and
C       thermal conductivity, KAY W/M-K  of charge
C
        MUA=145.8
        MUB=110.4
        DO 350 J=47,73
 350    MU(J)=(MUA*Tair(J)**1.5)/((Tair(J)+MUB)*10.**8.)
C
        KAYA=0.6325*(10.**(-5.))
        KAYB=245.4
        KAYC=12.
        DO 360 J=47,73
 360    KAY(J)=(KAYA*418.68*(Tair(J)**0.5))/(1.+(KAYB*
     Z(10.**(-(KAYC/Tair(J)))))/Tair(J))
C
        TYPE 365
 365    FORMAT(/' Enter 0 = to go on                                   '/
     Z          '         1 = to print J,CA,TAIR,MU,KAY,RHO,MASS,VOL>'$)
        ACCEPT 30,IGO
        IF (IGO.EQ.0) GO TO 420
        TYPE 370
 370    FORMAT(/'     J  C.A   Tair(K) MUkg/m-s)  K(W/m-k)  RHO
     Z(kg/m**3)  Mass(KG)  VOLUME(M**3)')
C
        DO 380 J=47,72
 380    TYPE 390,J,ARRAY(1,J),Tair(J),MU(J),KAY(J),RHO(J),Mass(J)
     Z,ARRAY(2,J)/(10.**6.)
 390    FORMAT(1X,I4,1X,F5.0,1X,F6.1,5(1X,E11.4))
C
 420    TYPE 425
 425    FORMAT(/' Enter 0 = to go on                                   '/
     Z          '         1 = to print J,CA,HJ1,HJ2,Hw         >'$)
        ACCEPT 30,IGO
```

```
         IF (IGO.EQ.0) GO TO 515
         TYPE 430
 430     FORMAT(/'   J  C.A. HJ1(W/m**2-K) HJ2(W/m**2-K) Hw(W/m**2-K)')
C
         DO 440 J=47,73
 440     TYPE 450,J,ARRAY(1,J),HJ1(J),HJ2(J),Hw(J)
 450     FORMAT(1X,I4,1X,F5.0,1X,3(E10.3,2X))
C
C        After omitting visually observed weird HJ1 and HJ2 values,
C        HJ1 and HJ2 are averaged within a user chosen range
C
 515     TYPE 520
 520     FORMAT(/' Enter 1st/last HJ1 (47to72) for ave. process >_,_'$)
         ACCEPT*,FHJ1,LHJ1
C
         IF (FHJ1.EQ.47) GO TO 521
         DO 522 I=47,FHJ1-1
 522     HJ1(I)=0.0
C
 521     IF (LHJ1.EQ.73) GO TO 524
         DO 523 I=LHJ1+1,73
 523     HJ1(I)=0.0
C
 524     TYPE 525
 525     FORMAT(' Enter # of HJ1(I)s to omit from ave. process   >_'$)
         ACCEPT 30,NDEL1
         IF (NDEL1.EQ.0) GO TO 535
C
         TYPE 530
 530     FORMAT(' Enter locations, I(from 47 to 72) to omit  >_,_,..'$)
         ACCEPT*,(IDEL1(I),I=1,NDEL1)
C
         DO 532 J=1,NDEL1
 532     HJ1(IDEL1(J))=0.0
C
 535     HJ1AVE=0.0
         DO 540 J=FHJ1,LHJ1
         IF (NDEL1.EQ.0) GO TO 545
         DO 550 I=1,NDEL1
 550     IF (J.EQ.IDEL1(I)) GO TO 540
 545     HJ1AVE=HJ1(J)+HJ1AVE
 540     CONTINUE
         HJ1AVE=HJ1AVE/FLOAT((LHJ1-FHJ1+1)-NDEL1)
C
         TYPE 5501
 5501    FORMAT(/' Enter 1st/last HJ2 (47to72) for ave. process >_,_'$)
         ACCEPT*,FHJ2,LHJ2
C
         IF (FHJ2.EQ.47) GO TO 5502
         DO 5503 I=47,FHJ2-1
 5503    HJ2(I)=0.0
```

```
C
 5502   IF (LHJ2.EQ.73) GO TO 5504
        DO 5505 I=LHJ2+1,73
 5505   HJ2(I)=0.0
C
 5504   TYPE 5506
 5506   FORMAT(' Enter # of HJ2(I)s to omit from ave. process   >_'$)
        ACCEPT 30,NDEL2
        IF (NDEL2.EQ.0) GO TO 5507
C
        TYPE 5508
 5508   FORMAT(' Enter locations, I(from 47 to 72) to omit  >_,_,..'$)
        ACCEPT*,(IDEL2(I),I=1,NDEL2)
C
        DO 5509 J=1,NDEL2
 5509   HJ2(IDEL2(J))=0.0
C
 5507   HJ2AVE=0.0
        DO 5510 J=FHJ2,LHJ2
        IF (NDEL2.EQ.0) GO TO 5511
        DO 5512 I=1,NDEL2
 5512   IF (J.EQ.IDEL2(I)) GO TO 5510
 5511   HJ2AVE=HJ2(J)+HJ2AVE
 5510   CONTINUE
        HJ2AVE=HJ2AVE/FLOAT((LHJ2-FHJ2+1)-NDEL2)
C
        ACTn=1.-((ALOG10(HJ1AVE/HJ2AVE))/(ALOG10(DJ2/DJ1)))
C
        TYPE 5513,HJ1AVE,HJ2AVE,DJ1,DJ2,GUESSn,ACTn
 5513   FORMAT(' HJ1AVE = 'E10.3/
     Z         ' HJ2AVE = 'E10.3/
     Z         '    DJ1 = 'E10.3/
     Z         '    DJ2 = 'E10.3/
     Z         ' GUESSn = 'F7.3/
     Z         '   ACTn = 'F7.3)
C
C       Evaluating Junction Nusselt #, Reynolds # and charge velocity
C
        NUJAVE=0.0
        REJAVE=0.0
        ICOUNT=0
        DO 552 J=47,73
        NUJ(J)=(HJ1AVE+HJ2AVE)*0.5*(DJ1+DJ2)*0.5/KAY(J)
        IF (NUJ(J).LT.(0.65)) GO TO 552
        IF (NUJ(J).GE.(0.65).AND.NUJ(J).LT.(1.41)) GO TO 553
        IF (NUJ(J).GE.(1.41).AND.NUJ(J).LT.(3.42)) GO TO 554
        IF (NUJ(J).GE.(3.42).AND.NUJ(J).LT.(29.3)) GO TO 555
        IF (NUJ(J).GE.(29.3).AND.NUJ(J).LT.(121.)) GO TO 556
        IF (NUJ(J).GE.(121.).AND.NUJ(J).LT.(773.)) GO TO 557
        GO TO 552
  553   REJ(J)=(NUJ(J)/0.891)**(1./0.330)
```

```
        GO TO 559
 554    REJ(J)=(NUJ(J)/0.821)**(1./0.385)
        GO TO 559
 555    REJ(J)=(NUJ(J)/0.615)**(1./0.466)
        GO TO 559
 556    REJ(J)=(NUJ(J)/0.174)**(1./0.618)
        GO TO 559
 557    REJ(J)=(NUJ(J)/0.0239)**(1./0.805)
 559    ICOUNT=ICOUNT+1
        V(J)=REJ(J)*MU(J)/(RHO(J)*(DJ1+DJ2)*0.5)
        NUJave=NUJ(J)+NUJAVE
        REJAVE=REJ(J)+REJAVE
 552    CONTINUE
        NUJAVE=NUJAVE/ICOUNT
        REJAVE=REJAVE/ICOUNT
C
        TYPE 560
 560    FORMAT(/' Enter 0 = to go on                            '/
     Z          '       1 = to print J,CA,NUJ,REJ,V          >'$)
        ACCEPT 30,IGO
        IF (IGO.EQ.0) GO TO 564
        TYPE 561
 561    FORMAT('   J  C.A.     NUJ           REJ        V(m/sec)')
C
        DO 562 J=47,73
 562    TYPE 563,J,ARRAY(1,J),NUJ(J),REJ(J),V(J)
 563    FORMAT(1X,I4,1X,F5.0,1X,3(E10.3,2X))
C
 564    TYPE 565,NUJAVE,REJAVE
 565    FORMAT(/'        NUJAVE       = 'E10.3/
     Z          '        REJAVE       = 'E10.3/)
C
        TYPE 590
 590    FORMAT(/' Enter 0 = to go on                                 '/
     Z          '       1 = to iterate on n (guessed/actual) >'$)
        ACCEPT 100,IGO
        IF (IGO.EQ.1) GO TO 2
C
C       After omitting visually observed weird Hw values, linear
C       interpolation is used as a 1st. approx. to replace omitted
C       points, before they are smoothed.
C
        TYPE 600
 600    FORMAT(/' Enter 1st/last Hw (47 to 72) for smoothing  >_,_'$)
        ACCEPT*,FHw,LHw
C
        IF (FHw.EQ.47) GO TO 602
        DO 604 I=47,FHw-1
 604    Hw(I)=0.0
C
 602    IF (LHw.EQ.73) GO TO 608
```

```
       DO 606 I=LHw+1,73
 606   Hw(I)=0.0
C
 608   TYPE 610
 610   FORMAT(' Enter # of Hw(I)s to omit from smoothing     >_'$)
       ACCEPT 30,NDEL
       IF (NDEL.EQ.0) GO TO 620
C
       TYPE 630
 630   FORMAT(' Enter locations, I(from 47 to 72) to omit  >_,_,..'$)
       ACCEPT*,(IDEL2(I),I=1,NDEL)
C
       Xa=0
       Spaces=2
C
       DO 640 J=1,NDEL
        IF (Xa.GT.0) GO TO 650
        Xa=IDEL2(J)-1
 650    IF (J.EQ.NDEL) GO TO 660
        IF ((IDEL2(J+1)-IDEL2(J)).GT.1) GO TO 660
        Spaces=Spaces+1
        GO TO 640
 660    Xb=IDEL2(J)+1
       TYPE 665,J,SPACES
 665   FORMAT(' Hw('I2') was deleted/replaced, gap size ='I3' spaces')
        deltHw=(Hw(Xb)-Hw(Xa))/FLOAT(Spaces)
          DO 670 I=1,Spaces-1
 670      Hw(Xa+I)=Hw(Xa+I-1)+deltHw
        Xa=0
        Spaces=2
 640   CONTINUE
C
 620   NPP=(LHw-FHw+1)-NDEL
C
       DO 680 J=FHw,LHw
 680   A(J-FHw+1)=Hw(J)
C
C      Calling Smoothing Subroutine RSMOT
C
       CALL RSMOT(A,NPP)
C
       DO 690 J=FHw,LHw
 690   Hw(J)=A(J-FHw+1)
C
C
C      Defining Dcyl(i) = cyl. vol.(i) / cyl. surface area (i)
C
       DO 692 J=1,73
 692   Dcyl(J)=CYLVOL(J)/CYLsa(J)
C
C      Evaluating the cylinder Nusselt # and Reynolds #
```

```
C
      DO 695 J=47,72
      NUw(J)=Hw(J)*Dcyl(J)/KAY(J)
      REw(J)=RHO(J)*Dcyl(J)*V(J)/MU(J)
 695  CONTINUE
C
      TYPE 700
 700  FORMAT(/' Enter 0 = to go on                                '/
     Z      '         1 = to print J,CA,Dcyl,CYLsa,Hw,NUw,REw   >'$)
      ACCEPT 30,IGO
      IF (IGO.EQ.0) GO TO 750
      TYPE 710
 710  FORMAT(/'   J  C.A.    Dcyl(m) CYLsa(m**2) Hw(W/m**2-K)   NUw
     Z     REw')
C
      DO 715 J=47,73
 715  TYPE 720,J,ARRAY(1,J),Dcyl(J),CYLsa(J),Hw(J),NUw(J),REw(J)
 720  FORMAT(1X,I4,1X,F5.0,5(1X,E10.3))
C
 750  TYPE 760
 760  FORMAT(/' Enter -1 = to analize FIRST disk                  '/
     Z      '          0 = to stop                              '/
     Z      '          1 = to write crunched data to  Disk #10  >'$)
      ACCEPT 100,IGO
      IF (IGO.EQ.-1) GO TO 50
      IF (IGO.EQ.0) GO TO 999
 765  PAUSE 'Insert Binary Data Disk #10 and press RETURN '
      DO 770 I=1,128
 770  DIR(I)=0.0
      IERR1=ISPFNW("377,ICHAN,0,DIBUF1,1)
      IF (IERR1.NE.0) TYPE 70,IERR1
      IF (DIR(1)-10.) 765,775,765
C
C     Choosing scaling factors in order to make use of the maximum
C     maximux integers available, +/- 32000.
C
 775  TYPE 780
 780  FORMAT(' Writing C.A.,deltaW/J/,deltaG/J/,Tair,Ts,P,TC#1,TC#2'/
     Z      '           to disk #10')
C
      DO 785 J=47,73
      ARRAY(2,J)=deltaW(J)*1000.
      ARRAY(3,J)=deltaG(J)*1000.
      ARRAY(4,J)=Tair(J)
 785  ARRAY(5,J)=Ts(J)
      KCOUNT=0
      GO TO 805
C
 790  KCOUNT=1
C
      DO 800 J=47,73
```

```
        ARRAY(2,J)=cumW(J)*1000.
        ARRAY(3,J)=cumG(J)*1000.
        ARRAY(4,J)=RHO(J)
        ARRAY(5,J)=V(J)
        ARRAY(6,J)=Hw(J)
        ARRAY(7,J)=NUw(J)
 800    ARRAY(8,J)=REw(J)
C
 805    DO 810 I=1,8
        DO 810 J=1,46
 810    ARRAY(I,J)=0.0
C
        DO 820 I=1,8
        DO 820 J=74,96
 820    ARRAY(I,J)=0.0
C
        DO 830  I=1,8
        RMIN(I)=32000.
 830    RMAX(I)=-32000.
C
        DO 840 I=1,8
        DO 840 J=1,96
        RMIN(I)=AMIN1(ARRAY(I,J),RMIN(I))
 840    RMAX(I)=AMAX1(ARRAY(I,J),RMAX(I))
C
        DO 850 I=1,8
        TYPE 855,I,RMIN(I),RMAX(I)
 855    FORMAT(' CHAN# 'I3' ,MIN= 'F7.0', MAX= 'F7.0)
 850    CONTINUE
C
 860    DO 870 I=1,8
        TYPE 880,I
 880    FORMAT(' Enter multiplier for ARRAY('I2',J)    >'$)
 870    ACCEPT*,Scale(I)
C
        DO 890 J=47,73
        ARRAY(1,J)=ARRAY(1,J)*Scale(1)
        ARRAY(2,J)=ARRAY(2,J)*Scale(2)
        ARRAY(3,J)=ARRAY(3,J)*Scale(3)
        ARRAY(4,J)=ARRAY(4,J)*Scale(4)
        ARRAY(5,J)=ARRAY(5,J)*Scale(5)
        ARRAY(6,J)=ARRAY(6,J)*Scale(6)
        ARRAY(7,J)=ARRAY(7,J)*Scale(7)
        ARRAY(8,J)=ARRAY(8,J)*Scale(8)
 890    CONTINUE
C
        DO 900  I=1,8
        RMIN(I)=32000.
 900    RMAX(I)=0.0
C
        DO 910 I=1,8
```

```
      DO 910 J=1,96
      RMIN(I)=AMIN1(ARRAY(I,J),RMIN(I))
 910  RMAX(I)=AMAX1(ARRAY(I,J),RMAX(I))
C
      DO 920 I=1,8
      TYPE 930,I,RMIN(I),RMAX(I)
 930  FORMAT(' CHAN# 'I3' ,MIN= 'F7.0', MAX= 'F7.0)
 920  CONTINUE
C
      TYPE 940
 940  FORMAT(' Enter 0 = to go on                          '/
     Z         '        1 = to change multipliers          >'$)
      ACCEPT 100, IGO
      IF (IGO.EQ.1) GO TO 860
C
      IF (KCOUNT.EQ.0) GO TO 945
      KBLOCK=KBLOCK+1
      TYPE 943
 943  FORMAT(' Writing C.A.,cumW/J/,cumQ/J/,RHO,V,Hw,NUw,REw'/
     Z          '         to disk #10.')
      GO TO 955
 945  TYPE 950
 950  FORMAT(' Enter block# to write to       >'$)
      ACCEPT*,KBLOCK
C
 955  JBLOCK=KBLOCK
      DO 960 I=1,256,8
      DO 960 ICOL=1,8
      IROW=(I-1)/8+47
      K=(I-1)+ICOL
 960  IBUF(K)=ARRAY(ICOL,IROW)
      IERR=IWRITE(256,IBUF,JBLOCK,ICHAN)
C
      TYPE 970 ,KBLOCK
 970  FORMAT(' Write accomplished in block #' I5)
C
      IF (KCOUNT.EQ.1) GO TO 985
      TYPE 975
 975  FORMAT(' Enter 0 = to go on                                    '/
     Z         '        1 = to write C.A,cumW/J/,cumQ/J/,RHO,V,Hw,NUw'/
     Z         '           REw to Binary data disk #10 as well     >'$)
      ACCEPT*,IGO
      IF (IGO.EQ.1) GO TO 790
C
 985  TYPE 990
 990  FORMAT(' Enter 0 = to stop                             '/
     Z         '        1 = to analyze Binary data disk #9      >'$)
C
      ACCEPT 100,IGO
      IF (IGO.EQ.1) GO TO 50
 999  STOP
      END
```

APPENDIX D: Detailed Cell Design

In designing the cell it was recognized that the glass windows would be the most critical parts of the system. As a result of this, a 1 cm thickness was chosen for the stainless steel cylinder thickness based on the thread reach of a standard 18 mm spark plug. Justification of this assumed cell wall thickness will be done here before description of the detailed glass design analysis.

Popov [25, p. 290] suggests using a thick cylinder wall approach when the wall thickness t, and the inside cell radius r_i, are related as follows.

$$t > 1/10\ r_i \tag{D$_1$}$$

Considering an annular thin disk, the plane stress condition (i.e. $\sigma_z=0$) governs. Furthermore at any point in an elastic cylinder, radial σr and tangential σt stresses are present, (D_2), and (D_3).

$$\sigma r = c_1 - c_2/r^2 \tag{D$_2$}$$

$$\sigma t = c_1 + c_2/r^2 \tag{D$_3$}$$

where:

$$c_1 = \frac{P_i r_i^2 - P_k\ r_k^2}{r_k^2 - r_i^2}$$

$$c_2 = \frac{(P_i - P_k)\, r_i^2 r_k^2}{r_k^2 - r_i^2}$$

$_i$ = inside
$_k$ = outside

For the special case here, where there is only internal pressure P_i

$$c_1 = \frac{P_i r_i^2}{r_k^2 - r_i^2}$$

$$\& \quad c_2 = \frac{(P_i r_i^2 r_k^2)}{r_k^2 - r_i^2}$$

$$\sigma r = \frac{P_i r_i^2}{r_k^2 - r_i^2}\left[1 - \frac{r_k^2}{r^2}\right] \qquad (D_4)$$

$$\sigma t = \frac{P_i r_i^2}{r_k^2 - r_i^2}\left[1 + \frac{r_k^2}{r^2}\right] \qquad (D_5)$$

For ductile materials such as stainless steel, which fail in shear rather than in direct tension, the maximum shear theory of failure should be used for design. This is

$$\tau max = \frac{\sigma_1 - \sigma_2}{2} = \frac{\sigma yp}{2} \qquad (D_6)$$

With internal pressure only, the maximum shearing stress occurs on the inner surface of the cylinder. At this surface both the tensile stress σt and the compressive stress σr

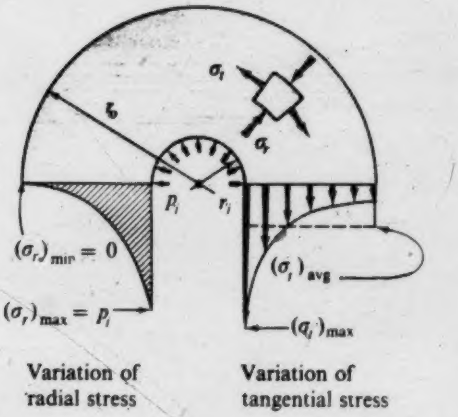

Figure D.1 Variation of Radial and Tangential Stresses in a Thick Wall Cylinder

reach their maximum values, see Figure D.1. Substituting into (D_6) the maximum and minimum principle stresses (D_5) and (D_4) respectively, (D_7) is obtained.

$$\frac{\sigma t - \sigma r}{2} = \frac{\sigma yp}{2}$$

$$\frac{\sigma yp}{2} = \frac{P_i r_i^2}{(r_k^2 - r_i^2)} \qquad (D_7)$$

solving for P_i

$$P_i = \frac{\sigma yp \ (r_k^2 - r_i^2)}{2r_k^2}$$

where:

$\sigma yp = 200$ MPa (representative value for 300 series stainless steel) [5, p. 370]

$r_i = 4$ cm

$r_k = 5$ cm

This results in an internal pressure of 36 MPa required for failure of the cell. Therefore, the wall thickness of 1 cm should be very sufficient to handle the expected pressure of 2 MPa even when allowances are made for the four access holes drilled into the cell body and a factor of safety.

The design of the glass windows was, for the most part based on a procedure outlined in the Glass Engineering Handbook [28]. However, before proceeding, it is important to appreciate some of the factors that affect the strength of glass.

First of all, flat glass or sheet glass is characterized by 3 elements of strength:

(i) The strength of the bulk

(ii) The strength of the surfaces

(iii) The strength of the edges

A sketch of the glass window is shown in Figure D.2.

In general, mechanical surface treatment such as sand-blasting, scratching, grinding, even polishing, reduces the strength of the glass from that with its natural surface intact. However, treating the surface chemically by etching with Hydrofluoric acid followed by lacquering greatly increases the glass strength.

The circumferential edge of the glass window has the lowest strength of the three listed above. This is because the edge contains the most critical defects as a direct result of its mechanical treatment, during grinding to shape. The strength of the natural surface of the glass which has been vertically drawn occupies an intermediate position between the strength of the edge and the inner parts of the glass. Polishing these surfaces, while further reducing its strength somewhat, does not change its relative position of strength with respect to the edges and the bulk. Another way of looking at this is to consider that the glass surface layer (with its natural surface intact) contains defects of a higher criticality than the inner layers of the glass but of a lower criticality than are the micro-cracks

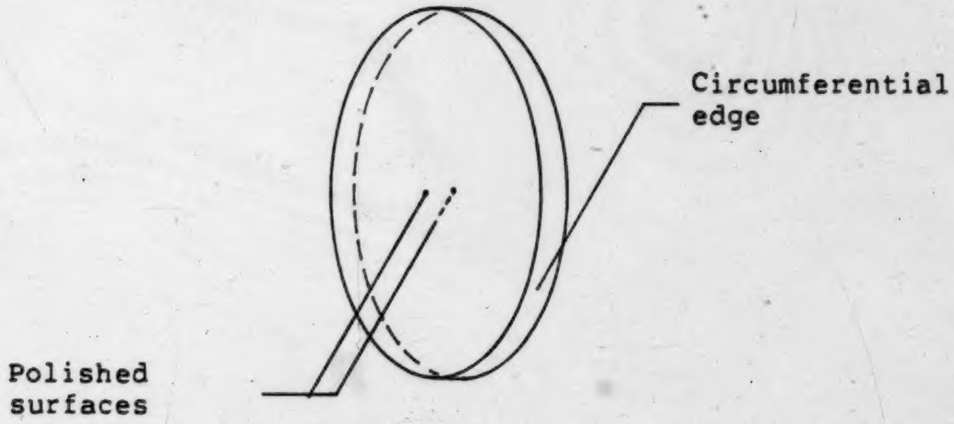

Figure D.2 Schematic of Glass Window

on the surface of a mechanically treated glass, by polishing for example.

The bulk strength obtained can be more or less chosen by knowlege of manufacturing and quality control procedures used.

Control over the strength of the edge is accomplished in much the same fashion as for the bulk strength. However, depending on the design application, particularly in this case because the edge is a minimum distance of 3.5 cm from the loaded part of the glass, the effect of the edge being the weakest part of the glass may indeed be negligible. Furthermore, recalling that the clamping technique used tends to distribute the clamping force evenly over the fixed region, the likelihood of creating a stress concentration in an already weakened area such as the circumferential edge is minimal.

Regarding the strength of the surfaces, one is given certain options. Two design criteria must be considered, material strength and the need for some mechanical surface treatment (polishing for example) to improve the photographic image resolution.

One option available for increasing the strength of the glass is tempering. This is a heat treatment technique that involves setting up high residual stresses and results in a tempered strength usually 2 1/2 to 3 times the annealed strength.

In the final analysis polishing was deemed an absolute necessity in order to achieve the required photographic quality. However, its effect was two-fold,

1. Tempering was automatically ruled out as hand polishing, which is required for this sort of quality optical work, would have been virtually impossible after heat treatment of the glass. On the other hand, heat treatment subsequent to polishing would have distorted the smooth surface.

2. The act of polishing is known to reduce the strength of the glass somewhat from that with its vertically drawn natural surface intact. Therefore, adequate strength is to be found in designing the glass thick enough to withstand the expected loads.

From the mechanical design aspect, the very minimum criteria required for the cell was being able to withstand the effects of the combustion of a stoichiometric mixture of a fuel like methane and air, initially at atmospheric pressure. It is however very desirable to be able to first pressurize the charge before igniting the mixture.

Assuming the combustion takes place adiabatically with no work added or changes in kinetic or potential energy involved, the temperature of the products is referred to as the adiabatic flame temperature. This is the maximum temperature that can be achieved for any given reactants when the "theoretical" amount of air is supplied (Stoichiometric Mixture, $\Phi=1.0$), i.e., complete combustion occurs so there will be no oxygen or CO in the combustion products. Incomplete combustion is to be avoided as it tends to lower the temperature of the products. The theoretical maximum adiabatic flame temperature for a stoichiometric methane/air mixture initially at 300 K, is 2240 K [14]. For combustion in a constant-volume bomb, the maximum peak pressure is found using (D_8)

$$P_2 = (T_2/T_1)P_2 \qquad (D_8)$$

$$P_2 = (2240\ \text{K}/300\ \text{K})\ P_1$$

$$P_2 \cong (7 \rightarrow 8)P_1$$

This shows that the expected peak pressure resulting from adiabatic combustion of methane/air mixture ($\Phi = 1.0$) is about 7 to 8 times the initial pressure.

However, the measured peak pressure was approximately four times the initial pressure. The lower values being a result of heat losses which occur during combustion. This prompts the following question: What is the maximum allowable initial pressure such that the resulting peak pressure does not cause over stressing of the glass? As a starting point it was decided to use a typical pressure-time trace obtained during the compression/ignition stroke, from an unthrottled Otto engine with a compression ratio of 10 to 1 (idealized cycle), Obert [24]. This was used to create a pressure-time design curve for a constant-volume combustion process like this, with an initial pressure of 2.07 MPa, the expected peak pressure 8.3 MPa. Figure D.3 shows this design loading-time curve.

For simplicity this loading time-curve is approximated to act like an impulse of 6.2 MPa with duration of 0.5 s.

The Engineering Materials Handbook [16] suggests using the following for determining the strength of sheet glass when subject to uniform pressure loading.

$$P = 3.12\ Mt^2/A \qquad (D_9)$$

where:

P = internal pressure (6.2 MPa)

t = thickness (cm)

A = unsupported area ($\pi(8)^2/4 = 50.3\ \text{cm}^2$)

M = modulus of rupture (41.36 MPa for annealed glass)

For the cell size the unsupported area of the glass window is 50.3 cm^2. Using a maximum internal design pressure of 6.2 MPa, a modulus of rupture of 41.36 MPa (for annealed glass [16]) was used to solve (D_9) resulting in a minimum required thickness of 1.4 cm.

The Pressure Vessel Design Handbook [18] suggests using equation (D_{10}) for pressurized circular flat heads.

$$t = d\sqrt{0.2\ P/S} \qquad (D_{10})$$

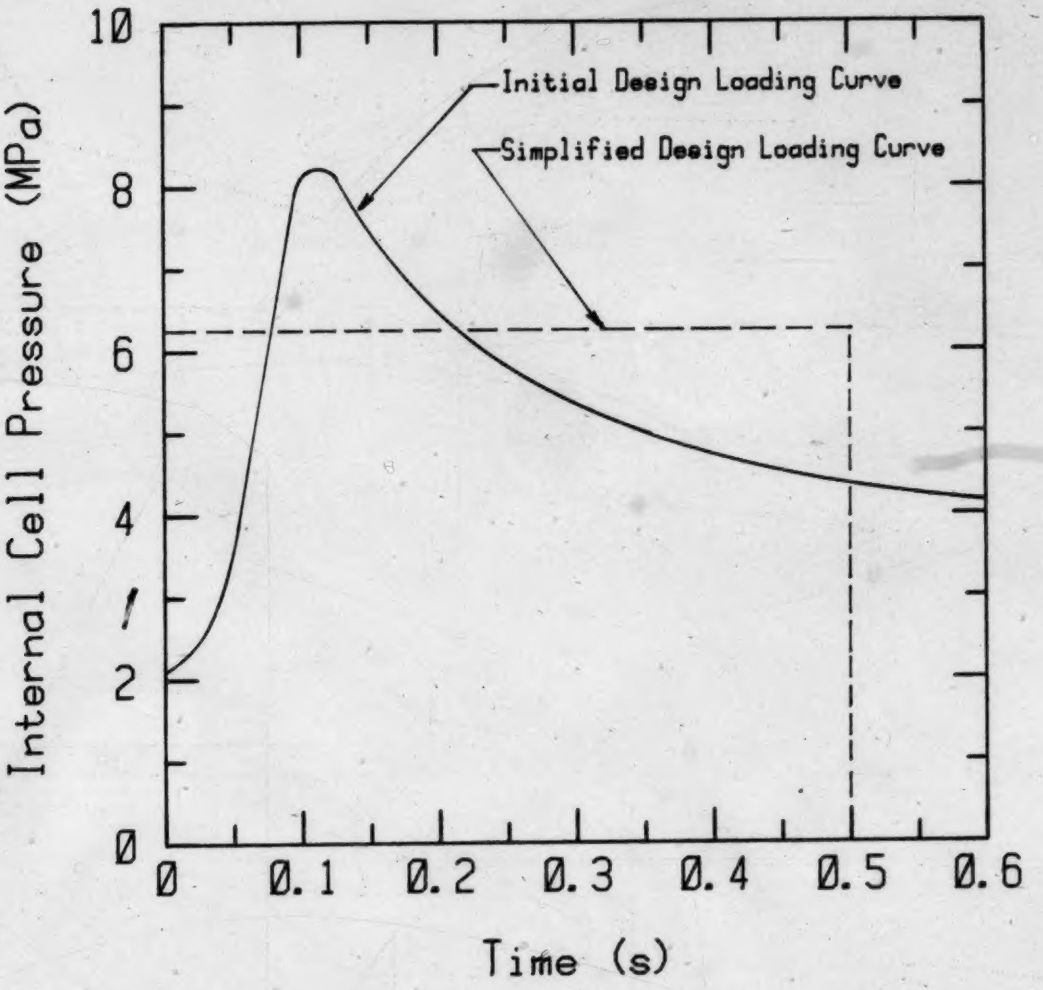

Figure D.3 Pressure-Time Trace used as the Starting Point in Glass Design

where:

S = maximum allowable stress value of material (MPa); used modulus of rupture for annealed glass (41.36 MPa)

P = internal design pressure (6.2 MPa)

d = inside diameter of shell (8 cm)

t = minimum required thickness of head (cm)

The result of this calculation was t = 1.4 cm

Finally using the theory of flexure to determine the stress in a circular plate with simply supported edges [27] gives:

$$\sigma = 3/8\ (3+\mu)\ \omega(r/t)^2 \qquad (D_{11})$$

where:

ω = uniformly distributed load/unit area (6.2 MPa)

t = thickness of plate (cm)

r = unsupported radius (4 cm)

σ = average bending stress at the surface of the plate at the diameter section (used modulus of rupture for annealed glass, 41.36 MPa)

μ = poisson's ratio for glass (0.21)

Solving for t gives a minimum thickness of 1.7 cm.

From these three results, a glass thickness of around 2 cm is suggested without making any substantial allowances for loading time, clamping conditions, mechanical surface treatment of glass or temperature boundary conditions.

Taking into account the loading time of 0.5 s with an internal pressure of 6.2 MPa, the allowable load is reduced by one third to a steady state load of 4.1 MPa. Making allowance for all other previously mentioned effects, a factor of safety of two was selected. This results in a recommended working pressure of 2.07 MPa, which is close to the 2.14 MPa that the Glass Engineering Handbook [28] suggests. Because the cell will be exposed to a pressure-time loading curve shaped similarly to Figure D.2 and not to a steady-state design pressure, it seems pertinent to suggest a maximum value for the initial cell pressure prior to the initiation of combustion, bearing in mind the expected peak pressure and overall loading time. There is sufficient flexibility in the steady-state design pressure of 2.1 MPa, to suggest that operation of the cell initially filled with a charge of 0.69 MPa, and having the pressure-time trace shown in Figure D.3 (note the similarity with Figure D.2) should be safe for both the operator and cell.

An initial cell pressure of 0.69 MPa translates into the capability to increase the initial density to about 7 times atmospheric which is equivalent to an engine with compression ratio of 7 to 1.

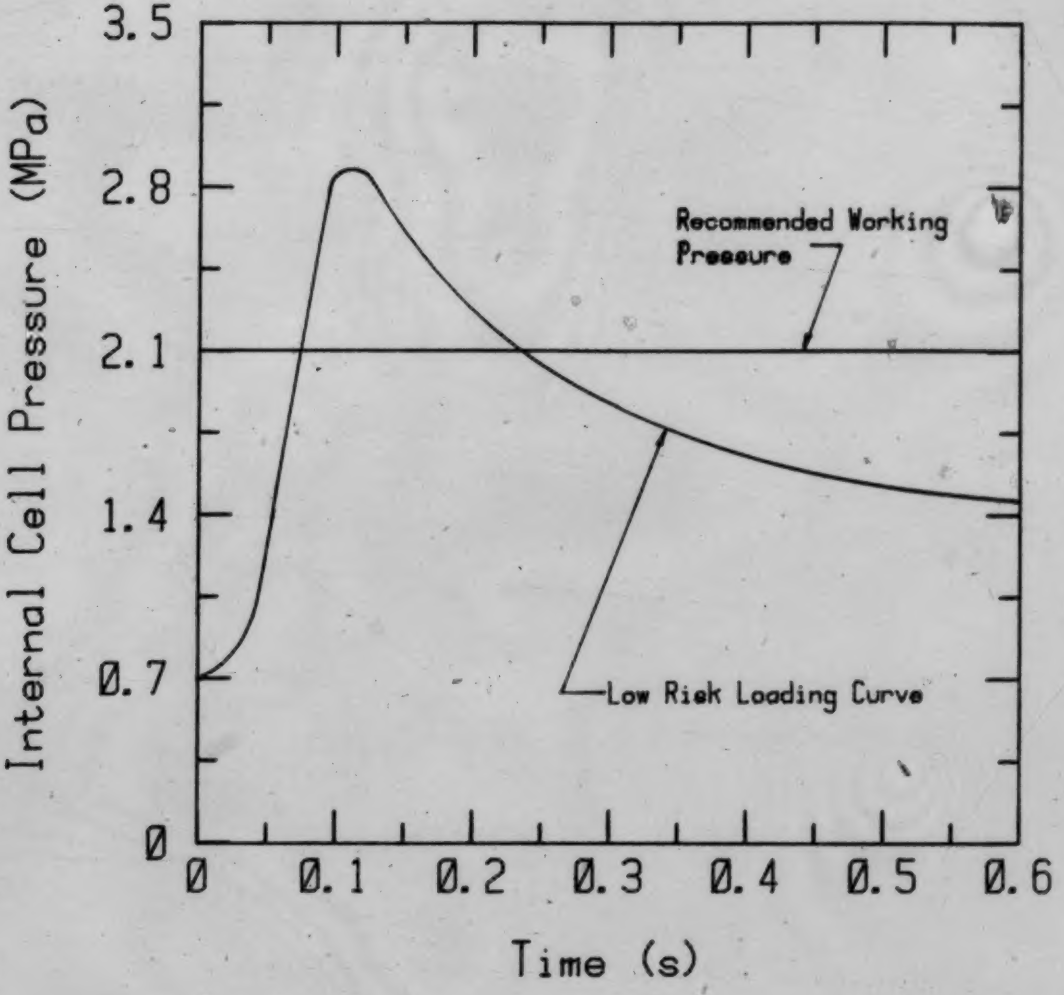

Figure D.4 Recommended Working Pressure and Low Risk Loading Curve for Glass

It should be noted that this analysis was done assuming a stoichiometric mixture of methane and air, $\Phi=1.0$. Here the pressures and temperatures at the end of the constant volume combustion, accounting for heat loss, are the upper limits. Therefore, if non-stoichiometric mixtures are ignited in the cell, the initial pressure may be boosted, as long as the resulting peak pressure is not greater than 2.8 MPa for a short duration, i.e., when the actual cell internal pressure-time trace is similar in shape to that of Figure D.3.

Some Suggested Precautions When Using the Cell and Handling the Glass

1. Apply a consistent torque that securely clamps the glasses in place. This is important in order to minimize glass failure.

2. At all costs avoid touching the flat glass surfaces with any thing other than lens paper, and then only for cleaning purposes. It is easy to scratch glass but expensive and time consuming to repair.

3. Prompt evacuation of combustion products is essential in order to stay within the design envelope. This is because of several reasons:

i) The material strength of glass is inversely proportional to its ambient temperature. This trend increases if there is a temperature differential across the glass as is the case when combustion occurs in the cell while the other surface is exposed to room temperature.

ii) Glass exhibits fatigue characteristics under static loads as a function time, somewhat similar to how metals behave under cyclic loads expressed as a function of the number of reversals. Hence reduction in loading time tends to increase the time until failure.

4. It is important to minimize exposure of the glass surfaces to the presence of moisture bearing atmosphere, as fatigue is closely associated with adsorbtion of water molecules.

5. It is suggested that cell pressure-deflection tests be done once a year in order to build a case history of the behaviour of the glass.

6. The Schlieren photographs can be used to monitor the glass bulk and surface conditions on an on going basis, particularly for locating surface scratches and internal flaws.

APPENDIX E: Surface Gap Plugs Used in Study

Figure E.1 - Homebuilt version

Figure E.2 - Champion G508V

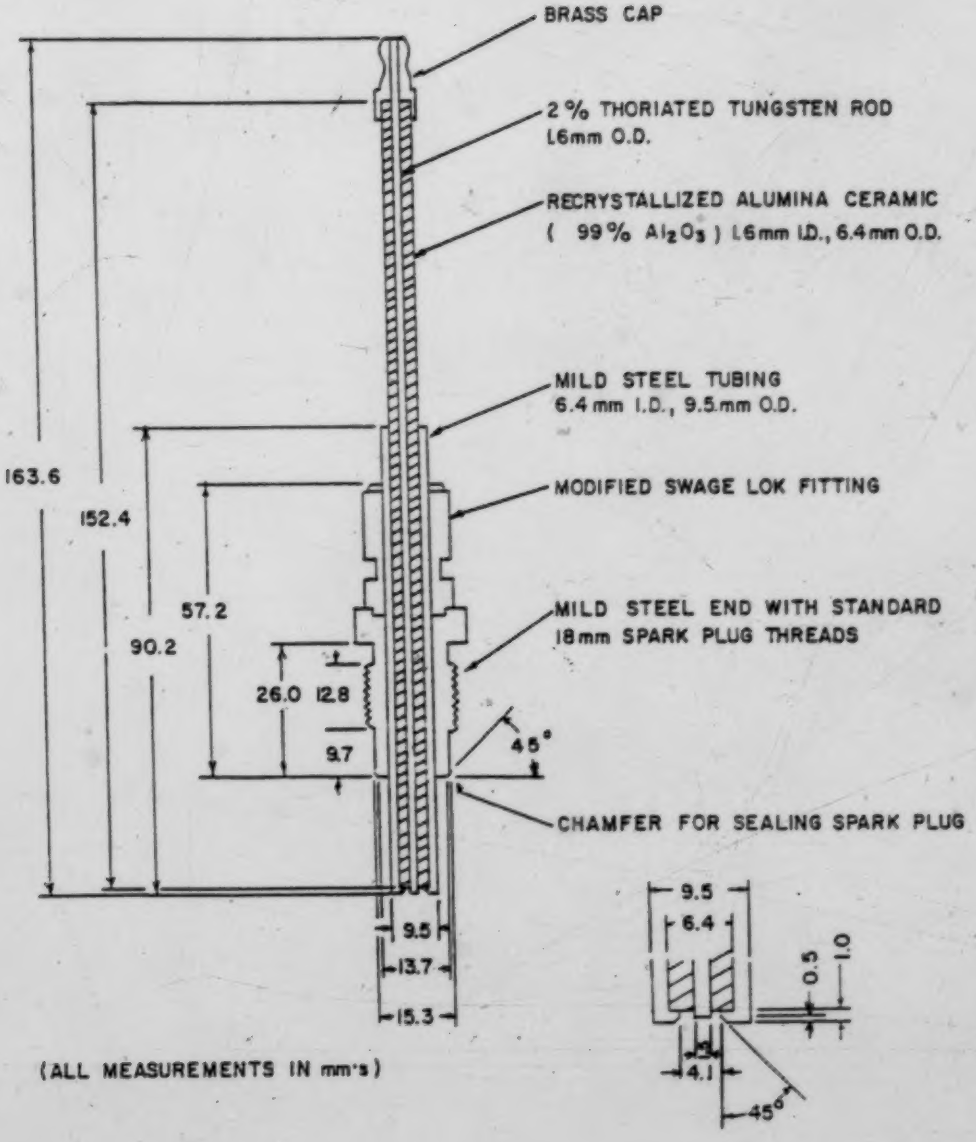
BRASS CAP
2 % THORIATED TUNGSTEN ROD
1.6mm O.D.
RECRYSTALLIZED ALUMINA CERAMIC
(99 % Al_2O_3) 1.6mm I.D., 6.4mm O.D.
MILD STEEL TUBING
6.4 mm I.D., 9.5 mm O.D.
MODIFIED SWAGE LOK FITTING
MILD STEEL END WITH STANDARD
18mm SPARK PLUG THREADS
CHAMFER FOR SEALING SPARK PLUG
163.6
152.4
90.2
57.2
26.0
12.8
9.7
45°
9.5
13.7
15.3
(ALL MEASUREMENTS IN mm's)
9.5
6.4
0.5
1.0
1.3
4.1
45°

Figure E.1 Homebuilt Surface Gap Plug

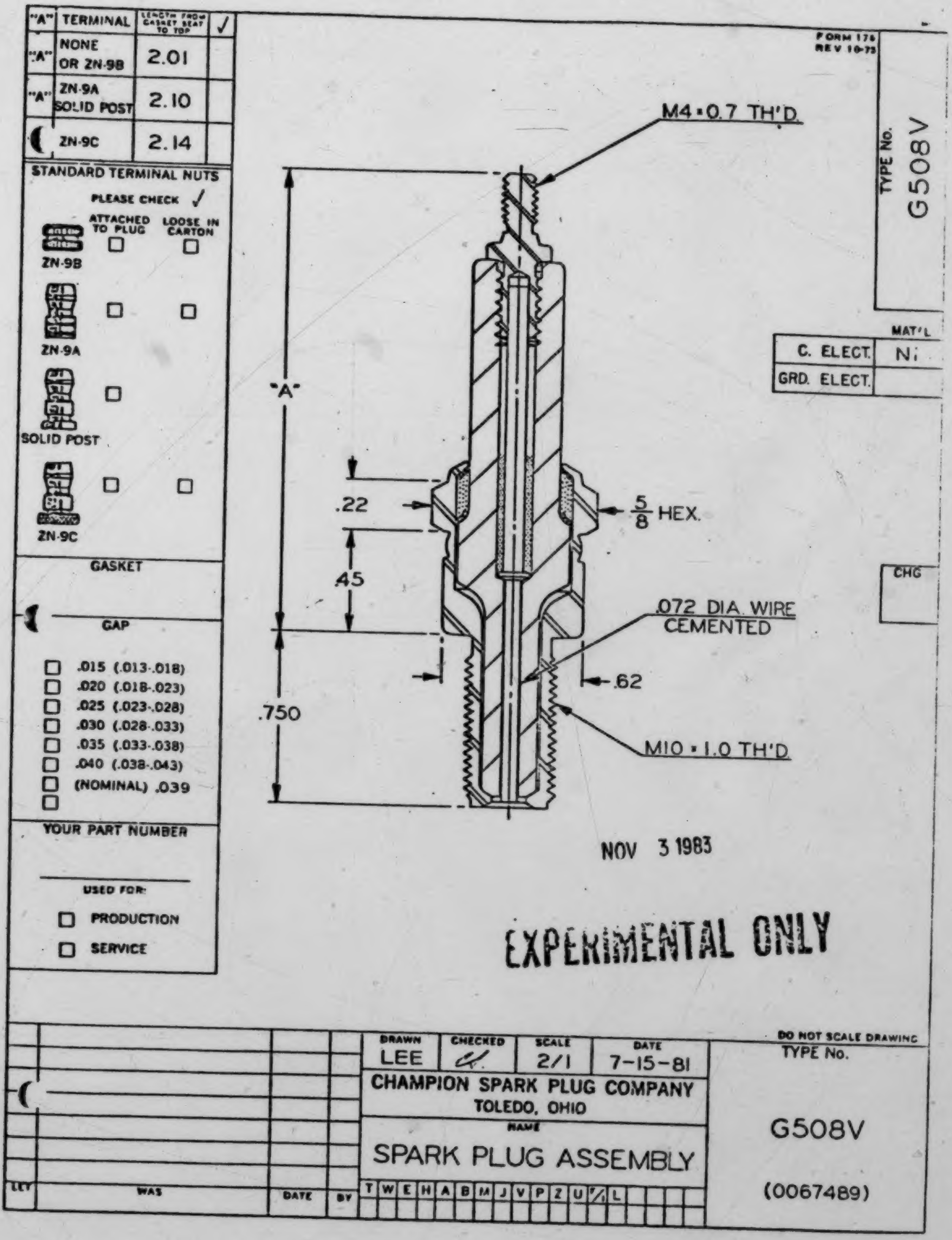

Figure E.2 Champion G508V Surface Gap Plug

APPENDIX F: Ignition System Parts List

For Figure F.1 Schematic of Ignition Circuit

(a) DC - DC Converter

(b) Main Discharge Capacitor

(c) Ignition Coil

(d) SCR Switched Capacitor

Resistors

R_1	3Ω, (10 W)
R_2	500Ω, (2 W)
R_3	390Ω
R_4	10 kΩ
R_5	3.9 kΩ
R_6	1.5 MΩ
R_7	10 kΩ 50 W
R_8	2 kΩ (50 W)

Capacitors

C_1	1000μF
C_2	100μF
C_3	600 pF
C_4	0.001μF (1000 V)

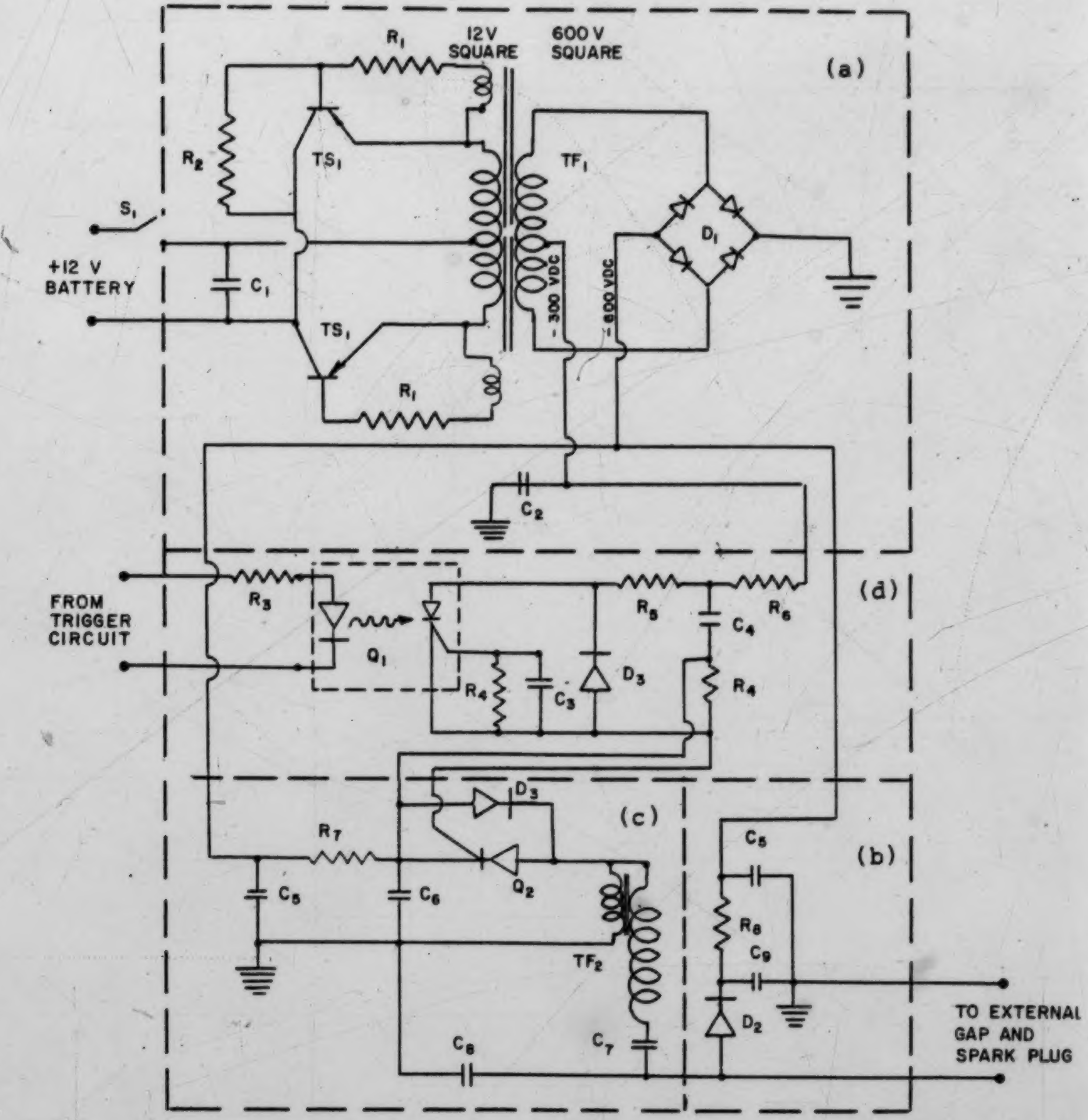

Figure F.1 Schematic of Ignition Circuit (a) DC-DC Converter,(b) Main Discharge Capacitor, (c) Ignition Coil (1 of 4),(d) SCR Switched Capacitor

C_5	10μF (1000 V)
C_6	4μF (1000 V)
C_7	0.005μF (30 kV)
C_8	0.0002μF (30 kV)
C_9	Main Discharge capacitor, 6μF(1000 V)

Transistors

TS_1	Motorola MJ4502

Transformers

TF_1	Toroidal Hammond T509
TF_2	Accel automotive ignition coil

Diodes

D_1	1N4007
D_2	VARO H1480 (40 kv)
D_3	1N10D8
D_4	1N5419

Switch

S_1	Main power switch (30A)

Others

Q_1	General Instruments Photo-SCR opto Isolator MCS 2400
Q_2	General Electric SCR C137PB

For Figure F.2 Schematic of Trigger Circuit (1 of 4) (e)

Resistors

R_1	33 kΩ
R_2	47 kΩ
R_3	0 → 1000 kΩ
R_4	100 kΩ
R_5	22 kΩ
R_6	2.2 kΩ

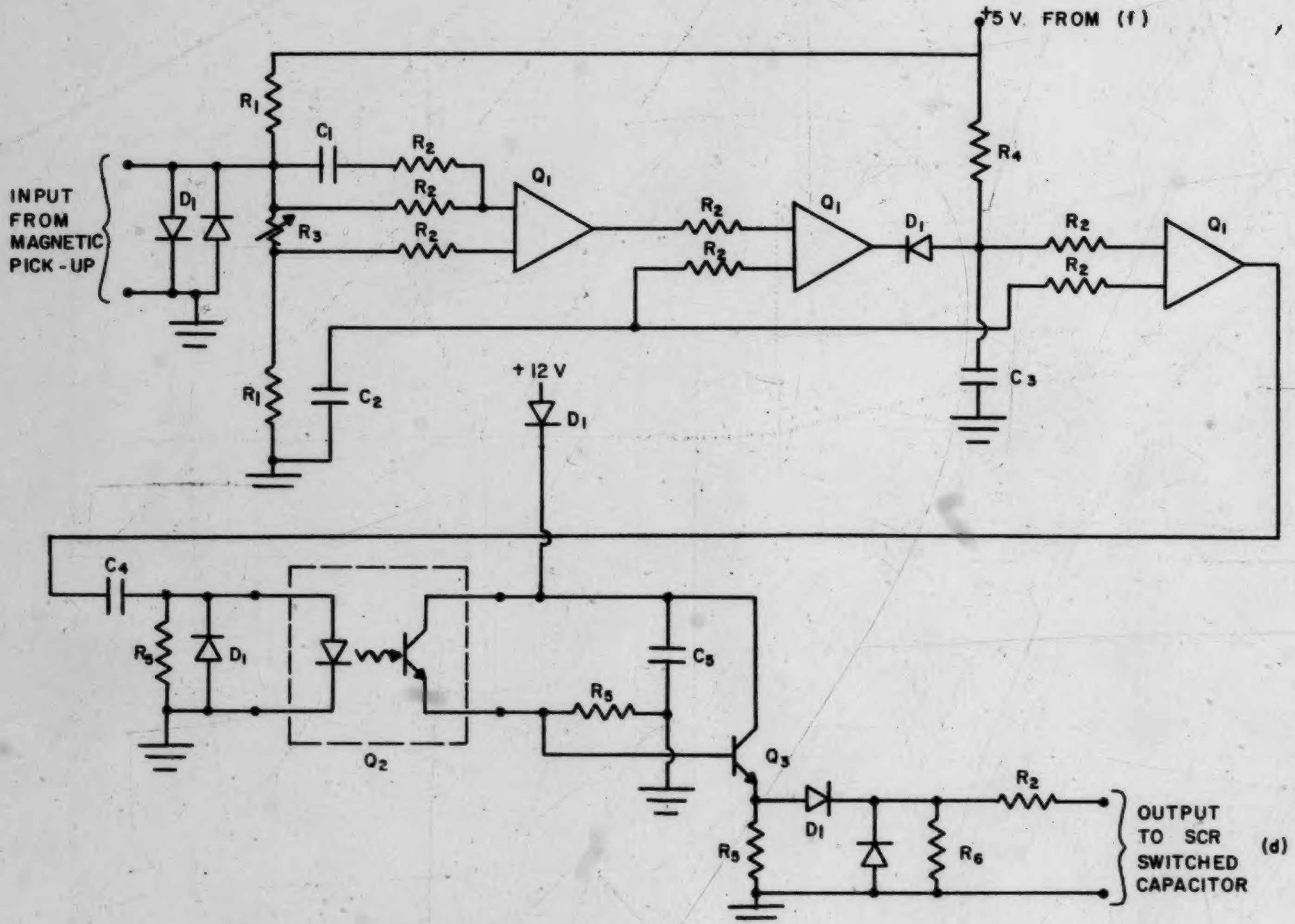

Figure F.2 Schematic of Trigger Circuit (1 of 4) (e)

Diode

D_1	1N4007

Capacitors

C_1	1μF
C_2	1μF
C_3	0.033μF
C_4	0.047μF
C_5	10μF

Others

Q_1	LM324
Q_2	4N25
Q_3	2N4401

For Figure F.3 Schematic of +5 V regulated power supply to trigger circuit (f)

Diode

D_1	1N4007

Capacitors

C_1	3000μF
C_2	10μF

Others

Q_1	LM 309

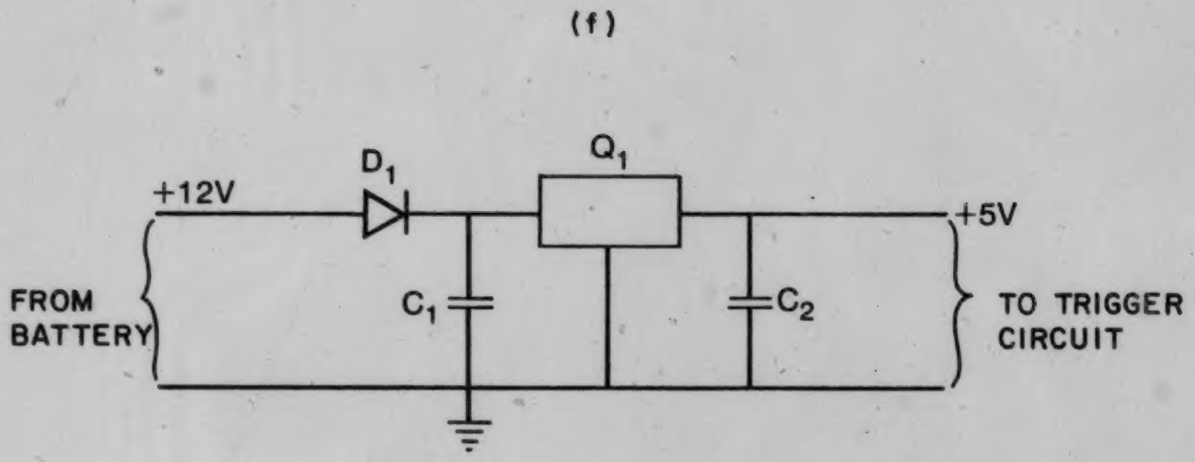

Figure F.3 Schematic of +5 v Regulated Power Supply to Trigger Circuit (f)

APPENDIX G: Technical Data on Diesel Fuel

The specifications for the Artic (AA) Diesel fuel is listed in Table G.1. while results of tests done by various laboratories are listed in Table G.2

TABLE G.1 Diesel Fuel Specifications

	Type AA	ASTM Method
Flash Point, °C, min.	40	D 93 or D 3828
Cloud Point, °C, max.	-48	D 2500
Pour Point, °C, max.	-51	D 97
Kinematic Viscosity 40°C, mm^2/s		D 445
min.	1.2	
max.	-	
Distillation:		D 86
90% recovered, °C, max.	290	
Water and Sediment, % vol., max.	0.05	D 1796
Total Acid Number, max.	0.10	D 974
Sulphur, % mass, max.	0.2	D 1552
Copper Corrosion, 3 h 100°C, max.	No. 1	D 130
Copper Residue (Ramsbottom), on 10% bottom, %mass, max.	0.15	D 524
Ash, %mass, max.	0.01	D 482
Ignition Quality, Cetane No., min.	40	D 613

TABLE G.2 Diesel Fuel Distillations, Cloud Point and pour point test results

	fuel AA[a]	fuel AA[b]
Distillation Range % Recovered °C (ASTM D86)		
IBP	154	157
10%	175	176.5
50%	202	204
90%	235	236
FBP	250	249
Cloud Point °C (ASTM D2500)	-54	-51
Pour Point °C (ASTM D97)	-51	-51

[a] National Research Council

[b] Alberta Research Council